Neuronal Circuitry of the Pigeon Retina (*Columba livia*) – The morphological classification and organization of various neuronal types

Angeliza Querubin

June 2013

A thesis submitted for the degree of Doctor of Philosophy of The Australian National University

To all the animals used in research: Without them this research would not have been possible.

Acknowledgements

Firstly, my utmost and sincerest thanks go to my three supervisors who I greatly admire and respect and to whom I am forever grateful. Firstly, my immense gratitude goes to Professor Jan Provis, my Honours supervisor and PhD adviser for taking me as her student back in 2006, opening up a world of opportunities, and for taking the time to help me with the final revisions of my thesis. Many thanks to my PhD supervisor, Dr Keely Bumsted O'Brien, for giving me the opportunity to conduct scientific research under her guidance and support, checking my work and giving useful advice. I also want to thank Dr Brendan O'Brien for sharing his knowledge and expertise and opening up my way of thinking about science, as well as giving good advice.

I am grateful for the advice that Dr Riccardo Natoli has provided during my PhD and honours years. His advice in regards to the final revisions and addressing the reviewers' comments on my thesis was very helpful and encouraging.

I am very grateful to Dr Lauren Marotte for allowing me to use her lab and equipment to do my experiments. I will not forget her generosity and assistance.

I am extremely grateful to Dr Spencer Whitney and his lab members for allowing me to use their gene gun equipment to do my experiments. Without their help, I would not have had obtained the data for my thesis.

Many thanks to Dr Krisztina Valter-Kocsi for allowing me to work with her and demonstrate in her course. It was a great pleasure and honour to work with her.

Sincere thanks to Professor Bill Stell for providing suggestions, advice on data analysis and sharing his knowledge to me. Bill has been very supportive and helpful during my PhD candidature and after my thesis submission.

I cannot forget Professor Jonathan Stone for providing his words of encouragement when I expressed my desire to do a PhD.

Thanks to the financial support, generous scholarship and student travel funding provided by the ARC Centre of Excellence in Vision Science. They have made it possible for me to attend and present at conferences and meetings and conduct research.

My sincerest thanks goes to all the lab staff members and students in the Provis lab and O'Brien lab in particular to Hie Rin Lee, Peter Kozulin, Owen Carr, Ray Wong, Matt Rutar, Rizalyn Albaraccin and Alex Hadjinicolaou.

I want to thank my family, especially my mother, Zenaida Querubin, who have all supported and loved me. Thanks to my aunties, Sr Lydia Marave and Sr Angelita Marave for their support, encouragement and prayers.

Big thanks to my best friend Ms Daria Sigma for her help in proofreading my thesis and looking after me throughout my PhD candidature. To my wonderful girlfriend, Ms Rebecca Press, I thank you for all your love, support and advice in writing the thesis and sharing your knowledge with me.

Abstract

The three studies presented in this thesis were conducted to advance our understanding of the retinal circuitry that contributes to processing high visual acuity in the pigeon. In the first study, the topographic density changes and degree of photoreceptor (PR) to retinal ganglion cell (RGC) convergence in the pigeon retina was determined. DAPI or Propidium iodide labelled PRs and RGCs were counted in the retina. Rod density was quantified by counting anti-rod opsin stained outer segments. The fovea and the red field contained significantly higher cone and RGC densities compared with the yellow field. Rods were missing from the fovea, but not in the red field, which suggests that a rod circuitry may be present in this area. The ratio of cones to RGCs was lower in both the fovea and red field, which is consistent with the higher visual acuities that have been reported in these regions.

The second study classified the types of DiO-labelled bipolar cells in the fovea, central red and yellow fields. Eight bipolar cell types were classified in the retina using a modification of Mariani's (1987) classification scheme. Eight BC types (B1 – B8) had similar dendritic morphology as the ones described by Mariani. Two bipolar cell types, B7 and B8, had comparatively smaller dendritic fields than the other types. It was estimated to receive input from possibly one photoreceptor in the fovea and the central red field. Based on the small dendritic field size, B7 and B8 may be good candidates for being the midget-like BCs in the pigeon retina.

The third study classified the RGC groups in the pigeon retina. Classification of RGCs labelled with DiI/DiO in the pigeon retina was based on the dendritic stratification pattern in the inner plexiform layer (IPL). Five morphological RGC groups were identified, the unstratified, monostratified, bistratified, tristratified and tetrastratified. The unstratified group was characterised by vertically oriented dendrites

occupying a thick portion of the IPL, whereas the other groups had horizontally oriented dendrites stratifying at narrow portion of the IPL. The unstratified RGC had the narrowest dendritic field (diameter ~ 18.5 μm). Based on the unstratified RGC's dendritic field size, it is a good candidate for a 'midget-like' RGC in the pigeon retina. However, it has a different morphology from the primate midget RGC. Further work is required to determine the physiology and differential distribution of the different types of bipolar and ganglion cells in the pigeon retina.

Table of Contents

Abbreviations

AD – *area dorsalis*

ANU – Australian National University

ATP – Adenosine triphosphate

BC – bipolar cell

DAPI - 4',6-Diamidino-2-Phenylindole

DB – diffuse bipolar cell

DMEM – Dulbecco's Modified Eagle Medium

ERG – electroretinogram

F – fovea

GCL – ganglion cell layer

INL – inner nuclear layer

IPL – inner plexiform layer

LGN – lateral geniculate nucleus

LWS – long wavelength sensitive

MA – monoamine-accumulating

MSP – microspectrophotometry

MWS – medium wavelength sensitive

nBOR – nucleus of the basal optic root

NFL – nerve fibre layer

NSW – New South Wales

OCT – Optimal Cutting Temperature

OD – optic disc

ONL – outer nuclear layer

OPL – outer plexiform layer

PBS – phosphate buffered saline

PI – Propidium iodide

PND – posterior nodal distance

PKC – protein kinase C

PR – photoreceptor

RF – red field

RGC – retinal ganglion cell

RPE – retinal pigment epithelium

SD – standard deviation

SEM – standard error of mean

SWS – short wavelength sensitive

UV – ultraviolet

YF – yellow field

Chapter 1 - Introduction

1.1 Introduction

The pigeon has been known to have a range of visual abilities, and these permit the bird to survive and perform various activities essential to its lifestyle. One of its most intriguing aspects of its visual capabilities is its good visual acuity or the ability to resolve fine detail. Although the pigeon's visual system has long been the subject of research to help us understand how this bird is able to achieve such good visual acuity, there has been little focus on examining the anatomy of the retinal circuitry subserving high visual acuity.

A number of studies since Cajal's (1889; 1972) anatomical study of the avian retina have revealed some of the various types and distribution of a few neuronal classes in the pigeon retina. Previous research have shown that there are two specialized areas in the pigeon retina, the fovea and the *area dorsalis,* which are densely populated by neurons in three nuclear layers of the retina (Galifret, 1968; Binggeli and Paule, 1969). Some of the types of neurons in these layers, such as photoreceptors, bipolar cells and a few retinal ganglion cells (RGCs), have been morphologically characterised (Mariani and Leure-Dupree, 1978; Lockhart, 1979; Hayes and Holden, 1980; Mariani, 1982; Hayes and Holden, 1983; Mariani, 1983b; Hayes, 1984; Mariani, 1987; Bowmaker et al., 1997). However, many more neuronal types, particularly RGC types in the ganglion cell layer, have not been classified and comparatively analysed in detail in terms of its density, distribution, and interconnectivity with each other at different retinal locations using recent more rapid techniques for neuronal labelling. Such knowledge is vital in order to begin to understand the mechanism in which the retina processes visual information and contributes to mediating high visual acuity.

Since both the pigeon and the primate retinas contain a fovea (Polyak, 1941; Walls, 1942; Galifret, 1968), the question of whether the pigeon retina features a midget

circuitry similar to the primate has been raised. The midget circuitry comprises a midget ganglion cell receiving input from only one cone photoreceptor via a midget bipolar cell in the primate fovea (Polyak, 1941; Boycott and Dowling, 1969; Kolb, 1970). A few investigators identified candidate 'midget-like' bipolar and RGCs in the pigeon retina (Lockhart, 1979; Mariani, 1987), but as Lockhart pointed out, the Golgi-impregnation methods used to identify these neurons may be selective and not random. Because not all the bipolar cell and RGC types across the retina have been classified, the difference between the midget-like neurons and other bipolar cell and RGC types in all areas of the retina remains poorly understood.

Therefore, this thesis aims to examine at the anatomical level the retinal circuitry in the two high cell density areas that may contribute to the ability to process high spatial visual stimuli - the fovea and the *area dorsalis*/red field. It also aims to investigate the potential existence of a midget circuitry in the pigeon retina. To achieve these aims, three studies were conducted using modern approaches that examine the types and distribution of photoreceptors, bipolar cells and RGCs. The aims of the first study were to determine the density of cone and rod photoreceptors, and estimate the amount of cone photoreceptor to RGC information convergence in the pigeon retina, and find a correlation with visual acuity (Chapter 3). The second study aimed to classify the different bipolar cell types in the pigeon retina and find a candidate midget-like bipolar cell (Chapter 4). The aims of the third study were to classify the different groups of RGCs, and to identify the best candidate midget-like RGC type (Chapter 5). Knowledge of the different neuronal types will shed light on the neuronal organization and circuitry of the pigeon retina and lead to a better understanding of how the avian retina processes various forms of visual information.

This thesis is set out in the following manner. The Chapter 2 reviews the literature documenting the current knowledge about the avian and mammalian retinas, and the factors that contribute to visual acuity at the retinal level. The methods used in the three studies are described in detail in Chapters 3 – 5. Chapter 3 compares the densities and the distribution of cone and rod photoreceptors and RGCs in the pigeon retina. It highlights the differences and similarities in photoreceptor and RGC distribution between the fovea and the *area dorsalis*. Estimates of photoreceptor to RGC convergence ratios in the retina indicate that the fovea and the *area dorsalis* have significantly lower convergence compared with the peripheral retina. Photoreceptors, however, send the information to RGCs through the bipolar cells, therefore it is vital to know the different bipolar cell types. The morphological characteristics of the different bipolar cell types are presented in Chapter 4. Then, using the dendritic and axon dimensions, the convergence ratios between the photoreceptors and bipolar cells were estimated. The estimates suggest that a bipolar cell type may possibly receive input from one photoreceptor in the fovea and central red field. Based on the morphology, two bipolar cell types are put forward as likely candidates for being the 'midget-like' bipolar cells in the pigeon retina. In Chapter 5, RGC groups were classified based on the dendritic stratification pattern. A likely midget-like RGC candidate is proposed based on its relative dendritic field size. The conclusions are drawn together in Chapter 6.

Chapter 2 - Literature Review

2. Literature Review

2.1 Introduction

Visual processing starts in the retina, a neuron-rich tissue lining the interior chamber of the eye. The avian retina, like that of many vertebrate animals, is a highly structured nervous tissue consisting of various types of neurons with distinct physiological and morphological properties. Our knowledge of the neuronal population in the avian retina has grown since Cajal's (1889; 1972) pioneering studies into various avian species, yet it is still incomplete. Despite the long recognition of the wide range of visual abilities the bird can achieve, the mechanism involved in processing visual information in the retina is far from being completely understood. Over the past fifty years, the pigeon has been the species of most interest for investigating the anatomy and function of the avian retina. These investigations have been attempts to understand this part of the visual system's contribution to mediating high visual acuity and other forms of visual information. The initial step to gain this understanding requires knowledge of the different types of neurons in the retina, their interconnectivity with each other and their distribution. Therefore, this chapter will begin with a review of the literature on the neuronal architecture of the avian retina and compare features of the retina between avian species, particularly in relation to the pigeon. After the avian retinal structure has been considered, I will review the methods used to characterise the bipolar cell and RGC types in the mammalian retina, as well as the factors contributing to high visual acuity based on numerous studies of the mammalian retina.

2.2 The pigeon retina

A cross-section of the pigeon retina reveals the neurons organized into several layers (Fig. 2.1). The pigeon retina has all the basic vertebrate retinal layers: the retinal pigment epithelium (RPE) and the neural retina. Light travelling through the retina first encounters the nerve fibre layer and must pass through the ganglion cell layer (GCL), inner plexiform layer (IPL), inner nuclear layer (INL), outer plexiform layer (OPL) and outer nuclear layer (ONL) before it reaches the outer segments of the photoreceptors. Through a series of chemical transduction events that are initiated in the outer segments, light is converted into an electrical signal that is then transmitted from the photoreceptors to the bipolar cells in the INL and onto the RGCs in the GCL. RGC axons from the retina exit via the optic nerve on its way to the brain where they terminate and synapse with other neurons.

The thickness of the retinal layers changes across the retina from relatively thin in the far periphery (also termed the yellow field) to a thicker section in the central and dorsal regions. For instance, the total thickness of the pigeon retina near the ora serrata is about 180 μm, while in the parafovea it increases to 290 μm (Hayes, 1982; Querubin et al., 2009). The central and dorsal regions of the pigeon retina have thicker layers because the density of cells in these areas is significantly higher compared with the periphery (Galifret, 1968; Binggeli and Paule, 1969; Hayes, 1983; Querubin *et al*., 2009). The INL is about 11 nuclei thick in the dorsal area of the retina and 18 rows of nuclei in the parafovea, while in the periphery the thickness decreases to about 5 nuclei (Hayes, 1982; Querubin et al., 2009).

The pigeon retina has a few prominent features. The central and dorsal areas of the pigeon retina contain two specializations characterised by increased densities of photoreceptors, cells in the INL, and RGCs (Galifret, 1968; Binggeli and Paule, 1969;

Hayes, 1983; Querubin *et al*., 2009). The central specialized area is where the fovea is located, characterised by a depression on the surface of the retina. In the dorsal retina, the second area with high cell densities, termed the *area dorsalis*, lacks a depression (Galifret, 1968; Querubin *et al*., 2009).

Another interesting feature is that the dorsal and ventral part of the pigeon retina can be distinguished by the colour of the oil droplets present in the cone photoreceptors (Walls, 1942; Mariani & Leure-Dupree, 1978; Querubin *et al*., 2009). The dorsal retina has an abundant population of cone photoreceptors containing red oil droplets and is thus called the red field or red area (Fig. 2.2). Surrounding the red field, extending to the peripheral edges of the retina, is the yellow field, where the majority of oil droplets are yellow or green in colour (Fig. 2.2). Within the central yellow field lies the central fovea. It is located on the nasal side of the optic nerve head.

One of the most intriguing aspects of the avian retina is the lack of vascularization. The source of oxygen and nutrients for the metabolically active retina is mainly from the choroid, which is thicker in birds than in mammals (Meyer, 1977). The pecten has been implicated as the secondary provider of nutrition and oxygen to the retina (Walls, 1942; Wingstrand and Munk, 1965). There is some evidence to support this theory, including the discovery of a network of capillaries within the pecten (Mihalkovics, 1873; Mann, 1924; Jasiński, 1973; Meyer, 1977), and retinal degeneration following removal of arterial blood supply to the pecten (Wingstrand & Munk, 1965).

2.3 Retinal Neurons

Upon light-induced chemical changes occurring in the photoreceptor, the chemical and electrical signals are sent to the interneurons located in the INL. Before

the RGC receives these signals, initiated in the photoreceptors, these interneurons, namely the bipolar cells, horizontal cells, amacrine cells and interplexiform cells, have modified and processed it using complex mechanisms that are only beginning to be unravelled. The retinal circuitry consists of various types of photoreceptors, bipolar cells, RGCs, horizontal cells, amacrine cells and interplexiform cells. Their interconnectivity has been investigated mainly in the mammalian retina. Therefore, much of the current understanding of the retinal circuitry was based on mammalian studies using various anatomical, immunocytological and physiological techniques.

Several morphological types of neurons have been identified in a number of avian retinas, although only a few types have been characterised in the pigeon retina. The photoreceptor types in birds are the most well-characterised. Various methods have been used to study the neuronal morphology and distribution of several types in the avian retina with some advantages and disadvantages. In earlier years, before immunohistochemistry became a common tool for specifically marking cell types in the nervous system, identification had relied mainly on morphological analysis of Golgi-impregnated neurons.

Photoreceptors

Retinal photoreceptors are light-sensitive neurons responsible for converting light into electrical signals. The basic structure of the photoreceptor consists of an outer segment, inner segment, cell body and axon terminal. The photoreceptor is oriented in such a way that the tips of the outer segment lie adjacent to the RPE. Its axon terminal can terminate in any of the three sublayers of the OPL – the outer, intermediate or inner sublaminas. At the OPL, photoreceptors communicate with the bipolar and horizontal

cells. Photoreceptors have been characterised in terms of their structure, morphology, opsin and oil droplet content, and topographical distribution.

Two types of photoreceptors are generally present in vertebrates, the rod and cone photoreceptors. The rod photoreceptor subserves dim light or night-time vision, while cones function in bright light or daytime vision. Studies have revealed that the structure and content of rods and cones bear some similarities and differences as will be discussed in the following sections.

Structure of the Photoreceptor

The outer segment of rod and cone photoreceptors consists of stacks of thin membrane discs. The stack of discs in the photoreceptor outer segment has a thin outer membrane that is not continuous with the outer membrane of the inner segment. The disc is composed of a double membrane separated by a very narrow space between the two membranes (Sjöstrand, 1953b; a; De Robertis and Lasansky, 1958). The double membranes are continuous, thus enclosing the narrow space between them.

The apex of the outer segment is ensheathed by RPE microvilli. As part of the normal renewal process of the outer segment, the RPE phagocytose the outer segments, which have been shed from the apex (Young, 1967; Young and Bok, 1969; Ishikawa and Yamada, 1970; Anderson et al., 1978). Newly formed discs migrate from the base of the outer segment to the apex and the cycle of renewal repeats.

In the inner segment, a number of organelles are present. At the distal end (adjacent to the outer segment) of the inner segment, there are numerous mitochondria, which form a dense mass called the ellipsoid (Sjöstrand, 1953a; De Robertis, 1956; De Robertis and Lasansky, 1958). The mitochondria provide ATP molecules to meet the high-energy demands of the photoreceptor. The endoplasmic reticulum is also present in the distal end of the inner segment. The proximal portion of the inner segment contains

the Golgi complex, a portion of the endoplasmic reticulum, dense particles and neuroprotofibrils. The Golgi complex plays an active role in the secretory activities of the cell (De Robertis, 1956; De Robertis and Lasansky, 1958).

A thin connecting non-motile cilium, also termed the connecting cilium, connects the outer and inner segments. The connecting cilium contains a bundle of filaments, which stretches into the outer and inner segments (Sjöstrand, 1953a; De Robertis, 1956).

Morphologically, cones and rods have a number of distinguishing features, including the shape of the cell and the presence of oil droplets. Rods have a relatively large cylindrical outer segment broader than cones and lack oil droplets in their inner segment (Morris and Shorey, 1967; Meyer and May, 1973; Mariani and Leure-Dupree, 1978; Mariani, 1987). In the pigeon retina, rod photoreceptors lack a fine axon fibre separating the soma from the rod spherules (axon terminals). Rod photoreceptors form synaptic terminals in the outermost stratum of the OPL in the pigeon red field (Mariani, 1987). Furthermore, rod photoreceptors in birds contain periodic-acid Schiff (PAS) positive-glycogen bodies (Meyer and May, 1973). In contrast, cone photoreceptors have short, conically shaped outer segments and oil droplets in the inner segments.

Cones can be further subdivided into several morphological types, which differ in shape, oil droplet colour and axon stratification in the OPL (Cajal, 1889; Morris and Shorey, 1967; Cajal, 1972; Meyer and May, 1973). The single cones in the avian retina can be classified as straight or diagonal, terms that refer to the way their axon fibres course through the OPL (Cajal, 1889; 1972; Mariani and Leure-Dupree, 1978). Mariani and Leure-Dupree (1978) identified two subtypes of straight cones in the pigeon red field. Both subtypes of straight cones have somas in the inner half of the ONL, but differ in the level at which their axon terminals stratify in the OPL and the oil droplet

colour. The single straight cone, which terminates in the intermediate sublamina of the OPL, has a red oil droplet, whilst the other one has an orange oil droplet and its axon pedicle lies in the outer sublamina of the OPL. The oblique or diagonal cone photoreceptor is characterised by having a long axon fibre, which bends to one side (Cajal, 1889; 1972). The axon fibre can lie almost horizontally or diagonally in the OPL and its cone pedicle terminates in the innermost sublamina of the OPL (Cajal, 1889; 1972; Mariani and Leure-Dupree, 1978).

In addition to single cones, the avian retina includes double cones. A double cone is composed of an accessory and a principal cone member in close contact with each other. Principal cones differ from accessory cones in the size of the outer segments and nucleus, the length of the axonal fibre and the sublamina in which their axons terminate in the OPL. Of the two members, the principal cone has a larger nucleus (Cajal, 1972). In the pigeon red field, the principal cone have cell bodies in the middle of the ONL, while the accessory cone's soma lies in the outer row (Mariani, 1987). The principal cone's pedicle terminates in the outermost sublamina. The accessory member's pedicle terminates in the outermost sublamina of the OPL also, with its basal processes sometimes terminating in the intermediate and innermost OPL substrata (Mariani, 1987).

Photoreceptor type distribution

The rod and cone photoreceptor distribution in the avian retina differs with retinal location and between diurnal and nocturnal species. Most diurnal birds examined have a cone-dominant retina (Walls, 1942). The Australian cockatoo (*Eolophus roseicapillus*) has single and double cones outnumbering the rod photoreceptors in a ratio of 3:3:1 (Braekevelt and Richardson, 1996). In the chick, Morris (1970) reported that the central retina contained fewer rod photoreceptors (14 %) than double cones (32

%) and single cones (54 %). In the peripheral chick retina, double cones (30 %) occurred less frequently than the rods (33 %) and single cones (37 %). Conversely, Meyer and May (1973) found that the ratio of rods to double cones is about 1:1 and that double cones occur twice as frequently compared to single cones in all areas of the adult chicken retina. The discrepancy in the reported distribution of rod and cone photoreceptors in the chicken retina may be due to the differences in the way the rod and cone photoreceptors were identified and counted by the different investigators. Meyer and May (1973) identified rod photoreceptors by their PAS-positive glycogen body labelling rather than relying on the absence of oil droplets, which Morris (1970) used in her study.

Another factor which may affect the ratio of different types of cones is the bird's age. In the pigeon's dorsal retina, it has been reported that single cone cell density changed minimally over the course of about 15 years (the average domestic pigeon lifespan), while double cones decreased significantly (Hodos et al., 1991). Furthermore, the density of the accessory cone member was greatly reduced in aged pigeons. The reason for the greater loss of double cones than single cones in pigeons is unknown.

While diurnal birds have a predominance of cone photoreceptors in their retinas, nocturnal birds have increased rod photoreceptor density. In the great horned owl retina, rod photoreceptors are more numerous than cones, including in the fovea (Fite and Rosenfield-Wessels, 1975). For birds, the frequency of cones or rods may be an adaptive mechanism to the light environment in which it is most active.

Spectral sensitivity of birds and absorption spectrum of their photoreceptors

The first steps in signal transduction occur in the outer segment of the photoreceptor. The plasma membrane of the outer segment contains light-sensitive visual pigments, which absorb photons of light. Each visual pigment consists of a

chromophore derived from vitamin A and an integral membrane protein called opsin (reviews Yokoyama, 1997; Hart and Hunt, 2007). The animal's spectral sensitivity and colour vision abilities are due to the spectral absorption properties of the visual pigments present in their photoreceptors. The interaction between the chromophore and opsin determines the spectral tuning of the visual pigment. Differences in the amino acid sequence of the opsin result in different maximum absorption profiles, which distinguish various types of cone and rod photoreceptors, as discussed below.

Four classes of cone visual pigments and a single rod pigment are present in most vertebrates. Each pigment has been classified according to the opsin's amino acid sequence and spectral sensitivity as follows: a) SWS1 or UV/violet-sensitive (UVS/VS) cone pigment; b) SWS2 or short wavelength-sensitive (SWS) cone pigment; c) RH1 and RH2 or medium wavelength-sensitive (MWS) pigments; and d) LWS or long-wavelength-sensitive cone pigments (Bowmaker and Hunt, 1999; Hart and Hunt, 2007). The wavelength absorption maxima for the four cone pigments in different bird species are shown in Table 2.1. These pigments show interspecies variation in the wavelength it absorbs.

Spectral sensitivity in different retinal regions

It has been studied to determine whether local regions of the pigeon retina are more sensitive to certain wavelengths using psychometric and electrophysiological methods. Spectral sensitivity refers to the maximum response of a particular retinal region to a specific wavelength stimulus measured by ERG. When wavelengths ranging between 580 and 600 nm and between 400 and 440 nm were presented to an unrestrained, freely moving pigeon's visual field, the pigeon responded correctly according to psychometric analysis (Romeskie and Yager, 1976). Romeskie and Yager (1976) thought that the red field was stimulated during the experiment. However,

because the pigeon may be turning its head during this experiment, it is unclear whether the red field or fovea was stimulated by the different wavelengths.

In other studies, the pigeon's red or yellow field was exclusively stimulated in anaesthetized non-moving pigeons, and the ERG responses were recorded. The studies showed that the yellow field was more sensitive to wavelengths between 450 and 550 nm compared with the red field (Wortel et al., 1984; Remy and Emmerton, 1989). The difference between the two regions is perhaps due to the composition of the cone classes in different regions of the retina. It has been found by MSP analysis that two oil-droplet types, located in the dorsal part of the pigeon retina, transmit light at longer wavelengths than those in the ventral part (Bowmaker, 1977; Bowmaker et al., 1997). This may partly explain the difference in the spectral sensitivities between the red and yellow fields, although other mechanisms involved are yet to be investigated.

Types of oil droplets

There are several types of oil droplets in the avian retina. Each type is distinguished by the colour, which varies between avian species. In the chicken and Japanese quail retina, five types of oil droplets based on their colour were identified: red, yellow, pale-green, pale-blue, and clear (Oishi et al., 1990). The clear oil droplet fluoresces intensely while the pale-green oil exhibits weak fluorescence under UV light. The five types of oil droplets found in the pigeon retina are slightly different, consisting of red, orange, yellow, yellow-green and colourless (Mariani and Leure-Dupree, 1978). Using MSP analysis, oil droplets have been classified into five types: red (R), yellow (Y), pale (P), clear (C), transparent (T). Each has a distinct absorbance cut-off wavelength and slight inter-species variation as summarized in Table 2.2.

The different types of oil droplets were found to be associated with a particular type of cone visual pigment. In the budgerigar, zebra finch, pigeon and chicken, the R-

type oil droplet was found in the LWS pigment, the Y-type droplet with the pigment MWS, C-type with the SWS, and the T-type with the UV or violet pigment (Bowmaker *et al*., 1997). The P-type oil droplet is present only in the principal cone member of the double cones which both contain the LWS pigment. The accessory cone rarely contains an oil droplet in the budgerigar, zebra finch, and pigeon, but it has been observed that the chicken retina has a small oil droplet (Bowmaker *et al*., 1997).

Each oil droplet is distributed in the retina in various frequencies. The presence or absence of particular oil droplets also varies between species. In the duck retina, the Y, P, C/T-type oil droplets occur in frequencies of about 24%, 50% and 5% respectively (Jane & Bowmaker, 1988). The penguin retina has a different distribution of oil droplet types where the pale and the yellow account for 70% of the total cone population (Bowmaker & Martin, 1985). While red oil droplets in the duck occur at 21% of the total cone population, none were reported in the penguin. In the pigeon retina, the red and orange oil droplets are predominantly present in the dorsal red field and the fovea (Mariani and Leure-Dupree, 1978).

Oil droplets in cone photoreceptors act as wavelength filters for incident light before it encounters the visual pigments. Above a certain cut-off wavelength threshold, the oil droplets transmit light of longer wavelengths, but shorter wavelength light that is below the cut-off point are absorbed by the oil droplet. Certain types of oil droplets were found to exhibit different cutoff wavelengths depending on the location of retina. The Y-type oil droplet in the dorsal pigeon retina has a cut off wavelength at about 539 nm, while in the ventral retina it is about 513 nm (Bowmaker *et al*., 1997). A similar regional difference in the cut off wavelength was observed for the R-type oil droplet in the pigeon retina. The R-type's cutoff wavelength in the dorsal retina was shifted to longer wavelengths compared with the ventral retina. It is unclear what the functional

significance of such differential absorption profiles of the Y and R-type oil droplets in the different regions of the pigeon retina.

Because the wavelengths transmitted through the oil droplets are longer than the visual pigment's maximum wavelength sensitivity, the maximum sensitivity of the cone photoreceptor is displaced towards longer wavelengths that the oil droplets allow. For instance, a cone containing the R-type oil droplet that has a cut-off wavelength at about 570 nm associated with a LWS visual pigment (λ_{max} = 567 nm), will displace the maximum sensitivity to about 600 – 620 nm (Bowmaker *et al*., 1997). Similarly, the Y-type oil droplet acts by displacing the sensitivity of cone photoreceptors to longer wavelengths. Other types of oil droplets, the C- and T-type, have a function that is yet to be clearly understood. Bowmaker *et al.* (1997) suggest that the C-type oil droplet may either narrow or broaden the sensitivity of SWS cone photoreceptors.

Bipolar cells

A number of bipolar cells have been classified morphologically in the avian retina. Cajal (1972) grouped the avian retinal bipolar cells into two groups: (1) the outer bipolar cells, which lie below the outer plexiform layer, and (2) the inner or small bipolar cells, which occupy the remainder of the bipolar cell layer.

The outer bipolar cell has a fully developed, very extensive dendritic arbour that appears to originate from the cell body. No Landolt's club was observed for the outer bipolar cell (Cajal, 1972). The axon terminal arborizations of the large or outer bipolar cells occur preferentially in the fifth sublayer of the IPL.

Unlike the outer bipolar cell, the inner bipolar cell has a long ascending fibre extending from the cell body, and from this ascending fibre, the dendrites branch into a small number of horizontally-oriented fibrils which lie on one of the three concentric

strata of the outer plexiform layer (Cajal, 1972). The axon of the small bipolars often sends out collateral branches at various sublayers of the IPL. The axon branches end with varicose ramifications or sometimes stratify at two different sublaminas in the IPL. Most axon processes extend their terminal arbourizations in between the fourth and fifth sublayers of the IPL.

In later studies, the classification of bipolar cells included more parameters, which yielded more bipolar cell types than Cajal's classification scheme. Seven bipolar cells types in the chicken (Quesada et al., 1988) and eight types in the pigeon red field have been reported (Mariani, 1987). In both studies, the bipolar cells were classified based on the presence of Landolt's club, shape and pattern of the dendritic tree, dendritic field size, and the location of the soma in the INL. However, axonal stratification level and number of axon branching was not included in the classification criteria for the chicken bipolar cells due to the high variation and lack of correlation between dendritic and axonal branching pattern. Nevertheless, a few bipolar cell types share similarities between the chicken, pigeon and primate retinas. According to Quesada and co-investigators (1988), the B1 ascending bipolar cell in the chicken retina resembles that of the B2, B6 and B7 of the pigeon retina. The chicken retina's B2 bipolar cell corresponds with Mariani's (1987) B3 cell type and with the primate flat bipolar cell type. Other bipolar cell types in the chicken retina did not show similarities with the pigeon bipolar cell types. Quesada and co-investigators compared the B1 bipolar cell of the chicken retina with the rod bipolar cell of the primate retina. However, care should be taken in interpreting this comparison. The chicken B1 and primate rod bipolar cells differ markedly in that the primate rod bipolar has a bushier dendritic arbour, while the chicken B1 is comparatively sparser. The numerous dendritic processes of the primate rod bipolar cell reflect the greater density of rod photoreceptors

in the primate peripheral retina. If the chicken's B1 bipolar cell connects with rod photoreceptors, the sparser dendritic processes may be a reflection of the lower density of rod photoreceptors in the chicken retina. It is yet to be investigated which types of photoreceptors provide input into each bipolar cell type in the avian retina.

Retinal ganglion cells (RGCs)

RGCs are the final output neurons that transmit different aspects of the visual scene to the brain. Cajal considered the avian retina the most complicated with respect to the structure of the IPL and the morphology of the spongioblasts and ganglion cells. Cajal (1972) divided the avian ganglion cells into single-layered and multi-layered cells, which refer to the number of dendritic stratifications it made in the IPL. Within the single-layered group, four types of ganglion cells were observed most frequently in the retina of the gallinaceous birds: (1) giant pyriform cells which form a very gnarled, flat arbourization at the level of the first sublayer; (2) middle-sized pyriform cells which form a varicose terminal arbourization in the second sublayer; (3) middle-sized multipolar cells which form a fine arbourization in the second sublayer; and (4) small pyriform cells whose granular and extremely dense arbourization lies within the fourth sublayer of the IPL (Cajal, 1972). Cajal also found these small pyriform cells in the sparrow, which despite their delicate, compact terminal arbourization, stratify in the third IPL sublayer. Cajal believed that the fine dendritic arbourizations occur in each of the five IPL sublayers originating from either single-layered or multi-layered cells.

Three types of ganglion cells were most frequently observed which belonged to the multi-layered group: (1) multipolar cells which furnish horizontal dendritic arbours to three IPL sublayers, namely to the second, third and fourth; (2) smaller multipolar cells with two horizontal dendritic arbours – a thicker arbour stratifying in the outer part

of the fifth IPL sublayer and the other stratifying in the third IPL sublayer; and (3) small multipolar cells which form three horizontal dendritic arbours stratifying in the second, fourth and fifth IPL sublayers (Cajal, 1972).

Cajal (1972) also found several odd types of multi-layered ganglion cells in the chaffinch and green finch: (1) cells whose ascending and singular process forms three very delicate dendritic arbours stratifying in the second, below the third and fourth IPL sublayers; (2) cells whose ascending trunk divides gradually and form two fine dendritic arbours stratifying in the second and fourth sublayers; (3) cells with three dendritic arbours stratifying in the first, third and below the fourth sublayers.

RGCs in the pigeon, chick and quail retina have been classified by a number of more recent investigators (Budnik et al., 1984; Ikushima et al., 1986; Thanos et al., 1992; Chen and Naito, 1999; Naito and Chen, 2004b). Given the diversity in the dendritic morphology and multi-stratification pattern of RGCs in birds, authors were unable to provide a complete classification of the entire RGC population. Hayes and Holden (1980) classified RGCs in the pigeon retina according to soma size. In the chicken retina, Thanos and co-investigators (1992) classified eight morphological groups based on the dendritic field size and dendritic density and also the levels in which the dendrites ramify in the IPL. Chen and Naito (1999) and Naito and Chen (2004a) used a different classification scheme and reported only four groups (Group I – IV) of RGCs. These were distinguished based on the different clusters on the scatter graph of dendritic field and soma sizes and eccentricity from the *area centralis*. The groups I – II were further subdivided into complex (c) and simple (s), which refer to the density of the dendritic branching pattern (Chen and Naito, 1999; Naito and Chen, 2004a). The complex subgroup of RGCs was characterised by highly branched dendritic patterns while the simple subgroup was sparsely branched. A slightly different

classification system was used in the quail where RGCs fell into seven types (Types I – VII) according to soma size, shape and location, and dendritic arborization pattern (Ikushima et al., 1986). Ikushima *et al*. (1986) included displaced RGCs (Types VI and VII) located in the INL in their classification. Despite the difference in the classification scheme between the chicken and quail, Naito and Chen (2004) compared their RGC groups to Ikushima and colleagues' (1986) types and found that a few types shared similarities: ie, chicken RGC groups Is corresponded to the quail type I; chicken group IIc with the quail types II and III; and chicken group IIIs with the quail types IV and V. A correlation between the two classified chicken RGC grouping of Naito and Chen (2004) and Thanos and co-investigators (1992) was also reported. Regardless of the classification scheme, it is possible that the same RGC types are present across different avian species, including the pigeon retina. However, the different morphological RGC types have not been previously classified in a similar way in the pigeon retina.

RGC organization in the retina in relation to visual processing

The organization of each RGC type in the retina has been hypothesized to be distributed in such a way that the dendritic fields of each type completely covers the entire retina (Wässle and Boycott, 1991). If a spot of light falls on a spot on the retina, would every type of ganglion cell be under that illumination? A homogeneous coverage by each type would allow every point in the visual field to be simultaneously analysed with respect to its contrast, colour, movement and resolution. Complete coverage of the retina has only been demonstrated for a few RGCs using methods that stain the entire cell and provide detailed analysis of their morphology and quantity. For alpha cells in the cat retina, it has been found that each subpopulation of ON- and OFF-alpha cells form a regular mosaic with their somas and uniformly tile the retina with their dendritic fields (Wassle et al., 1981). It has been shown in the cat retina that a type of RGC called

monoamine-accumulating (MA) provides uniform coverage. To determine whether the MA cells provide uniform coverage in the retina, the extent of the dendritic overlap of adjacent filled MA cells was examined and it was calculated that a coverage factor of 2.2 was maintained from central to peripheral retina (Dacey, 1989). The evidence suggests that different RGC types tile the retina, although it is still yet to be confirmed for the other types.

Displaced ganglion cells

Displaced ganglion cells, whose cell bodies lie in the inner margin of the INL, are a common feature of the avian retina. These cells are the sole source of retinal projection onto the accessory optic system, the nucleus of the basal optic root (nBOR) (Karten et al., 1977; Fite et al., 1981). The distribution of displaced ganglion cells in the pigeon retina is reported to be concentrated in the central and temporal yellow field with highest densities found in the most peripheral region (Fite et al., 1981; Hayes and Holden, 1983). Displaced ganglion cells in the pigeon retina were found at much lower densities in the red field and fovea. This supports the hypothesis that displaced ganglion cells are involved in initiating rapid oculomotor responses to peripheral moving stimuli (Brecha and Karten, 1979).

The thalamofugal and tectofugal pathways

These two visual pathways are implicated in playing a role in high visual acuity functions in the avian system. Other visual pathways present in birds include the accessory optic system (see Simpson 1984 for review) and the retinohypothalamic system (Bons, 1976); however, they are not reviewed here because they have not been implicated in high visual acuity.

The thalamofugal and tectofugal are two parallel visual pathways that carry axon projections from the retina to the telencephalon in birds. The two pathways differ in

their target regions within the telencephalon. The thalamofugal pathway, carries retinal projections to the thalamus and then to the telencephalon (Meier et al., 1974), and is analogous to the mammalian geniculostriate pathway (Shimizu and Karten, 1993). The tectofugal pathway sends retinal projections to the optic tectum and to the nucleus rotundus in the thalamus and then to the telencephalon (Karten and Revzin, 1966; Revzin and Karten, 1967). This pathway is similar to the colliculo-thalamo-cortical pathway in mammals. In birds, the target projection of the thalamofugal pathway in the telencephalon is the visual Wulst, while the tectofugal pathway's target is the ectostriatum (or entopallium, as the new nomenclature names this area (Reiner et al., 2004)).

In addition, the retinal location of the RGCs that project to the thalamus differs from those that relay to the tectum, depending on the placement of the eye and the degree of binocular vision of the bird. In the owl, which has frontally placed eyes, the thalamus receives its retinal input largely from the temporal side of the optic nerve head, especially from the fovea (Pettigrew, 1979; Bravo and Pettigrew, 1981). The owl's optic tectum receives retinal input from RGCs in the horizontal elongated streak including the fovea (Bravo & Pettigrew, 1981). In birds with laterally placed eyes, such as the pigeon, the thalamus receives the axon terminals of RGCs from the yellow field with higher numbers from the nasal region and much fewer from the red field and temporal yellow field (Remy and Güntürkün, 1991; Miceli et al., 2006). Conversely, a much higher number of RGCs from the pigeon red field was found to project to the tectum. Furthermore, the pigeon's retinal projections onto optic tectum are topographically organized. The nasal and temporal RGCs project to the posterior and anterior tectum respectively, while the inferior and superior retina project to the dorsal and ventral tectum (Remy and Güntürkün, 1991).

It has been hypothesized that the pathway from the temporal retina to the thalamus is important for establishing binocular convergence in owls. In support of this hypothesis is the demonstration of neurons in the visual Wulst responsive to binocular disparity (Pettigrew and Konishi, 1976). In pigeons, however, there are a low number of RGC axons from the temporal retina projecting to the thalamus. Therefore, the thalamofugal pathway in pigeons may not be involved in binocular processing to the same extent as in frontal-eyed species, but may be involved in the visual detection of objects in the lateral field of view (Güntürkün et al., 1993).

The thalamofugal pathway has been implicated in processing high visual acuity based on the electrophysiological recordings from the thalamus and Wulst of pigeons consisting of neurons with small receptive fields (Revzin, 1969; Jassik-Gerschenfeld et al., 1976). It is likely that the thalamofugal pathway also processes high visual acuity in raptors given that it receives large retinal input from the fovea (Bravo & Pettigrew, 1981). The tectofugal pathway is involved in motion detection and directional selectivity based on electrophysiological recordings in the tectum demonstrating large number of neurons exhibiting these properties (Jassik-Gerschenfeld and Guichard, 1972). Given the receptive field sizes of the tectal neurons range from small to large, it is possible that certain areas in the tectum may also be involved in processing high visual acuity.

The thalamus and tectum receive different RGC types. The size of the RGCs that innervate these regions is variable. In the owl, the RGCs innervating the tectum were heterogeneous in size consisting of small and large RGCs, while those that project to the thalamus were homogenous and had uniform morphology ranging in the medium to large size (Bravo & Pettigrew, 1981). In the pigeon, RGCs projecting to the thalamus were larger compared with the cells innervating the tectum (Remy and Güntürkün,

1991). Secondly, it has been demonstrated that the thalamus receives different proportions of distinct RGC types compared with the tectum. DiI application into the dorsal anterior thalamus labelled RGC groups IIc, IIs, and IIIs (Chen and Naito, 2009). An injection of DiI into the tectum labelled all the groups, but group Ic (52.6%) was the most frequently labelled group, followed by group IIc (27.1%), Is (6%), IVc (6%), IIs (4.5%), and IIIs (3.8%) (Chen & Naito, 2009).

Horizontal cells

Horizontal cells are located in the outer retina where they make lateral synaptic contacts with photoreceptors and modify the physiology of photoreceptors and bipolar cells (Perlman et al., 2007).

Avian horizontal cells have been classified based on their morphological and immunocytochemical characteristics. Cajal (1889) classified avian horizontal cells into two types, the brush-shaped and the stellate cells. Both types have an axonal process that runs along the outer portion of the INL beneath the OPL and terminates in an arbour in the OPL. In contrast, Gallego (1975) reported only a single type of horizontal cell with an axon in both diurnal and nocturnal bird species. Mariani (1987) reported two main horizontal cell types in the pigeon retina, one bearing an axon termed H1, the other an axon-less type. The horizontal cell type without an axon was subdivided into three further types, H2-H4. The H1 horizontal cell type has the narrowest dendritic field, then H2, H3, and H4 has the broadest. The four horizontal types can be further classified according to differential immunoreactivity to markers such as calretinin, trkA, GABA, islet-1, Lim 1 + 2, prox1, AP2α, and Pax6 (Fischer et al., 2007). The use of immunolabelling horizontal cells may be useful for future studies of its differential distribution and coverage in the avian retina.

Amacrine cells

Cajal (1889) identified two groups of amacrine cells in the bird retina, the diffuse and the stratified. These cells differ in the pattern of their processes and the level in which the processes stratify. The processes of the diffuse amacrine cell group ramified in several layers of the IPL, and had long delicate processes with short branches and varicosities. The stratified amacrine cells were categorized into five types according to IPL stratification, amacrine cells of the first, second, third, fourth and fifth sublayers (Cajal, 1889). Mariani (1982) classified the amacrine cells in the pigeon retina into two distinct classes. Class I amacrine cells are characterised by lack of an axon and radially spread dendrites, and include cells with multiple stratification. Class II amacrine cells have an axon with a short terminal arborization, and typically do not have a radially organized dendritic arbour as seen in the Class I cells. Mariani (1983b) identified another amacrine cell called asymmetric which he thought to be involved in directional selective responses recorded in the pigeon retina, but the electrophysiological properties of this cell class have yet to be studied.

Interplexiform cells

Vertebrate retinas contain interplexiform cells, neurons whose cell body lies in the INL and whose processes extend in both the OPL and IPL (Dowling and Ehinger, 1978; Mariani, 1987). The function of this class of neurons is not well understood, but these cells may provide a centrifugal pathway within the retina, allowing information to flow from the inner to outer plexiform layers (Dowling, 1979). Unlike bipolar cells, interplexiform cells do not synapse with photoreceptors and ganglion cells, but form synaptic connections with horizontal cells and amacrine cells, and rarely with bipolar cells in the goldfish retina (Dowling & Ehinger, 1978). In the pigeon retina, Mariani

(1987) described an interplexiform cell identified by Golgi-impregnation. However, caution should be taken when using the term interplexiform to describe the one found in the pigeon retina by Mariani (1987) as it is very different from those identified by Dowling (1979) and Dowling and Ehinger (1978). The interplexiform cell identified by Dowling (1979) and Dowling and Ehinger (1978) has its cell body in the innermost part of the INL among the amacrine cells, while the one Mariani found has a cell body that may be in the middle or outer part of the INL. Further investigation is required to confirm whether an avian interplexiform cell exists by means of immunohistochemical labelling of the dopamine presence and determining its synaptic connections with other retinal neurons.

2.4 Classification of bipolar cell types

Although several neuronal types have been identified in the avian retina, their interneuronal connectivity and physiology are still poorly characterised compared to those in the mammalian retina. In contrast, distinct cell types in the mammalian retina can be distinguished from each other on several aspects, such as dendritic morphology, neuronal synaptic connections, the number of neuronal convergence, and stratification level in the IPL. The following section will be a review of these parameters used to anatomically identify and classify different neuronal types in various species, with a main focus on bipolar cells.

Dendritic morphology of bipolar cells

Bipolar cells can be morphologically classified based on dendritic morphology. A rod bipolar cell's dendritic branching pattern has been described as 'moplike' or

tufted (Polyak, 1941). In primates, the rod bipolar cell was found to have as many as 45 dendritic processes in the OPL (Boycott & Dowling, 1969).

Cone bipolar cells exist in different types. In the primate retina, there are several different types of cone bipolar cells, such as the midget, diffuse, giant bistratified, and the blue-cone (Polyak, 1941; Boycott and Dowling, 1969; Kolb, 1970; Mariani, 1981; 1983a; Mariani, 1984; Boycott and Hopkins, 1991; Boycott and Wässle, 1991; Kolb and Dekorver, 1991; Boycott and Hopkins, 1993; Calkins et al., 1994; Wässle et al., 1994; Calkins et al., 1996; Chan et al., 2001a; Chan et al., 2001b; Kolb and Marshak, 2003). These cone bipolar types have different dendritic morphology. The midget has the smallest dendritic field compared to the diffuse, giant bistratified, and blue-cone bipolar cells. Furthermore, the bipolar cell types can be further classified as either flat or invaginating which refers to the shape of the dendrites in the OPL.

Photoreceptor connectivity with bipolar cells

The number of contacts that a bipolar cell type makes with a photoreceptor has been determined by a number of methods. The bipolar cell's dendritic field size can be used to estimate the amount of cone contact it can receive when compared with the size of the cone pedicle, but is not a direct way of determining the photoreceptor contacts with bipolar cells (Boycott & Dowling, 1969). Another way is to identify the types of cones and bipolar cells using light microscopy of labelled neurons and count the number of cones overlying the dendritic field of the bipolar cell. Using this method, the diffuse bipolar were observed to contact seven (Mariani, 1981) to ten cones in the primate retina (Boycott and Wässle, 1991). A more direct way to determine cone input is to use electron microscopy. Based on electron microscopic studies, the number of cone inputs to a midget bipolar cell ranged from a minimum of 1 to 3 (Kolb & Marshak, 2003),

while approximately 16-20 rods converge onto a rod bipolar cell in the cat retina (Freed et al., 1987a; Sterling et al., 1988a).

Some investigators have reported that rod bipolar cells contact both cone and rod photoreceptors as seen by light microscopy (Polyak, 1941) and by electron microscopy (Dacheux and Raviola, 1986). The rod bipolar cell found in the rabbit retina contacted mostly rod photoreceptors and very few cones (Dacheux & Raviola, 1986). However, others have revealed that only rod photoreceptors contact the rod bipolar cell in the primate retina using neuronal labelling and electron microscopic reconstruction (Boycott and Dowling, 1969; Kolb, 1970; Chan et al., 2001a). The electrophysiological recordings from the rod bipolar cell in the rabbit retina strongly suggest that its light responses were dominated by rod photoreceptors.

Bipolar cell connectivity with RGCs

The ON and OFF bipolar cell and RGC types in the mammalian retina have been shown to stratify in specific sublaminas of the IPL and make synaptic connections. In the cat retina, an OFF cone bipolar cell, also named the flat cone bipolar, synapses with an OFF ganglion cell in sublamina a (also the OFF sublayer, close to the amacrine cell layer) of the IPL (Nelson et al., 1978; Kolb, 1979). Conversely, the investigators have also shown that ON cone bipolar cells, termed the invaginating cone bipolar, made contacts with an ON ganglion cell in sublamina b (inner layer close to GCL). Similar to the cat retina, electron microscopic reconstruction has revealed the synaptic connections between the ON and OFF subtypes of midget bipolar cells and the respective midget RGC subtype at the same sublaminas in the primate retina (Kolb and Dekorver, 1991; Calkins et al., 1994). Although the bipolar cells in these studies have been shown not to make synaptic contacts in the opposite sublaminas (e.g. ON bipolar cell synapses with a

RGC in the OFF sublamina), it has recently been shown that this rule is not always obeyed by other types (Hoshi et al., 2009). Hoshi and co-investigators (2009) have found that ON cone bipolar cells make ribbon synapses as they pass through the OFF sublayer of the IPL in rabbit retinas. Therefore, caution must be observed when inferring the synaptic connections between neuronal types in the IPL based on the co-stratification of the dendritic and axonal processes.

2.5 Morphological RGC classification in the mammalian retina

RGC types in the mammalian retina have been well documented in a number of species including the cat (Boycott and Wässle, 1974; Kolb et al., 1981; Berson et al., 1998; Berson et al., 1999; Isayama et al., 2000), ferret (Isayama et al., 2009), rabbit (Amthor et al., 1983; Amthor et al., 1984a; Amthor et al., 1989b; Amthor et al., 1989a), rat (Sun et al., 2002), mouse (Kong et al., 2005; Coombs et al., 2006), and primates including humans (Dacey and Petersen, 1992; Kolb et al., 1992; Dacey and Lee, 1994; Peterson and Dacey, 1999; Peterson and Dacey, 2000). The classification of RGCs is often based on the dendritic field size, dendritic branching pattern, soma size, dendritic stratification in the IPL. Another way to identify RGC types is to plot the cell's soma or dendritic field size as a function of eccentricity from the *area centralis*, which was how the alpha, beta and gamma cells were categorized in the cat retina (Boycott and Wässle, 1974). The alpha and beta cells have different non-overlapping size ranges at certain eccentricities in the cat retina, with alpha cells being larger compared with the beta cells at any eccentricity. Furthermore, by plotting RGCs' dendritic field size against eccentricity from the *area centralis*, it was revealed that the alpha and beta cell types' dendritic fields increase with greater eccentricity (Boycott and Wässle, 1974; Isayama et

al., 2009). This change in dendritic field size in relation to cell density ensures that the cell provides efficient coverage of the retina.

To determine which parts of the brain a RGC type projects to, a retrograde dye is injected into a specific part of the brain revealing the different morphological RGC types it receives input from. For instance, the primate midget ganglion cell projects to the parvocellular lamina of the lateral geniculate nucleus (LGN) and the parasol ganglion cell project to the magnocellular layer of the LGN (Leventhal et al., 1981; Perry et al., 1984). Three non-midget, non-parasol RGC types were found to send projections to the LGN's koniocellular layer, namely the small-bistratified, sparse and broad thorny (Szmajda et al., 2008). Retrograde injection into a specific lamina in the LGN has allowed investigators to label the RGC type of interest and study its synaptic inputs in the marmoset retina (Percival et al., 2009; Percival et al., 2011).

The distribution of certain RGC types has been shown to be non-uniform across the retina and that specific areas of the retina contain different proportions of various RGC types. In the cat retina, beta cells are predominantly distributed in the *area centralis*, representing about two-thirds of all RGCs, but in the nasal visual streak, beta cells were half as frequent as the other ganglion cells (Stein et al., 1996). Gamma cells comprised only about a third of the RGCs in the *area centralis*, and just under half in the nasal retina (Stein and Berson, 1995). It is thought that the X (or beta) cells' tendency to concentrate in the *area centralis* was because they subserve high acuity visual functions, while the gamma cells or W cells are specialized for 'ambient' vision (Stone, 1983).

2.6 Techniques used to label neurons

Immunohistochemistry labelling of bipolar cells

Certain types of cone and rod bipolar cells have been identified using immunohistochemistry, the most widely used being Protein Kinase C (PKC) (Negishi et al., 1988; Cuenca et al., 1990; Greferath et al., 1990; Kato et al., 1990; Suzuki and Kaneko, 1990; Young and Vaney, 1990; Grünert and Martin, 1991; Müller and Peichl, 1991; Wässle et al., 1991; Zhang and Yeh, 1991; Kolb et al., 1993; Grünert et al., 1994; Koistinaho and Sagar, 1994; Osborne et al., 1994; Euler and Wässle, 1995; Strettoi and Masland, 1995; McCord et al., 1996; Vaquero et al., 1997; Job and Lagnado, 1998; Minami et al., 1998; Caminos et al., 1999; Caminos et al., 2000; Chan et al., 2001a; Fyk-Kolodziej et al., 2002). Eleven isoforms of PKC have been identified α, βI, βII, γ, δ, ε, η, θ, μ, ζ and λ. When immunoreactivity to distinct PKC isoforms was investigated in different species, it was revealed that antibodies against certain isoforms labelled different cell types depending on the animal species. Osborne and collaborators (1994) found that PKCδ antibody labelled Muller cells in rat, rabbit and guinea pig, but the same antibody labelled a subpopulation of RGCs only in the goldfish, and only photoreceptor inner segments in the chick retina. Antibodies against PKCα, PKCβI and PKCζ labelled rod bipolar cells, while cone bipolar cells have been labelled by antibodies against PKCβII in the cat and rabbit retinas (Koistinaho and Sagar, 1994; Fyk-Kolodziej et al., 2002). In the marmoset retina, antibodies against PKCα labels not only rod bipolar cells, but also a population of diffuse 'ON' cone bipolar cells (Chan et al., 2001a). In the macaque retina, antibodies against PKCα, PKCβI and PKCβII labelled rod and cone bipolar cells, some amacrine cells, and occasionally, astrocytes and Muller cells (Grünert and Martin, 1991; Grünert et al., 1994). Antibodies against

PKCε labels both rod and cone bipolar cells, as well as horizontal cells, some types of amacrine cells and RGCs in cat and rat retinas (Koistinaho and Sagar, 1994; Fyk-Kolodziej et al., 2002). Therefore, rod bipolar cells cannot be specifically identified by PKCα antibody labelling alone in certain species without confirming photoreceptor inputs by electron microscopic examination.

Other markers have been used to label different types of cone bipolar cells in the primate retina. However, certain markers do not label the same bipolar cell types depending on the primate species. In the macaque retina, antibodies against CD15 label DB6 cone bipolar cells, while in the marmoset retina, the same antibody labels flat midget bipolar cells in addition to DB6 bipolar cells (Grünert et al., 1994; Chan et al., 2001b; Chan et al., 2001a).

The morphology of the bipolar cells labelled by antibodies against PKCα also revealed interspecies differences. In the chicken and rat retinas, the axon terminals of PKC-like bipolar cells (PKCα-positive rod bipolar cells) are small and 'knob-shaped' (Caminos et al., 2000). In contrast, in goldfish, tench and zebrafish retinas' PKC-like bipolar cells, labelled with the same antibodies, have bulky and large axon terminals. Caminos and collaborators (2000) also reported that the axon terminals of PKC-like bipolar cells never reached the GCL in the chicken, tench, goldfish and zebrafish, but do so in the rat retinas. It would be interesting to find out whether such differences in stratification of PKC-like bipolar cell axon terminal in the IPL represents distinct rod circuitry in different species.

Immunolabelling bipolar cells has allowed detailed analysis of the density of various bipolar cell types at various eccentricities (Martin and Grünert, 1992; Grünert et al., 1994; Massey and Mills, 1996; Chan et al., 2001a; Wässle et al., 2009). Overall, it has been determined that PKC-labelled rod bipolar cells account for approximately 10%

of all bipolar cells in the rabbit retina, reaching its peak in the visual streak (Strettoi and Masland, 1995). In the zebrafish, tench and goldfish, a greater number of PKC-like bipolar cells (rod bipolar cells) in the peripheral retina were observed (Caminos et al., 2000). In the rat retina, rod bipolar cell density, labelled with L7 antibody, was higher in the inferior temporal retina and upper mid-peripheral retina (Euler and Wässle, 1995). This differs from the macaque retina, where the density of rod bipolar cells labelled with antibodies against PKCα increased from the fovea up to 2 mm eccentricity reaching a peak of 13,000 cells/mm^2, and from there the density decreased toward the peripheral retina (Grünert et al., 1994). This trend of rod bipolar density change is similar to that found in the chicken, where the density of PKC-like labelled bipolar cells (rod bipolar cells) were greater in the central retina than the peripheral regions (Caminos et al., 2000). This finding is interesting considering that the chicken and primate retinas have rod-free and cone-rich areas in the *area centralis* and fovea in the central retina.

DiI and DiOlistics labelling

One of the most useful technique for filling neurons to enable morphological examination is DiI labelling. DiI – a lipophilic dye – have been used to fluorescently label various types of neurons, including the horizontal cells, bipolar cells and ganglion cells. Horizontal and bipolar cells were labelled in the goldfish retina by filling micro glass pipette tips with DiI, inserting it into the retina, breaking the pipette tip and leaving it for a few days. The labelled horizontal cells and bipolar cells have been classified in the zebrafish retina using this method (Song et al., 2008; Li et al., 2009; Li et al., 2012). Labelling ganglion cells requires placement of the DiI crystals on the optic nerve and allowing the dye to retrogradely diffuse back to the cell body and the

dendrites. The zebrafish ganglion cells have been classified using this method (Mangrum et al., 2002). By combining DiI labelling with other methods of labelling, it is possible to determine the interconnectivity between different types of neurons in the retina.

Another way of delivering the DiI into the retina is to use a gene gun, called DiOlistics. To do this, micro-tungsten particles are coated with DiI or DiO and delivered to the retina *ex vivo* via a gene gun (Gan et al., 2000; Grutzendler et al., 2003). Upon contacting the cell, the dye diffuses into the cell membrane, thereby staining the cell. Using DiOlistics to fill RGCs in the mouse and rat retinas, four groups based on soma size, dendritic-field size, branching pattern and level of stratification were classified: RG_A, RG_B, RG_C and RG_D (Sun et al., 2002; Sun and He, 2002). Although the DiOlistics technique offers ease in obtaining well-stained cells in a short period of time than other techniques like the Golgi method, there are some disadvantages with the method. According to the authors, the random nature of the sampling method may be affected by the probability of a cell type being stained, which in turn is proportional to the total cross-sectional area of the somas in the entire population. Another potential problem with the DiOlistics technique is that some cells may be understained due to insufficient dye diffusing through the cell membrane, which was said to be difficult to control. Lastly, the DiOlistics technique does not allow analysis of the cell density and percentage of cell populations due to the low number of cells (< 10) labelled in each retina (Sun and He, 2002; Sun et al., 2002).

Photofilling

Another novel technique of staining cells is photofilling. It involves irradiating cells filled with a fluorescent molecule in the presence of diaminobenzidine. This results

in oxidation of the diaminobenzidine into an insoluble, electron-opaque product, which can be visualized by either a light or electron microscope (Maranto, 1982). Photofilling has been a valuable tool in identifying and classifying the different types of bipolar and amacrine cells in the mammalian retina (MacNeil and Masland, 1998; MacNeil et al., 2004). MacNeil and Masland and their collaborators (1998; 2004) used the photofilling method to estimate the relative percentage of each cell type out of the total sample of photofilled cells in the rabbit retina. However, the photofilled cells were sampled only from a particular region in the midperiphery/periphery, not from the entire retina, which raises the question of the usefulness of photofilling in determining cell type distribution and coverage across the retina. In addition, the possibility of missing certain cell types by photofilling was reported by MacNeil and collaborators (2004) when they failed to identify one bipolar cell type, the wide-field 'OFF' cell, observed by Famiglietti (1981). Therefore, it should be borne in mind that the relative percentages and the catalogue of the different cell types reported by MacNeil and collaborators (1998; 2004) are only an estimate of the true population.

Transgenic Mice

Transgenic mice carrying recombinant genes that allow certain retinal neurons to be labelled have been used to classify the different neuronal types. In Badea and collaborators' study (2003), they used mice carrying two genetic components, which took advantage of the Cre/loxP recombination system. The first component was the Cre recombinase gene fused to a mutated estrogen receptor ligand binding domain (CreER), that selectively binds the estrogen analog – 4-hydroxytamoxifen (4HT) (Feil et al., 1996). The CreER was targeted to the Rosa26 locus to obtain ubiquitous expression of CreER recombinase (Friedrich and Soriano, 1991). They used a line of mice referred to

as R26CreER, in which they can achieve optimal translation efficiency of the CreER message.

The second genetic component, referred to as ZAP, was a ubiquitously expressed Cre-sensitive reporter transgene (Lobe et al., 1999). The ZAP reporter contains a cytomegalovirus enhancer/β-actin promoter driving the lacZ coding region followed by transcription termination sites. The lacZ coding region and termination signals are flanked by loxP sites. The loxP sites are recognized by Cre recombinase, which catalyses the excision of the region between the loxP sites. An alkaline phosphatase (AP) coding region is located immediately distal to the loxP flanked sequences, but is not expressed unless the upstream cassette is removed by Cre recombinase. Tissue from the transgenic mice can be stained for AP activity by incubating the tissue with NBT/BCIP stain and be visualized by light microscopy.

When Badea and collaborators (2003) exposed the R26CreER;ZAP mice post-natally to 4HT (3 mg), photoreceptors, bipolar cells and an amacrine cell in the retina as well as diverse cell types in the brain were labelled AP positive. When mice were injected with 80 μg of 4HT at various embryonic and post-natal developmental ages, Badea and collaborators (2003) found a progressive shift of labelled cell types from ganglion cells, amacrine cells and cone photoreceptors (early developmental stages) to rods, bipolar cells and Muller glia at later stages. Therefore, it was possible to selectively label particular cell types by choosing a developmental stage to inject 4HT.

In the (2004) study, Badea and Nathans used the transgenic mice carrying the R26CreER;ZAP genes, which were injected with 1 μg/g of bodyweight of 4HT during embryonic day 10. Using cluster analysis to group the different cell types, they classified the horizontal cells, bipolar cells, amacrine cells and ganglion cells in the mouse retina. In relation to the bipolar cells, eight clusters of bipolar cells were found

which differed in various parameters including axon stratification level in the IPL and axon arbor size. Nine clusters were classified for the ganglion cells, which differed in dendritic arbor stratification, size and pattern. Included among the amacrine cell types identified were the AII amacrine cells and starburst amacrine cells.

Using the DiOlistics technique, Lucifer Yellow injections and transgenic mice expressing green fluorescent protein (GFP) to stain RGCs, Kong et al (2005) have analysed 219 RGCs and placed them into eleven morphological cluster groups, in addition to the bistratified and melanopsin ganglion cells present in the mouse retina. All eleven clusters shared similar morphological characteristics with the ganglion cell types classified by other investigators in the mouse retina (badea and nathans; Sun et al 2002).

There are several limitations to the CreER;ZAP labelling method described by Badea (2003). First, the time course of CreER action after a single exposure to 4HT is likely to extend over 1-2 days, limiting the temporal resolution of the marking event, although the non-linear 4HT dose-response curve should sharpen the time window of Cre activity. Second, Cre-ER-mediated recombination may be more effective in some cell types than in others, thereby biasing the population of labelled cells. Third, as with viral or particle delivery of genetic reporters, there is an obligatory several day delay between the time at which gene activation begins and the accumulation and transport of sufficient AP to visualize the distal processes. Fourth, the current genetic system uses two independently segregating loci. It would be more convenient to have a single locus carrying both the CreER and ZAP cassettes. Fifth, in targeting selected cell types, the method is limited by the range of promoter specificities that are currently available.

2.7 Factors limiting high visual acuity

Most of the current theories of how the retina is organized and processes high spatial resolution have come from studies in mammalian retina. Those studies have demonstrated that the mammalian retina, particularly the primate, has specializations with distinct morphological, connectivity and topographical features that are important in establishing high visual acuity. The relatively few studies in avian retina have demonstrated that there are some similarities between the avian and mammalian retinas. This section will consider the retinal specializations associated with high visual acuity, the unique primate foveal circuitry, the organization of RGCs and the contributions of photoreceptor and optical design in achieving high visual acuity.

Retinal specializations associated with visual acuity

The vertebrate retina contains specialized areas associated with high visual acuity. These specialized areas are referred to as either an *area centralis* or a *fovea centralis*. The term fovea, herein, is reserved for referring to an area containing a pit or a depression on the retinal surface. The shape of the foveal depression varies among species, but can be classified as either convexiclivate or concaviclivate. Walls (1942) described convexiclivate fovea as having a deep depression and a convex-shaped slope, whereas the concaviclivate fovea is shallower and concave shape. The central fovea of the hawks, nuthatch, sunbird and Blue jay are convexiclivate (Fite and Rosenfield-Wessels, 1975). Pigeons (Galifret, 1968; Binggeli and Paule, 1969), primates, and some fishes have a concaviclivate fovea (Walls, 1942).

Photoreceptor and RGC density in the *area centralis* and fovea are considerably greater compared with the surrounding area, causing a local thickening of the retina. The presence of an *area centralis* characterised by peak RGC density has been well

documented in a number of avian species such as the chicken (Morris, 1982), Japanese quail (Budnik et al., 1984; Ikushima et al., 1986) and ostrich (Boire et al., 2001a). In the jungle crow, two areas of high RGC density were identified, one in the central, the other in the dorsal retina (Rahman et al., 2006).

Birds may either have one or two foveas on the retina. A single fovea has been identified in the Blue jay, nuthatch, sunbird, great horned owl, and pygmy owl (Fite and Rosenfield-Wessels, 1975) and the pigeon (Galifret, 1968). The fovea of the great horned owl and pygmy owl are temporally located, whereas those of the Blue jay, nuthatch, sunbird and pigeon are in the central area closer to the optic nerve head. Bifoveate birds include the red-tailed hawk, goshawk, sparrow hawk, and the Least Tern (Fite and Rosenfield-Wessels, 1975). These birds have one central fovea, which is much deeper than the temporal fovea. Although the cell densities are much higher in the two foveal regions compared with the peripheral retina, the central fovea contains a higher peak photoreceptor and RGC density than the temporal fovea.

In a few bird species, a combination of an *area* and *fovea centralis* are present on the retina. The *area dorsalis* and the fovea in the pigeon have been demonstrated to subserve high acuity in the frontal and lateral field of view, respectively (Nalbach et al., 1990; Hahmann and Güntürkün, 1993; Rounsley and McFadden, 2005). This raises the question of whether both retinal areas process information via similar mechanisms that contribute to high acuity. This question deserves further examination, particularly in relation to the retinal circuitry in these regions. Some evidence based on electron microscopic analysis of the number of amacrine and bipolar cell synapses in the pigeon IPL indicates that the red field has a more complex circuitry compared with the central fovea and surrounding peripheral retina (Yazulla, 1974).

Studies in the primate retina have revealed that the fovea has several more distinguishing features. Among these are an absence of rod photoreceptors, a marked increase in the density and packing of cone photoreceptors (Curcio et al., 1990), and the presence of a midget circuitry (see below). All these features are hypothesized to contribute in establishing high visual acuity in the primate.

Cone to RGC convergence

One of the most striking features of the primate fovea is a high density of both cones and ganglion cells. The density of cone photoreceptors reaches its peak in the primate foveal centre, between approximately 193,000 and 210,000 cells/mm^2, while peak ganglion cell density is between 32,000 and 68,000 cells/mm^2 (Packer et al., 1989; Curcio and Allen, 1990; Curcio et al., 1990; Wilder et al., 1996). Based on these figures, one can estimate the number of cones per ganglion cell, which is 3–5 cones/ganglion cell in the fovea. In the peripheral retina, cone photoreceptor and ganglion cells decrease markedly with greater eccentricity from the fovea to a minimum of approximately 1,500 cones/mm^2 and 200 ganglion cells/mm^2, thus increasing the cone to ganglion cell ratio to about 7.5:1 (Packer et al., 1989; Curcio and Allen, 1990). The increased photoreceptor and ganglion cell density as well as the lower cone to ganglion cell ratio compared with the periphery have been associated with the fovea's greater spatial resolving power.

Midget circuitry

There is considerable evidence from the primate fovea that it contains a one-to-one cone to ganglion cell circuitry with highly specialized cell types mediating increased spatial resolution. The bipolar and ganglion cells forming this circuitry are

called ‘midget’ because of the small size of their dendritic fields. Midget cells were first described by Polyak (1941). He stated that a midget ganglion cell receives input from a midget bipolar, which is in turn connected to only one cone. Kolb (1970) later showed using electron microscopy that the midget bipolar contacts only one cone pedicle in the foveal region. Moreover, electron microscopic evidence has revealed that a midget bipolar cell contacts a midget ganglion cell near the foveal pit (Kolb and Dekorver, 1991; Calkins et al., 1994). The importance of having a one-to-one connectivity between a cone photoreceptor, a midget bipolar cell and a midget ganglion cell is in the creation of a pathway at the retinal level that preserves the high spatial resolving capacity.

The question of whether midget circuitry similar to that present in the primate fovea exists in the avian retina, particularly in the fovea and *area centralis,* has been addressed by a limited number of studies previously. The presence of a midget bipolar cell similar to the primate was reported in the two high acuity regions of the pigeon (Lockhart, 1979; Mariani, 1987) and the chicken retina (Quesada et al., 1986). In both the chicken and pigeon retina, a ‘midget’ bipolar cell type was named with a very small dendritic width of 2.5 μm (in the pigeon red field, Mariani, 1987) to 2-5 μm (in the chicken retina (Quesada et al., 1986; Quesada et al., 1988). However, the midget-like ganglion cell found in the pigeon retina did not resemble that of the primate midget ganglion cell in terms of its morphology (Lockhart, 1979). The pigeon midget-like ganglion cell had a dendritic field diameter of 10 μm in the fovea (Lockhart, 1979). This size is larger compared with the primate midget ganglion cell diameter of 5–7 μm (Kolb et al., 1992). Furthermore, unlike the primate midget RGC, which only has one dendritic process, the pigeon midget-like ganglion cell has multiple dendritic processes emanating from the soma. The evidence suggests that the midget ganglion cell in the

pigeon retina might be receiving input from more than one bipolar cell and that a one-to-one ratio between photoreceptor and ganglion cell is unlikely to be present in this high acuity region.

RGC density and dendritic field size

RGCs receive input from bipolar cells and the number of inputs they receive may be associated with the ganglion cell's dendritic field size and density at a particular eccentricity (Wässle and Boycott, 1991).

As discussed previously, the primate fovea includes a midget circuitry where one ganglion cell receives input from only one cone. This arrangement is thought to form the basis of high spatial resolution at the fovea. The dendritic field size of the midget ganglion cell around the fovea is so small as to permit contact with only one midget bipolar cell. However, in the primate peripheral retina, the midget ganglion cell's dendritic field diameter increases (Rodieck et al., 1985; Watanabe and Rodieck, 1989; Dacey and Petersen, 1992; Dacey, 1993b). As a result of this, the number of cones converging onto the midget RGC increases and this causes a reduction in the spatial resolving power in the periphery.

In the cat retina, there is a RGC, called the beta cell or X-cell, which has been implicated in subserving high visual acuity because it is characterised by a small dendritic field diameter and receptive field, and is distributed predominantly in the *area centralis* (Boycott and Wässle, 1974; Saito, 1983; Stanford, 1987; Stein et al., 1996). Like the midget ganglion cell organization in the primate retina, the dendritic field size of the cat beta cell increases with eccentricity from the *area centralis*. The beta cell characteristics and systematic variation of field size across the retina has also been documented in the ferret retina (Isayama et al., 2009). The widening of the dendritic

field size in the periphery would mean an increase in the number of bipolar cell inputs into the RGC and possibly lower visual acuity.

The variation in the dendritic field size of the midget and beta cells may also be a common feature in avian retina as well, although this has not been systematically studied. In the pigeon retina, RGC dendritic field size was comparatively smaller in the fovea and red field than in the periphery (Lockhart, 1979). The chicken RGC groups showed an increase in dendritic field size with respect to the *area centralis* (Chen and Naito, 1999; Naito and Chen, 2004b; Naito and Chen, 2004a). However, it is unclear which RGC types are predominant in these avian areas of high cell density regions of avian cell density.

Photoreceptor packing, eye size, and pupil diameter contribution to visual acuity

Several theories have been proposed that may contribute to the ability of the eye to resolve two points in space. The centre-to-centre distance between foveal cones (d_{cc}) is one of the important factors in determining the limits of visual acuity (Miller, 1979). The closer the distance between the foveal cones, the more likely that two points in space can be resolved.

Another significant factor in determining the extent of visual resolution is the *f*-number. The *f*-number is the ratio of the anterior focal length or the posterior nodal distance (PND) to the pupil diameter. According to Miller (1979), the *f*-number determines the actual image size on the retina. The larger the PND, the higher the *f*-number, which means the image of the object is projected onto a larger retinal area. The relationship between the *f*-number, d_{cc}, and pupil diameter is given by this equation: $d_{cc} = \lambda f/\sqrt{3}$ where λ is the wavelength (Miller, 1979).

In the human fovea, it has been reported that cones reach a peak density between 98,000 to 324,100 cones/mm^2 and the calculated d_{cc} = 3.4–1.9 μm, respectively (Curcio et al., 1990). The theoretical visual acuity for these individuals ranges from 47.5–86.3 cycles/degree. It has been calculated that the human eye with a 2.4 mm pupil diameter can resolve 60 cycles/degree and a cut off at 76 cycles/degree in the absence of aberrations or anomalies (Campbell and Gubisch, 1966). The spatial frequencies measured in humans using pyschophysics suggest that the spatial frequencies passed over 60 cycles/degree by the human pupil are of low contrast, and that the photoreceptor spacing is set to resolve a maximum of 55–60 cycles/degree (Westheimer, 1960; Campbell and Green, 1965).

In comparison to human visual acuity, the maximum anatomical resolving power of the Falconiforms is double that of human (Fox et al., 1976; Reymond, 1985). The visual acuities of two raptorial species, the American kestrel (*Falco sparverius*) and the eagle (*Aquila audax*), are higher than other bird species studied to date. The kestrel's visual acuity is 160 cycles/degree (Fox et al., 1976), while the maximum acuity of the eagle is between 132–143 cycles/degree (Reymond, 1985). When the focal length (*f*) of fresh and fixed eyes were measured, only a slight difference between the human and a few species of Falconiforms was reported, which is about f = 15.6 mm for the Falconiforms and f = 17 mm for the human (Snyder and Miller, 1978). To attain twice the visual acuity of the human, the PND of the Falconiform's eye must be larger to afford a larger retinal image and the foveal inter-cone spacing must be less than that measured in humans. In support for this hypothesis, the wedge-tailed eagle's central fovea was found to have a PND of 22.6 mm and an inter-cone spacing of 1.6 μm (Reymond, 1985). Using these values, Reymond (1985) estimated that the maximum anatomical resolving power of the wedge-tailed eagle is around 140 cycles/degree.

Furthermore, the smallest pupil diameter of the wedge-tailed eagle is larger compared with the human, measured to be around 5 mm (Reymond, 1985). This allows for more light to enter the eye and stimulate more photoreceptors while compromising between the limitations of diffraction and optical aberrations. In addition, the deep spherical bottom of the central fovea of falconiforms has been hypothesized to act as a negative lens which, in conjunction with the cornea and lens, functions as a telephoto optical system (Snyder and Miller, 1978). The overall optical design and retinal specializations of the eagle is exquisitely adapted for achieving a very high visual acuity.

Unlike the diurnal raptors described above, the barn owl's visual acuity lies at the lower end of the scale, ranging from 2.6 to 4.0 cycles/degree (Harmening et al., 2009). It is unclear why the owls have a very low visual acuity despite having excellent optics with a large axial length capable of producing a large retinal image (Schaeffel and Wagner, 1996; Harmening et al., 2007). One possible reason for the owl's low visual acuity may be due to the predominance of rod photoreceptors rather than cone photoreceptors in its retina including its fovea (Fite and Rosenfield-Wessels, 1975). Rod photoreceptors are not involved in processing high visual acuity and the rod circuitry involves a high degree of convergence from rods to a bipolar cell (Freed et al., 1987b; Sterling et al., 1988b). Another possible reason for not having a high visual acuity may be the owl's reliance on detecting other forms of stimuli, such as sound and movement, to capture its prey accurately, and therefore may not be necessary for survival.

2.8 Summary

The pigeon retina has several distinguishing features, such as the presence of two high cell density areas, including a fovea and an *area dorsalis*, the retina with two differently coloured areas and an unvascularized retina. Like other avian species, it

contains different types of cone photoreceptors which can be characterised based on the absorption spectra of various visual pigments and oil droplet types. Other neuronal types, such as the horizontal and bipolar cells, have been morphologically documented in the avian retina, including the pigeon, but it is still unknown what the physiological properties of these cell types are in birds. Experiments done in the mammalian retina to characterise the morphological types of bipolar cells and RGCs and their synaptic connectivity with other neurons can be applied to similar investigations of neuronal type classification and connectivity into the avian retina. A number of factors have been correlated with mediating high visual acuity in the mammalian retina, such as the presence of a fovea or *area centralis*, convergence ratios of cone photoreceptors to RGCs, a midget circuitry, RGC density and field size, and photoreceptor packing. Since the pigeon retina also has specialized areas of high cell density, the issue of whether other factors might be involved in processing high acuity vision has been raised. Based on a few earlier morphological studies in the pigeon and chicken retinas, there is some evidence suggesting that a midget circuitry may have partial similar connectivity between photoreceptors and bipolar cells. However, in order to demonstrate the exact number and type of neurons interconnected in the avian retina, an in depth examination using modern methods that have proved useful in mammalian studies is vital.

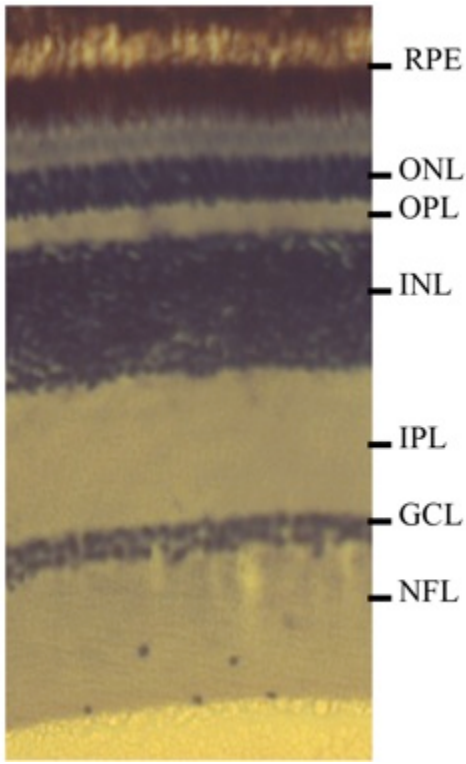

Figure 2.1. Cross-section of the central yellow field in the pigeon retina showing the layers. Retina stained with Haematoxylin and Eosin. RPE = retinal pigment epithelium; ONL = outer nuclear layer; OPL = outer plexiform layer; INL = inner nuclear layer; IPL = inner plexiform layer; GCL = ganglion cell layer; NFL = nerve fibre layer.

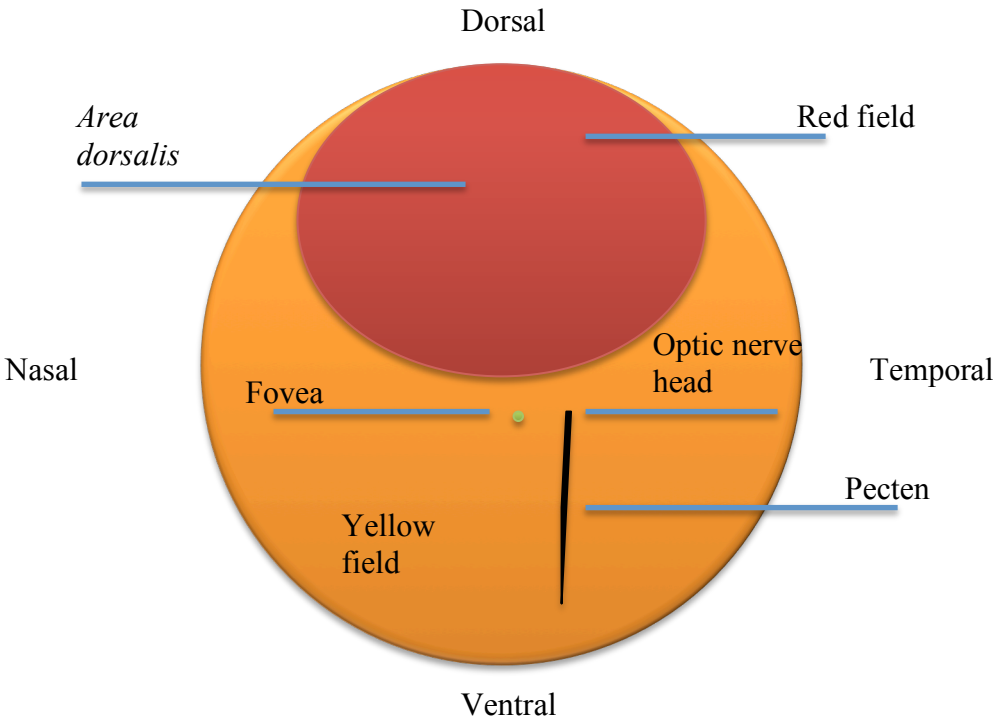

Figure 2.2. A schematic diagram of the pigeon retina showing the different regions.

Table 2.1. Maximum absorption wavelength (λ_{max}) of cone photoreceptor visual pigments in different avian species measured by MSP

Species	λ_{max}				
	LWS (red)	MWS (green)	SWS (blue)	UV/violet	Reference
Leiothrix lutea red-billed robin	568	499	454	355	(Maier and Bowmaker, 1993)
Spheniscus humboldti penguin	-*	543	450	403	(Bowmaker and Martin, 1985)
Anas platyrhynchos Mallard duck	570	502	452	420	(Jane and Bowmaker, 1988)
Melopsittacus undulattus budgerigar	564	509	444	371	(Bowmaker et al., 1997)
Taeniopygia guttata Zebra finch	567	503	429	360-380	(Bowmaker *et al.,* 1997)
Columba livia pigeon	567	507	453	409	(Bowmaker *et al.,* 1997)
Gallus gallus chicken	570	508	455	419	(Bowmaker *et al.,* 1997)

* The LWS pigment may not have been included in the sample of cone visual pigments due to the sampling limitations of MSP technique (Bowmaker & Martin, 1985).

Table 2.2. Absorbance cut-off wavelength (λ_{cut}) of cone photoreceptor oil droplets in different avian species measured by MSP

Species		λ_{cut} (nm)				
	R	Y	P	C	T	Reference
Leiothrix lutea red-billed robin	568	506	-	<400	<370	Maier & Bowmaker, 1993
Spheniscus humboldti penguin	-	525	-	<400	-	Bowmaker & Martin, 1985
Anas platyrhynchos Mallard duck	580	515	475-500	450	370	Jane & Bowmaker, 1988
Melopsittacus undulattus budgerigar	560-580	500-540	410-450, 480	410-450	-	Bowmaker *et al.,* 1997
Taeniopygia guttata Zebra finch						
Columba livia pigeon						
Gallus gallus chicken						

Chapter 3 -

Photoreceptor and Ganglion Cell Topographies Correlate with Information Convergence and High Acuity Regions in the Adult Pigeon (*Columba livia*) Retina

Authors: Angeliza Querubin, Hie Rin Lee, Jan M. Provis, and Keely M. Bumsted O'Brien

The work presented in this Chapter 3 was already published in The Journal of Comparative Neurology in 2009, Volume 517:711-722.

Abstract

The fovea and *area dorsalis* are high acuity vision regions in the pigeon retina. However, the degree of neural convergence (an important determinant of acuity) has not been quantified consistently in this bird. The purpose of the study was to determine the topographic density changes and degree of photoreceptor to ganglion cell convergence in the fovea and the *area dorsalis*. Total photoreceptor and ganglion cell densities were calculated on the horizontal and vertical meridians. In four eyes, retinal topography was mapped for photoreceptors and ganglion cells. Rod density was quantified by counting anti-rod opsin stained outer segments across the retina. The ratio of cone photoreceptors to ganglion cells, a rough measure of information convergence, was calculated. The fovea and the red field contained significantly higher mean cone and ganglion cell densities compared with the yellow field. Rods were missing from the fovea. Outside the fovea, rods comprised 20 % of the photoreceptor population with no significant density changes across the retina. The ratio of photoreceptors to ganglion cells was highest in the yellow field suggesting a high degree of information convergence and low acuity. Our data indicated that convergence of cones onto ganglion cells in the red field is similar to that observed in the fovea. Convergence ratios in both the fovea and red field suggested greater visual acuity compared to that of the surrounding yellow field, which is consistent with the higher visual acuities that have been reported in these regions.

3.1 Introduction

High acuity vision is mediated by specializations in the retina where a high density of cone photoreceptors (PR) and retinal ganglion cells (RGC), coupled by their synaptic circuits, conveys high resolution spatial information to the brain. There are many strategies for mediating high visual acuity, which range from small local regions of higher cell density as observed in *area centrales* to well defined foveae (Stone, 1965; Provis, 1979; Curcio et al., 1987; Packer et al., 1989; Curcio and Allen, 1990; Garciá et al., 2005; Salinas-Navarro et al., 2009). The fovea is a small pit at the centre of gaze consisting of inner retinal layers which are displaced laterally to form a pit, overlain by densely packed cone PR, which mediate colour vision and fine spatial acuity (Curcio *et al*., 1987; Curcio *et al*., 1990; Packer *et al*., 1989). Among mammals, the presence of a fovea is restricted to primates. However, other vertebrates (Slonaker, 1897; Walls, 1942), such as some birds (Fite, 1973; Fite and Rosenfield-Wessels, 1975; Inzunna and Bravo, 1993), some teleosts (Collin and Collin, 1999; Pettigrew et al., 1999; Collin et al., 2000), and some anolis lizards (Fite and Lister, 1981; Pettigrew et al., 1999), have a fovea. In addition, some birds have a second area of high visual acuity located in more peripheral retina (Fite & Rosenfield-Wessels, 1975; Slonaker, 1897; Walls, 1942). Understanding how these diverse structures mediate high visual acuity as compared with the human visual system is an important question in visual neuroscience. The pigeon (*Columba livia)* is an excellent model to study these high acuity regions.

The pigeon has two high acuity regions, the fovea and the *area dorsalis*. Located at the intersection of horizontal and vertical meridians, the pigeon fovea is concaviclivate, similar to the primate (Galifret, 1968), and other birds such as the northern Blue jay - *Cyanocitta cristate* (Fite & Rosenfield-Wessels, 1975) and the ostrich - *Struthio camelus* (Boire et al., 2001b). Unlike birds of prey and some lizards,

pigeon foveal depth is variable and overall the pit has a less well differentiated depression (Fite & Lister, 1981; Fite & Rosenfield-Wessels, 1975). The fovea lies close to the optic axis and subserves the monocular lateral field (Blough, 1973). The *area dorsalis* is located in the dorsal retina, and views a binocular frontal field below the beak (Slonaker, 1897; Walls, 1942; Galifret, 1968; Blough, 1971; Blough, 1973; Fite and Rosenfield-Wessels, 1975; Bloch and Martinoya, 1982; Reymond, 1985; Hodos and Erichsen, 1990). At the fovea there is a retinal excavation forming a depression in the retina, while the *area dorsalis* shows no macroscopic differences other than the presence of red oil droplets, which define the red field, as compared with surrounding retinal regions. The fovea and *area dorsalis* each project to different areas of the brain and subserve separate perceptual functions (Güntürkün and Hahmann, 1999). Rather surprisingly, although their morphologies and projection patterns are distinct, the mean visual acuity of these two regions is similar. Foveal acuity measured behaviorally is 12.6 cycles/degree (Hodos et al., 1991) while the *area dorsalis* visual acuity is 12.8 cycles/degree (Hodos et al., 1985; Hodos et al., 1991; Rounsley and McFadden, 2005).

Visual acuity can be limited by the spatial resolution of PR packing density and the types of connections made to RGC via bipolar cells. The primate fovea contains a midget system in which one cone PR provides input to a pair of ON and OFF bipolar cells. The ON bipolar cell in turn connects to one ON RGC and the OFF bipolar to one OFF RGC. This results in a 1:2 ratio of cones to RGC and provides the anatomical basis for high acuity, which in *Macaca* monkeys and humans typically is 30-45 cycles/degree or higher (Yarczower et al., 1966; Kolb and Dekorver, 1991; Calkins et al., 1994; Boycott and Wässle, 1999; Kolb and Marshak, 2003). By contrast, in the peripheral primate retina, the number of cone/bipolar sets converging onto a single RGC increases, so that the ratio decreases to 1:5 or more. This correlates with decreased peripheral

acuity (Walls, 1942; Boycott and Wässle, 1999). Whether birds with high visual acuity have a similar midget-like system is unclear. Midget-like bipolar and RGC with relatively small dendritic fields have been described in both the pigeon fovea and in the dorsal red field (Lockhart, 1979; Mariani, 1987), although their morphology is not completely analogous to the primate midget system (Polyak, 1941; Boycott and Dowling, 1969). As expected, the pigeon fovea and *area dorsalis* correlate with regions of high PR and RGC density. However, the densities previously reported in the fovea and the *area dorsalis* differ between studies and the ratio of PRs to RGC has not been analysed in detail (Binggeli & Paule, 1969; Galifret, 1968; Hodos *et al*., 1991). Furthermore, little information is available concerning regional variations in rod PR distribution at the fovea or *area dorsalis*. The purpose of this study was to determine the densities of rod and cone PRs, and RGCs in the red field containing the *area dorsalis*, in the fovea and in the peripheral retina of the pigeon (the yellow field). As a first step towards determining the morphological basis of high visual acuity in the pigeon, we determined the ratio of cone PRs to RGCs across the retina as a measure of convergence in the retinal circuitry. Although convergence ratios are only an indirect indication of the circuitry responsible for high acuity and other visual functions, they have been widely applied for this purpose (Boycott and Wässle, 1999) and serve as a useful starting point for understanding the morphological basis of acuity in the pigeon.

3.2 Materials and methods

Tissue collection and processing

Ten eyes from adult pigeons (*Columba livia*) of both sexes were obtained from the University of Auckland, New Zealand and a pigeon farm in NSW, Australia, with

ethical approval from the University of Auckland Animal Ethics committee and The Australian National University (ANU) Animal Ethics committee, respectively. Eyes were either enucleated and immersion fixed in 4% paraformaldehyde (PFA) in 0.1 M phosphate buffered saline (PBS; pH 7.4) or enucleated from pigeons perfused with the same fixative.

The cornea, lens, vitreous and sclera were removed. For wholemounts, radial cuts were made at the retinal margin to relax the retina such that it would lie flat and the tissue was either immediately mounted on glass slides and coverslipped, or further processed for immunocytochemistry. For cryosections, the eyes were cryoprotected in 30% sucrose in PBS at 4°C overnight and then incubated at 45°C for 3 hours in a solution containing 14% gelatin in 30% sucrose in PBS. The retinas were laid flat in a Petri dish and the gelatin solution was allowed to set at 4°C. The gelatin-embedded retina was frozen at a known orientation in equal parts of 30% sucrose solution in PBS and Optimal Cutting Temperature (OCT, Tissue Tek) mounting medium. The block was serially cross-sectioned at 20 μm in a cryostat (Leica, Wetzlar, Germany) starting 1-2 mm from the ventral edge of the yellow field to 2 mm from the dorsal edge of the red field (Fig. 3.1 A and B)

Histology, immunolabelling, and antibody characterization

Every tenth slide was stained with haematoxylin and eosin to reveal retinal morphology and viewed in bright field and photographed with an AxioVision HRC camera (AxioVision, Zeiss, Germany, software Release 4.6). Sections and wholemounts were immunolabelled with an antibody to rod opsin (RET-P1; 1:500). Ret-P1, a gift from Colin Barnstable, is an IgG1 mouse monoclonal antibody generated against rat retinal membranes (Barnstable, 1980). The antibody recognized a 39 kD m.w. band on

Western blots of pigeon retina (Silver et al., 1988), and can be blocked by peptides derived from the N-terminus of rhodopsin (Hargrave et al., 1986). The specificity was also defined in Hicks and Barnstable (1987). Our observed staining pattern and cellular morphology of rods is identical with previous reports (Barnstable, 1980; Fekete and Barnstable, 1983; Akagawa and Barnstable, 1986; Hicks and Barnstable, 1986; Hicks and Barnstable, 1987; Silver et al., 1988; Sheedlo et al., 1993; Matsuura et al., 2010). To block non-specific binding, tissue was pre-incubated with normal goat serum (Zymed Laboratories, South San Francisco, CA, 01-6101) diluted 1:10 in 0.01% Triton X- 100 in PBS (TPBS): sections for 1.5 hours, while wholemounts were left overnight at 4°C. Sections were incubated in the primary antibody overnight and wholemounts for 3-4 days at 4°C. After a thorough wash in PBS, Alexa Fluor 488 conjugated goat anti-mouse (Molecular Probes Inc., Eugene, OR, A11029; 1:1000), was applied for 3 hours to sections and overnight to wholemounts, followed by PBS washes to decrease background. Sections and wholemounts were coverslipped with Aqua Poly/Mount (PolySciences Inc.,Warrington, PA, USA; 18606). Controls were the primary was omitted showed no specific labelling in the tissues. Immunolabelled sections were examined using a confocal Laser-Scanning Microscope (LSM 5, Zeiss). All figures were generated and individual images manipulated to optimize contrast and brightness using Adobe Photoshop CS3.

Cell counts

Sampling in wholemounts

The pigeon retina was subdivided into a number of regions identifiable macroscopically. The pigeon retina contains a very prominent ventrally located pecten,

which is a pigmented vascular structure extending out into the vitreous (Fig. 3.1A). The retina was further subdivided for convenience into dorsal/ventral and nasal/temporal quadrants, bordered by the horizontal and vertical meridians (boxed regions, Fig. 3.1B). The fovea is located in the middle of the horizontal and vertical meridians (Fig. 3.1 A, B). The vertical meridian was an arbitrary axis that intersects the retina almost in half but slightly to the nasal side of the pecten, dividing the retina into the nasal and temporal halves. The horizontal meridian intersected the retina in half, dividing the retina into the dorsal and ventral halves. Counts made along the horizontal meridian included the central yellow field stretching from the nasal to the temporal edges. Counts along the vertical meridian include near the ventral edge of the yellow field to the dorsal part of the red field, which include part of the *area dorsalis*. Retinal wholemounts (n=6) in the region between the fovea and optic disc (OD) were photographed PR side up using a Leica microscope with DIC optics. Montages from the fovea to the OD were generated using a 40x wide-field objective (250 μm field diameter). Only the PRs were counted in the wholemount retinas. The number of PR inner segment profiles (both rods and cones) was counted in twenty 10 μm x 10 μm sampling boxes in a 250 μm-wide field, and the average number of inner segment profiles per mm^2 was determined. Counts were made in eight 250 μm-wide fields from the foveal centre to the OD.

Sampling in sections

Photoreceptor and RGC density measures also were performed in serial 20 μm frozen sections covering the entire retina (n=4). The flatmounting of the retina in gelatin prior to frozen sectioning allowed for the production of high quality retinal cross sections. Only cross sections showing all the retinal layers were analysed. Any sections showing a skewed or enface retinal orientation were not used for cell density analysis.

Starting at the ventral edge and ending at the dorsal edge, a series of slides approximately 500 μm apart was stained with either DAPI (Sigma; St. Louis MO, USA: diluted 1:10 in PBS) or propidium iodide (PI) solution (Sigma; diluted 1:500 in PBS) for 2 minutes, followed by a 10 minute PBS wash. Slides were coverslipped with Aqua Poly/Mount (PolySciences Inc, Warrington, PA, USA). In the central retina and *area dorsalis*, the distance between sampled sections was decreased to 250 μm to increase the amount of retina sampled. For most of the tissue sections, two to six sampling points were imaged across the retina. In sections containing the fovea, the sampling points included the fovea, 0.5 mm from the fovea and every 1 mm until the edge of the nasal and temporal periphery was reached. A Z-stack series of images centreed on the outer nuclear layer (ONL) were taken at each sampling location using a confocal Laser-Scanning Microscope (LSM 5, Zeiss). The total thickness of the Z-stack was 5.50 ± 0.08 μm, and the image size was 225 μm x 225 μm. Each Z-stack individual image was less than 0.5μm thick to ensure overlap between cells in each stack. The Z-stack images were opened in Adobe Photoshop CS3 and compiled into layers. An additional layer was added. All the cells in the Z-stack were marked with a dot on the additional layer. Both photoreceptors and ganglion cell nuclei were counted in the images. By counting only the newly appearing cells on the overlapping layers, it was assured that no cell was counted twice. Once all the cells were marked, the layer containing the dots (indicating cells) was imported into Image J and counted using the 'analyse particles' plug-in. To obtain the number of cells in square millimeters (mm^2), the cell counts were multiplied by a factor taking into account the thickness of the section, Z-stack height, and width of the sampling window.

Because the GCL also contains displaced amacrine cells along with a small number of glial cells, we applied a correction factor based on data from retrograde

filling of RGC in pigeon retina (Hayes, 1984). Regional variations in these counts showed that in the red field only 2% of cells were non-RGC, while in the fovea 15% were non-RGC and in the yellow field 23% were non-RGC (Hayes, 1984). A small percentage of RGC or Dogiel's cells (0.02-0.1%) were displaced to the inner nuclear layer (INL). These cells project independently to the accessory optic system (Hayes & Holden, 1983b) and were not included in our estimates.

For each of the sampling points on the sectioned retina, the percentage of non-RGCs was calculated from the cell density in cells/mm^2 which gave the density of ganglion cells. RGCs in the yellow field, outside the fovea, were calculated using the 23% correction factor, while those located in the fovea, the correction factor of 15% was used. For RGCs in the *area dorsalis* and red field, the correction factor used was 2%. It was assumed that the *area dorsalis* had a similar percentage of non-RGCs.

Graphing the PR and RGC densities

For every millimetre along the horizontal or vertical meridians, the average PR densities from both wholemounts and sections were plotted on a graph against eccentricity (distance in millimetres) from the fovea. Before averaging the PRs, the densities of PRs were compared for every millimetre between the wholemounts and sections. No significant differences were observed in the PR densities between the wholemounts and sections.

Since RGCs were counted from sections of different eyes only, the average RGCs was calculated for every millimetre along the horizontal or vertical meridians and were plotted on a graph against eccentricity (distance in millimetres) from the fovea.

Rod counts and ratio calculation

Rod density was determined using the same method to calculate cell density in wholemounts and sections. However, instead of counting inner segment profiles (wholemounts) or cell nuclei (in sections), the number of Ret-P1 labelled rod outer segments was counted. The average rod PR densities in the yellow and red fields were subtracted from the total PR cell density at each retinal location to give an estimated cone PR density for each retinal location. The ratio of cone PRs to RGCs was obtained by dividing the cone PR density with the corrected RGC density at each sampled point on the retina. This value was plotted on a reconstructed retinal map.

Topographic map construction

Topographic maps of PR and RGC densities were drawn from density calculations derived from only the retinal sections of four eyes. The length of each section was measured using a stage micrometer, drawn to scale, and the X-Y co-ordinates of each sampling location were plotted on the drawing in Adobe Illustrator CS3. The calculated densities were added for each sampling point and isodensity lines were drawn manually to connect regions of equivalent cell density.

Ratio of PR to RGC mapping

The densities of cone PRs and RGCs were averaged for each location sampled on the four sectioned retinas. The ratio of cone PR to RGC was calculated at each of the locations and the ratios were mapped. Colours were arbitrarily assigned to represent the range of ratios in the different regions of the retina. The map of PR to RGC ratios across the pigeon retina is shown in Fig. 3.7.

Statistics

The densities of PRs (sum of cones and rods) and RGC in the red field, fovea and yellow field were analysed using non-orthogonal analysis of variance. Cell density variation between retinas was also analysed. To determine whether a significant difference in mean cell densities existed between the red field, fovea and yellow field, the means and the least significant differences were obtained using a residual maximum likelihood (REML) statistical analysis. Computations were carried out in the statistical package GenStat 11.

3.3 Results

The fovea is evident as a small depression nasal to the tip of the pecten. The red field is evident in dorsal retina due to the high concentration of reddish oil droplets present in the cones (Fig. 3.1A (arrows)). Sections through the fovea showed a distinct thinning of the INL, inner plexiform layer (IPL) and GCL layers (Fig. 3.1 C, D). In the foveal centre the INL was 63 μm and the IPL was 38 μm, compared to the marked thickening of these layers on the surrounding foveal rim (100 μm and 60 μm; respectively; Fig. 3.1D). Thinning of the GCL centrally and thickening of the outer nuclear layer (ONL) was also apparent, although changes compared to the foveal rim in these layers were less pronounced (Fig. 3.1C, arrow; D, left edge of image). Regional variations were also observed for laminar thickness. The thickness of the ONL was 25 μm in the fovea, where PRs were densely packed. By contrast, near the OD (Fig. 3.1E), the ONL thickness was 15 μm. In the mid peripheral yellow field (Fig. 3.1F) and in the far periphery (Fig. 3.1G), the ONL was 10 μm thick. Generally in the periphery, the PRs were less tightly packed. Throughout the red field, the ONL was thicker (20 μm) than in other retinal locations, except at the fovea (Fig. 3.1 D-H). Ventrally, in the

yellow field, the INL was 30-40 μm thick (Fig. 3.1 F, G), but was thicker dorsally (55 μm) in the red field (Fig. 3.1H). The GCL was 20 μm thick on the foveal rim (Fig. 3.1C, arrowheads), compared with 15 μm in the central fovea and 10 μm in the red field (Fig. 3.1D and H). In the mid peripheral and peripheral yellow field, the GCL was 5-10 μm thick (Fig. 3.1 F, G).

PR and RGC density on the horizontal and vertical meridians

On the horizontal meridian in the fovea, total PR reached a peak density of 328,564 PR/mm^2 and RGC densities reached a peak density of 108,313 RGC/mm^2 (Table 3.1, Fig. 3.2A). Both PR and RGC densities dropped rapidly along the horizontal meridian between 0 and 1 mm eccentricity, in both temporal and nasal directions. On the temporal side there was a plateau in PR densities between 1 and 3 mm eccentricity, which ranges between 160,000 and 180,000 PR/mm^2, beyond which there was an approximately linear decrease out to the peripheral margin of the retina to > 10,000 PR/mm^2. On the nasal side, the decline in PR densities was approximately linear from about 1 mm out to the periphery (Fig. 3.2A). The density profiles for RGC along the horizontal meridian showed a rapid decline between 0 and 1 mm eccentricity. On the temporal side there was a plateau in RGC density between approximately 1 and 4 mm eccentricity, then a gradual decline to about 10,000-12,000 RGC/mm^2 at the peripheral margin. On the nasal side RGC density dropped faster to 9,500 RGC/mm^2 by about 4 mm eccentricity.

Along the vertical meridian outside the fovea, higher PR and RGC densities were detected in the red field (277,195 PR/mm^2 and 77,283 RGC/mm^2) with the highest densities observed in the *area dorsalis* (312,807 PR/mm^2 and 88,395 RGC/mm^2). The large variability observed in the RGC densities in the red field, including the *area*

dorsalis, is due to the variation between the retinas and possibly the ages of the retina. The overall average density of PR and RGC in the red field was significantly lower compared with the fovea; however, there was no significant difference of PR density in the *area dorsalis* (Table 3.1). Densities of both RGC and PRs were much lower in the ventral yellow field (30,216 RGC/mm^2 and 175,720 PR/mm^2). The red field along the vertical meridian showed the highest variability (increased SEM; Fig. 3.2) of all retinal regions analysed. This was due to a range of individual variation that was most marked in the PR population in the red field of one animal (Fig 3.3A and 3.4A). If the densities from this animal were removed from the analysis, the SEM is significantly reduced.

PR and RGC topography

PR and RGC densities were mapped topographically in four eyes (Fig. 3.3), which showed the same basic distribution patterns. There were two areas of high PR density in each retina; one in the fovea, the other in the *area dorsalis*. In all but one eye (Fig. 3.3A) the fovea had the highest density of PRs (Fig. 3.3 B, C, and D). In two of the retinas (Fig. 3.3 B and C) there was a band of high PR density extending nasally from the fovea. In the red field, the region of high PR density was, in most cases, located close to the vertical meridian, but slightly more temporal to the fovea (Fig. 3.3 B, C, and D). PR densities in the periphery were similar in all retinas (Fig. 3.3A, B, C, and D).

In the red field of all retinas, there was a localized region of high RGC density corresponding to the *area dorsalis* (Fig. 3.4), and in one retina this was the region of peak RGC density (Fig. 3.4A). In the other retinas (Fig. 3.4 B, C, and D), RGC density was highest in the fovea, ranging between about 104,000 and 146,000 RGC/mm^2. A band of elevated RGC density extending nasal and temporal from the fovea (a ‘visual

streak') was detected in 3 of the 4 retinas mapped (Fig. 3.3 B-D), but was not seen in the fourth retina which had higher RGC densities and an annular pattern of RGC distribution centred on the fovea. The density of RGCs in the yellow field was 10,000-100,000 RGC/mm^2, similar in each of the retinas mapped (Fig. 3.4).

Rod and cone densities

We detected a 350-400 μm diameter 'rod free' region centreed on the fovea, colocalizing with a peak in cone PR density (Fig. 3.5). On the margins of this region, rod PR density rose sharply to 23,000 rods/mm^2 at 0.5 mm eccentricity (Table 3.1; Fig. 3.6). Outside the fovea, rod PRs were uniformly distributed with an average of 23,000 rods/mm^2, comprising about 20% of the total PR population in the yellow and red fields, including the *area dorsalis* (Fig. 3.6). When the contribution of the rod PRs was considered, cone PR density was highest at the fovea and 1.3-3 times higher in the red field compared with the yellow field. The peak cone PR density in the red field appeared to occur at the *area dorsalis* (Table 3.1).

PR to RGC convergence

The map showing the convergence ratios of cone PRs onto RGC at various locations across the retina is shown in Fig. 3.7. In the fovea and the *area dorsalis* there were 2.1-2.5 cones for each RGC. A region of intermediate convergence ratios, between 2.6 and 4.5:1 (red and yellow regions in Fig. 3.7), is observed extending between the foveal region and the *area dorsalis*, while along the margins of the red field, and throughout the yellow field, the convergence values are much higher at 4.67 - >7.2:1 (green, purple and blue regions, Fig. 3.7). In addition, the maps detected an elongated band extending nasal and temporal from the fovea at about 30° to the horizontal,

suggestive of a visual streak. When this map of convergence ratios was superimposed on a map of visual space in the pigeon (Fig. 3.7B), there was a close correspondence between high visual acuity and low PR to RGC ratios.

When the ratio of PR to RGC was calculated based on the averages presented in Table 3.1, the ratios were slightly different from that presented in Fig. 3.7. In the fovea, the ratio of cone PR to RGC was 2.7:1. The ratio of cone PR to RGC was greater (3.3:1) in the *area dorsalis* than that in the fovea and red field. In the red and yellow fields, the ratios were 2.9:1 and 4.1:1, respectively. The ratios obtained from the map (Fig. 3.7) and Table 3.1 were reasonably comparable. The slight differences may be attributable to the fact that the map shows the ratios at multiple locations in more detail, while the averages in Table 3.1 were obtained from the whole region of the fovea, *area dorsalis*, the red and yellow fields.

3.4 Discussion

This paper is the first to report rod and cone PR and RGC topography and cone PR and RGC ratios across the entire pigeon retina. The study confirms previous reports of the topographic variation of PR and RGCs in the pigeon retina (Galifret, 1968; Binggeli and Paule, 1969; Hodos et al., 1991). PR densities were significantly higher in the fovea compared with the red and yellow fields, but not statistically different compared with the *area dorsalis*. RGC densities in the fovea were statistically higher compared with all other regions sampled although there was a large amount of individual variation (Table 3.1). These changes in cell density were reflected in the different thickness of retinal layers at various retinal sampling locations. Similar to Hodos and colleagues, our rod PR density data in the red field showed that rod PRs comprised 20% of the PR population throughout the red (including the *area dorsalis*)

and yellow fields (Hodos *et al*., 1991). A new finding in the present study was the absence of rods from the fovea, similar to primate retina (Curcio *et al*., 1990). Our novel calculations of rod versus cone density allowed us to determine that the calculated ratio of cone PRs to RGCs followed the same pattern as cell density, with the lowest convergence ratio found in the fovea and the red field.

Regional variations in cell density

Our qualitative data indicating that the thickness of the INL changes with retinal eccentricity agreed with the data reported by Galifret (1968). Although we did not quantify density changes in the INL, the small proportion of RGCs displaced to the amacrine cell layer was insignificant. Hayes and Holden (1983) demonstrated the percentage of displaced RGCs was 0.06% in the red field, 0.28% in central retina (the foveal pit only contained one displaced cell), and 0.54% in the yellow field. In addition, these cells projected to the basal optic root and were likely to be involved in the optomotor reflexes and visuomotor behavior rather than in finer visual discrimination functions that involved the geniculate, tectal, and higher brain centres (Karten et al., 1977; Brecha and Karten, 1979; Brecha et al., 1980; Fite et al., 1981).

Previously reported PR and RGC densities in the pigeon fovea and *area dorsalis* were widely variable (Galifret, 1968; Binggeli & Paule, 1969; Hayes & Holden, 1983b; Hodos *et al*., 1991). Each of these previous studies reported densities for specific regions of the retina without providing a comprehensive account of topography, except for Hayes and Holden (1983b). Galifret (1968) reported density data for PRs and RGCs along the vertical meridian and a topographic map of cells in the INL. Our observed trend that PR and RGC density varied across the retina in a coordinated fashion was similar to that reported by Galifret (1968); however, we provided a more detailed

analysis of the PR and RGC densities. When Galifret's data were converted to cells/mm^2, our RGC densities were between 2.7 and 1.1 times lower with the largest difference in the fovea and red field. The higher cell densities reported by Galifret (1968) may be due to the inclusion of displaced amacrine cells and glial cells in his RGC layer counts. In our study, we used the correction factor from Hayes (1984) to calculate the RGC density. Hayes (1984) reported that displaced amacrine cells and glial cells account for 2 to 23% of the overall GCL population depending on retinal eccentricity.

This difference in reported density in central to peripheral retina was also observed when comparing our RGC densities to Binggeli and Paule (1969). In the far periphery, the densities reported in this chapter were similar. In the central retina, though, the RGC density reported by Binggeli and Paule (1969) was 2.5 times lower than the densities we observed. These variations in the central retina may be explained by differences in sampling methods. Binggeli and Paule (1969) counted axons in the optic nerve, while we counted the RGCs themselves at high resolution on specific sampling locations in the retina.

Hodos *et al*. (1991) focused on the red field PR and RGC densities, but did not provide a topographic map. Our data was in good agreement with Hodos *et al*. (1991) for the total density of rod PRs, cone PRs, and RGCs in the red field. Our topographic density and ratio maps clearly showed that within the red field there was a local region of high cone PR and RGC density. This data provided a good distinction between the larger region of the red field and the smaller behaviourally-defined *area dorsalis*, which we were able to pin-point with our approach. Although we investigated cone density in the red field, we did not differentiate between double and single cones in our study. Hodos *et al*. (1991) reported that in young pigeons, two thirds of the cones in the *area*

dorsalis are double cones. Taken together, our data provided an overview of PR and RGC densities and convergences across the entire red field and the smaller *area dorsalis* in the dorsal retina.

There was a large amount of individual variation between our specimens for PR and RGC densities. In three of the retinas (Fig. 3.3 & 3.4 B, C, D), the highest PR and RGC densities were found in the fovea. The second highest cell densities were found in the *area dorsalis*, except for one retina (Fig. 3.3 & 3.4A). This was not surprising, because the variation in cones in the human retina was reported to be 4.08-5.29 million, with foveal cone densities ranging from 100,000 to 324,000 cones/mm^2 (Curcio *et al*., 1990). Despite these differences in density, when the ratio of cones to RGCs was calculated, a high PR density was always paired with a high RGC density to produce a topographic map of convergence ratios that was remarkably similar between retinas. The convergence map, when superimposed on a map of visual space (Fig. 3.7B; (Nalbach *et al*., 1990)) provided an excellent correlation between morphology and behavior. Another potential contribution to the individual variation in PR and RGC density was the age of the pigeon. The exact age of the birds used in this study was unknown. Pigeons were shown to exhibit age-related decreases in PR number and acuity (Fitzgerald et al., 2001). It is possible that the pigeon with the higher densities was younger than the others.

Implications for retinal circuitry

The current study has shown an important difference in the distribution of rod photoreceptors between the fovea and the *area dorsalis*, which has implications in the circuitry and scotopic sensitivity in these areas. Our data has shown for the first time that rod PRs were absent from the pigeon fovea, but comprised 20% of the PR

population in the red and yellow fields. The absence of rod photoreceptors in the fovea suggests that a rod circuitry is not present in this area. In contrast, there is a possibility that a rod circuitry is in place in the *area dorsalis*, which conveys output signals from rod photoreceptors to second and third order neurons in the retina. Furthermore, because rod photoreceptors are highly sensitive to low light levels and scotopic sensitivity decreases in the foveal area of the rhesus monkey retina (Crawford, 1977), the lack of rods of the pigeon fovea may also produce a low measurement of scotopic sensitivity. Compared with the fovea, scotopic sensitivity might be better in the *area dorsalis* and the surrounding peripheral region as the density of rod photoreceptors is greater. An investigation into the relationship between scotopic sensitivity and rod density would be valuable in testing this hypotheses.

The presence of rods in the two high acuity areas also implies that rods do not preclude high visual acuity *per se*. The lack of rods in the primate fovea was argued to increase acuity because the high degree of spatial summation caused by the rod circuit was missing (Freed et al., 1987a; Sterling et al., 1988a). Without the rods, the cones were able to pack together at higher density. Because visual acuity was usually measured in photopic conditions when the rods were less active, their contribution to acuity was minimal. In the pigeon, the behaviorally measured acuity of the fovea and the *area dorsalis* were similar: 12.6 cycles/degree (fovea) versus 12.8 cycles/degree (*area dorsalis*) (Hodos *et al*., 1991), although these values were variable depending on the method used, the age of the bird, and the viewing distance. The density of cones in the *area dorsalis* was slightly lower compared with the fovea, but was significantly higher compared with cone densities in the yellow field. Our data indicated that the presence of rods did not significantly interfere with packing of cones in the *area dorsalis* compared to the fovea. The higher cone densities and cone packing in the fovea

and *area dorsalis* are perhaps more important determinants in achieving high spatial acuity.

The PR:RGC ratios calculated in this paper were based on densities after correction factors for rods and non-RGCs in the GCL were applied. Previous reports of lizard and bird PR and RGC counts provided an overall density of cells in the ONL and GCL. In order to compare the data presented in the current study with previous results, our pigeon PR:RGC ratios were recalculated without the correction factors and compared with other foveate species (Table 3.2) (Fite and Rosenfield-Wessels, 1975; Fite and Lister, 1981; Curcio and Allen, 1990; Collin et al., 2000). Among animals that contain a temporal fovea/*area dorsalis*, the Blue jay and sparrow hawk had PR:RGC ratios higher than the pigeon, the red tailed hawk PR:RGC ratio was similar to the pigeon, while all other PR:RGC ratios in animals with a temporal fovea/*area dorsalis* were lower than the pigeon (Table 3.2). In the central fovea, the pigeon PR:RGC ratio was most similar to the sparrow hawk , the sunbird, and *A. equestris*. The nuthatch, *A. cuvieri*, *A. cristatellus* and *A. distichus* all had much lower PR:RGC ratios in the central fovea (Fite & Rosenfield-Wessels, 1975; Fite & Lister, 1981). Birds of prey such as the red tailed hawk, the goshawk, and Least Tern showed much higher PR:RGC ratios compared with the pigeon in the central fovea (Fite & Rosenfield- Wessels, 1975). The highest PR:RGC ratio in the central fovea for any animal was reported in the deep sea fish *C. macroptera* (Collin *et al*., 2000). Therefore, low convergence ratios are a common feature of the fovea and *area dorsalis* in many species, not just the pigeon. This type of circuitry may be one of the fundamental ways that allows these specialized areas of the retina to mediate high visual acuity. In addition, the convergence ratios indicate that the limit of acuity is not at the level of cone photoreceptors, but at the RGC level.

The foveal PR:RGC ratio in humans is 1:3 (Table 3.2), which in conjunction with the midget system is the basis for high acuity (Boycott and Dowling, 1969; Curcio and Allen, 1990; Boycott and Wässle, 1999). Whether the pigeon retina contains a synaptic arrangement similar to the primate midget system is still an open question. Using the Golgi method, Lockhart (1979) showed midget-like bipolar and RGCs with relatively small dendritic fields in both the pigeon fovea and red field although their morphology was not completely analogous to that of the primate midget system. Mariani (1987) identified eight different types of bipolar cells in the pigeon retina, including one that resembled a primate midget bipolar cell. The smallest bipolar cell dendritic fields were small enough to mediate a one-to-one PR/bipolar contact (Lockhart, 1979). The dendritic field sizes of RGCs indicated that one-to-one contact between bipolar and RGCs was unlikely. Quesada *et al*. (1986) arrived at a similar conclusion after identifying midget-like bipolar cells in the chicken retina.

The third finding is that two high acuity areas can have similar PR and RGC densities, but different functions. The fovea was capable of resolving distant spatial detail in the lateral visual field as well as detecting motion (Bloch and Martinoya, 1982; Martinoya et al., 1983). In contrast, the *area dorsalis* was shown to be myopic in the frontal vision and was only capable of detecting static objects (Bloch and Martinoya, 1982; Martinoya et al., 1983; Hodos and Erichsen, 1990). Given that the *area dorsalis* or red field is used for binocular vision, one would expect a squared visual acuity for this area. However, behavioural acuity measurements reveal that the fovea and the red field have similar visual acuities of about 12 cycles/degree (Hodos et al., 1991; Hahmann and Güntürkün, 1993; Rounsley and McFadden, 2005). The most likely purpose of the *area dorsalis* is for locating food on the ground, such as small grains, which requires acute resolution. Nalbach *et al*. (1990) estimated that the visual field

subserved by the *area dorsalis* was located in the fronto-ventral quadrant of the visual hemisphere 45° below the horizon, which was ideally positioned to view the visual field below the beak. Because the pecten was oriented 45° from the horizon in a normal resting head position (Nalbach *et al*., 1990), our maps were rotated by 45°. The predicted location of the *area dorsalis* was close to the highest density of cones and RGCs. The lowest information convergence in the red field was between 30° and 60° dorsal to the horizontal meridian in the temporal retina.

In addition to a fovea and an *area dorsalis*, our topographic maps revealed a visual streak intersecting the fovea in the horizontal meridian, a common feature in many mammals, including cats, rabbits, rats, pigs, monkeys and humans (Stone, 1965; Provis, 1979; Packer *et al*., 1989; Curcio *et al*., 1990; Garciá *et al*., 2005; Salinas-Navarro *et al*., 2009). The presence of a visual streak and an *area centralis* was hypothesized to be a reflection of the lifestyle, habitat, and feeding habits of terrestrial animals (Hughes, 1977). It is possible that the visual streak is used for not only in maintaining flight along the horizon, but also for detecting predators approaching on the ground or in the air, as in ground-dwelling mammals.

3.5 Conclusions

The present study provided insights into the different but equally effective ways of mediating high acuity. One of the important factors that may contribute to mediating high visual acuity by the fovea and the *area dorsalis* is significantly higher cone PR and RGC densities and low cone PR to RGC convergence. Importantly, the pigeon retina showed a proof of principle that high acuity can be achieved without a foveal depression and in the presence of rods. The study has also identified an important difference between the fovea and the *area dorsalis*, which suggests that the remaining

parts of the rod circuitry are present in the *area dorsalis*, but not in the fovea. This study provided the framework for future studies investigating the development of circuitry of two high acuity regions, the central fovea, analogous to the human fovea, and the non-foveate *area dorsalis*.

Acknowledgements

Angeliza Querubin, Keely Bumsted O'Brien and Hie Rin Lee carried out the cell counting, capture cell images and conducted the experiments. Angeliza Querubin did the topographical mapping of the photoreceptor and ganglion cell densities and the cone to ganglion cell ratios in the four retinas. Angeliza Querubin and Keely Bumsted O'Brien generated the figures and tables in the paper and carried out the data analysis. Keely Bumsted O'Brien and Jan M Provis provided advice on the methodology. All four authors co-wrote the paper.

Chapter 3 figures & tables

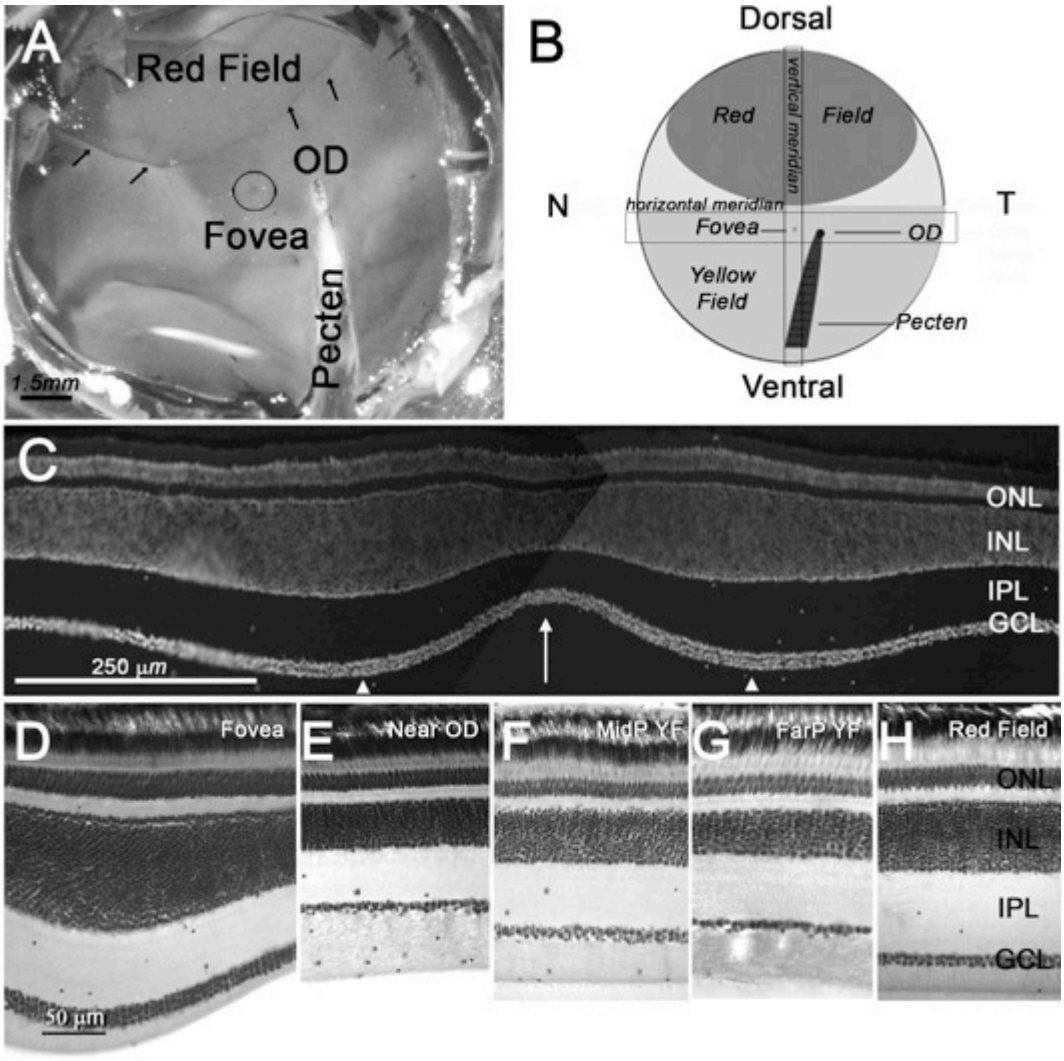

Figure 3.1.

Figure 3.1. The Adult Pigeon Retina. A) View of the pigeon retina in an open eye cup with the cornea and lens removed. The red field, the margins indicated by the arrows, is located dorsally. The optic disc (OD) is located at the dorsal tip of the pecten. The fovea (circled) is located nasal to the OD. A fold in the retina is visible near the pecten - this is an artefact. B) Schematic representation of a pigeon retina. The fovea (circled) is centred on the horizontal and vertical meridians (boxed areas). The outer nuclear layer (ONL), inner nuclear layer (INL), inner plexiform layer (IPL), and ganglion cell layer (GCL) are indicated. C) Adult pigeon foveal section, cell nuclei stained with DAPI. The arrow indicates the centre of the fovea and the arrowheads indicate the foveal slope. D-H) Nissl-stained cross-sections of the adult pigeon retina at different retinal eccentricities, the Fovea (D), Near the OD (E), mid peripheral yellow field (MidP YF; F), far peripheral yellow field (FarP YF; G), and the Red Field (H).

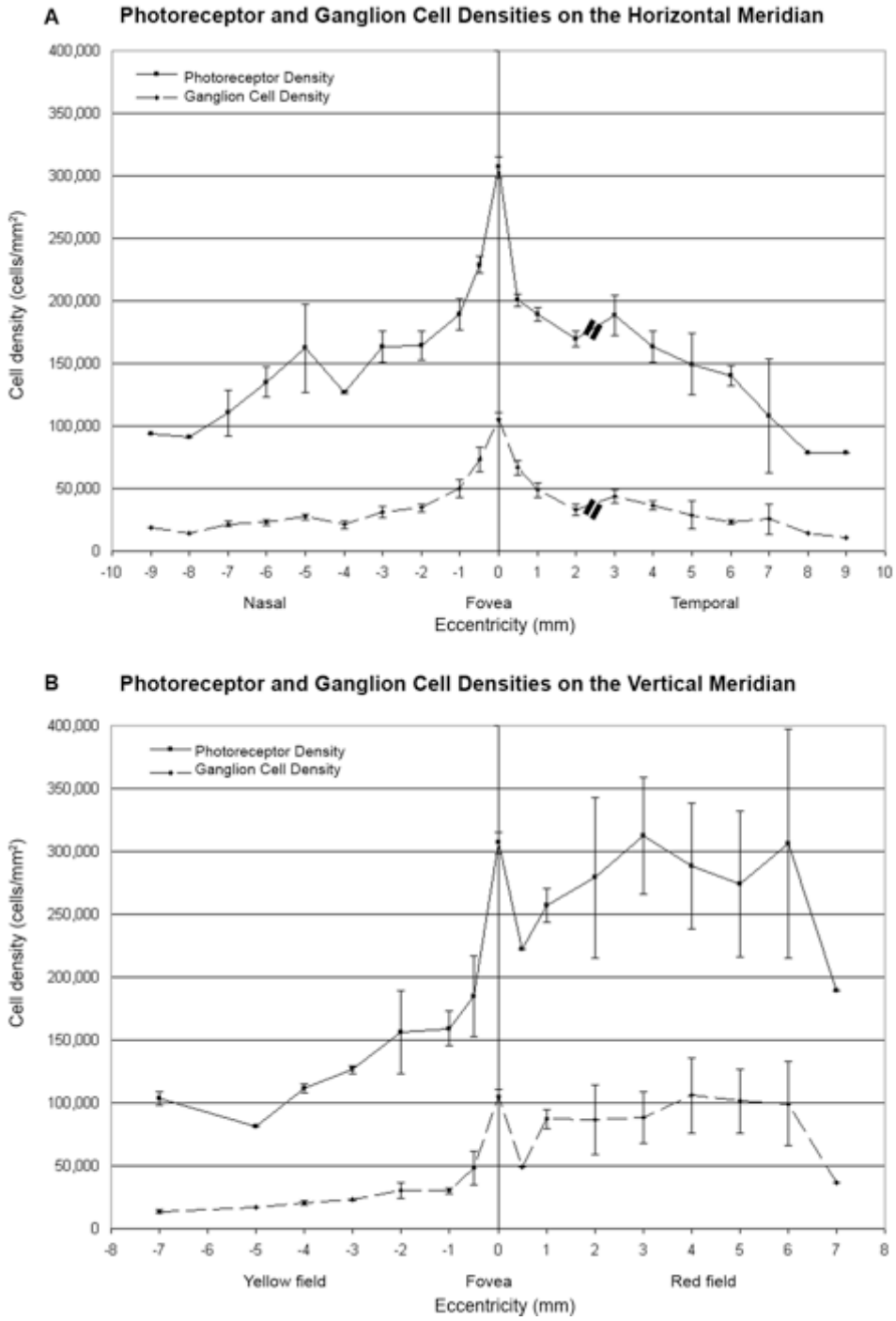
A
Photoreceptor and Ganglion Cell Densities on the Horizontal Meridian
Photoreceptor Density
Ganglion Cell Density
Cell density (cells/mm²)
400,000
350,000
300,000
250,000
200,000
150,000
100,000
50,000
0
-10 -9 -8 -7 -6 -5 -4 -3 -2 -1 0 1 2 3 4 5 6 7 8 9 10
Nasal
Fovea
Temporal
Eccentricity (mm)
B
Photoreceptor and Ganglion Cell Densities on the Vertical Meridian
Photoreceptor Density
Ganglion Cell Density
Cell density (cells/mm²)
400,000
350,000
300,000
250,000
200,000
150,000
100,000
50,000
0
-8 -7 -6 -5 -4 -3 -2 -1 0 1 2 3 4 5 6 7 8
Yellow field
Fovea
Red field
Eccentricity (mm)

Figure 3.2.

Figure 3.2. Graphs of photoreceptor and ganglion cell densities in the horizontal and vertical meridians. A) The mean densities of photoreceptors (n = 10) and ganglion cells (n = 4) +/- standard error of the mean (SEM) are plotted across the horizontal meridian. The optic disc is temporal to the fovea (two black bars). B) The mean densities of photoreceptors (n = 10) and ganglion cells (n = 4) +/- SEM was plotted across the vertical meridian.

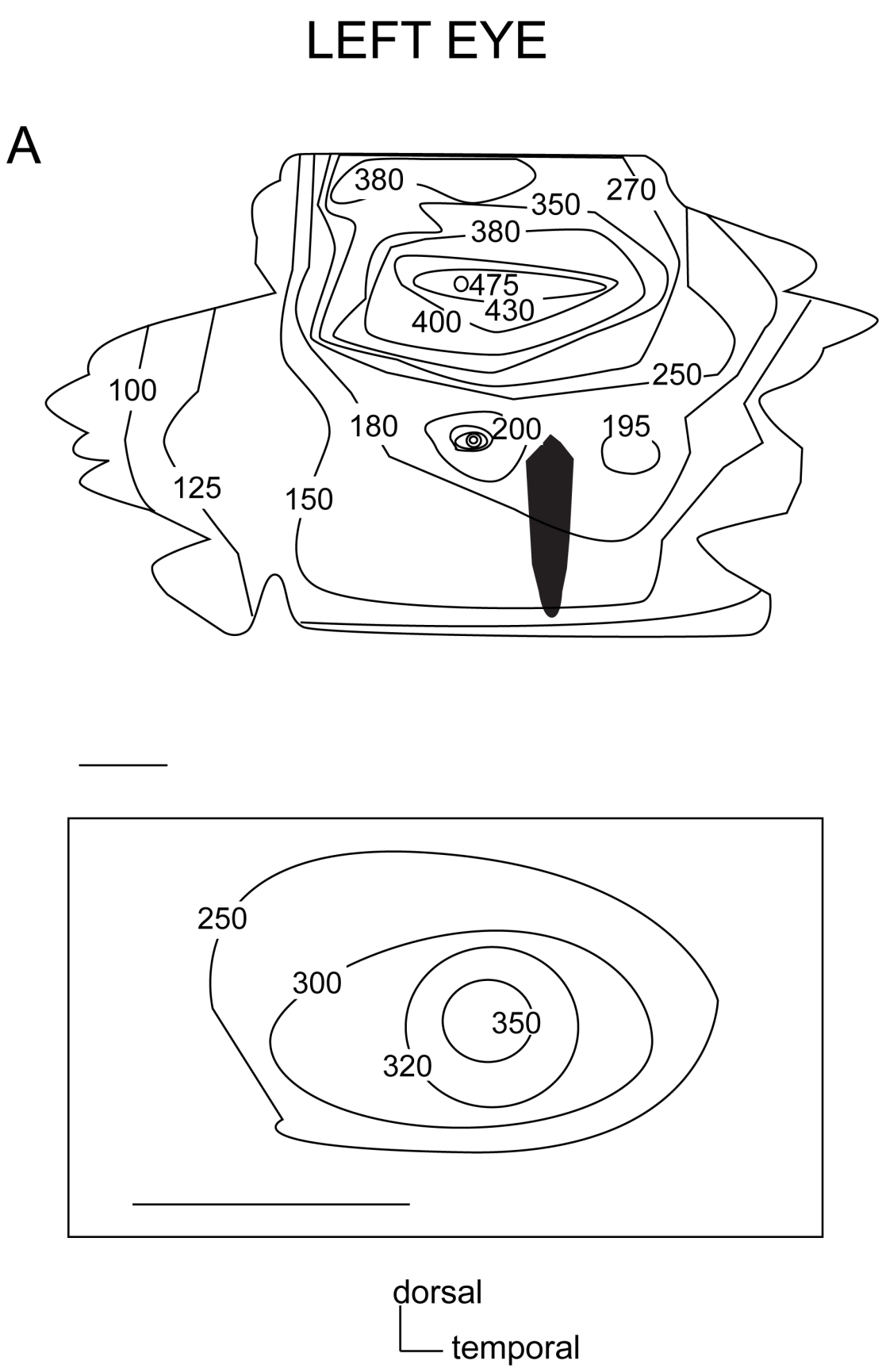
LEFT EYE
A
380
350
270
380
475
430
400
250
100
180
200
195
125
150
250
300
350
320
dorsal
temporal

Figure 3.3A.

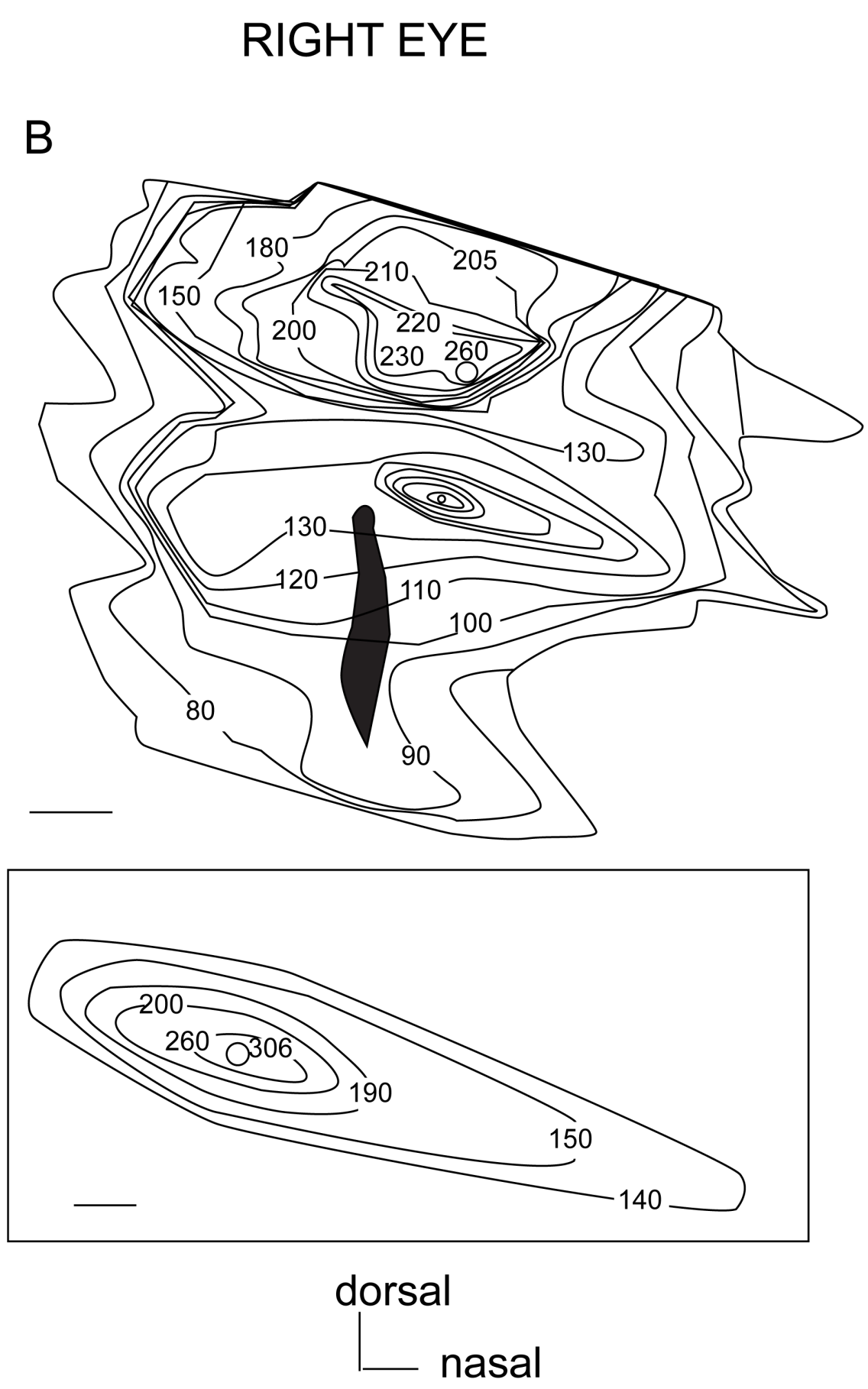
RIGHT EYE
B
180
205
210
150
220
200
230
260
130
130
120
110
100
80
90
200
260
306
190
150
140
dorsal
nasal

Figure 3.3B.

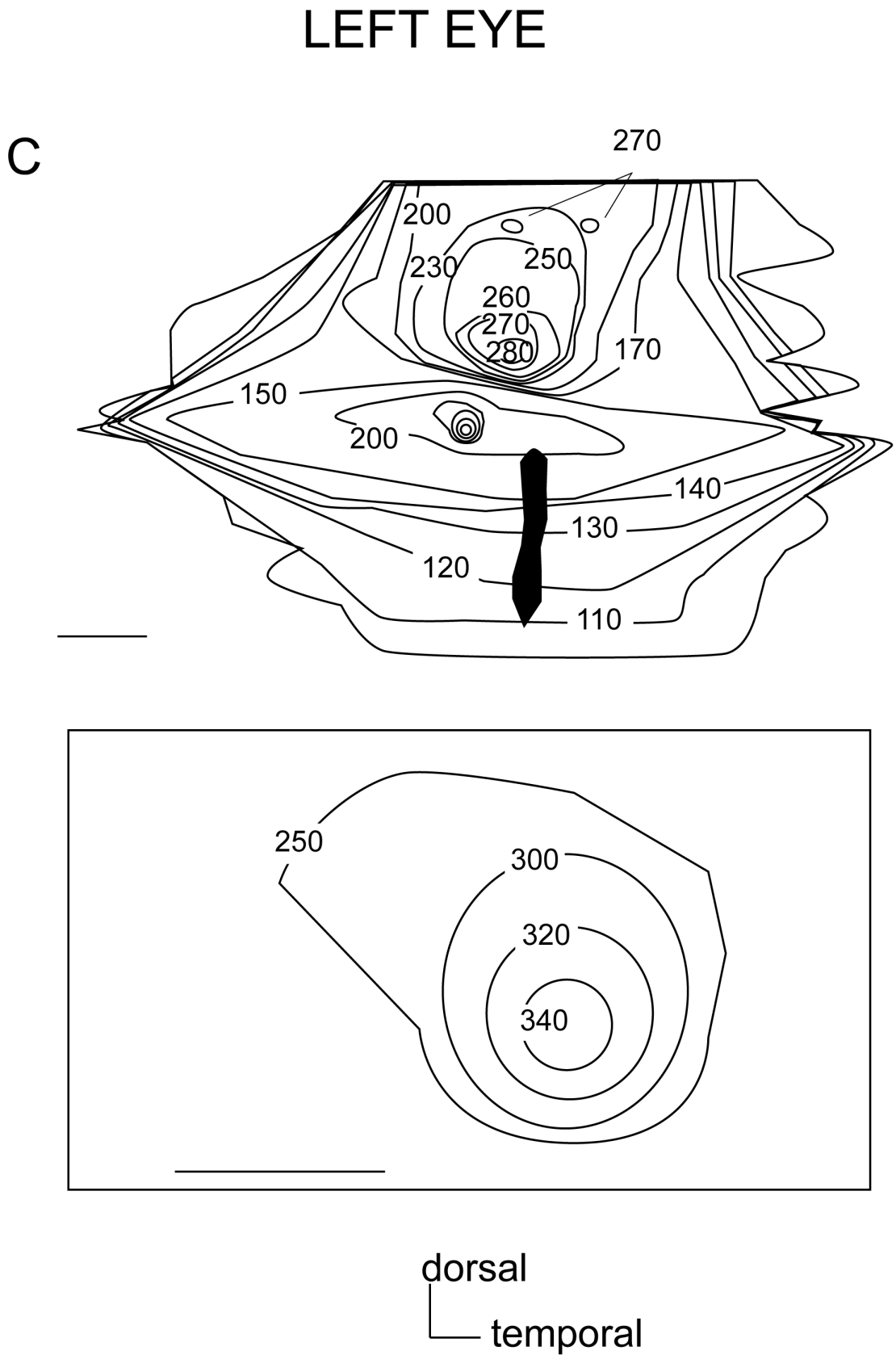
LEFT EYE
C
270
200
230
250
260
270
280
170
150
200
140
130
120
110
250
300
320
340
dorsal
temporal

Figure 3.3C.

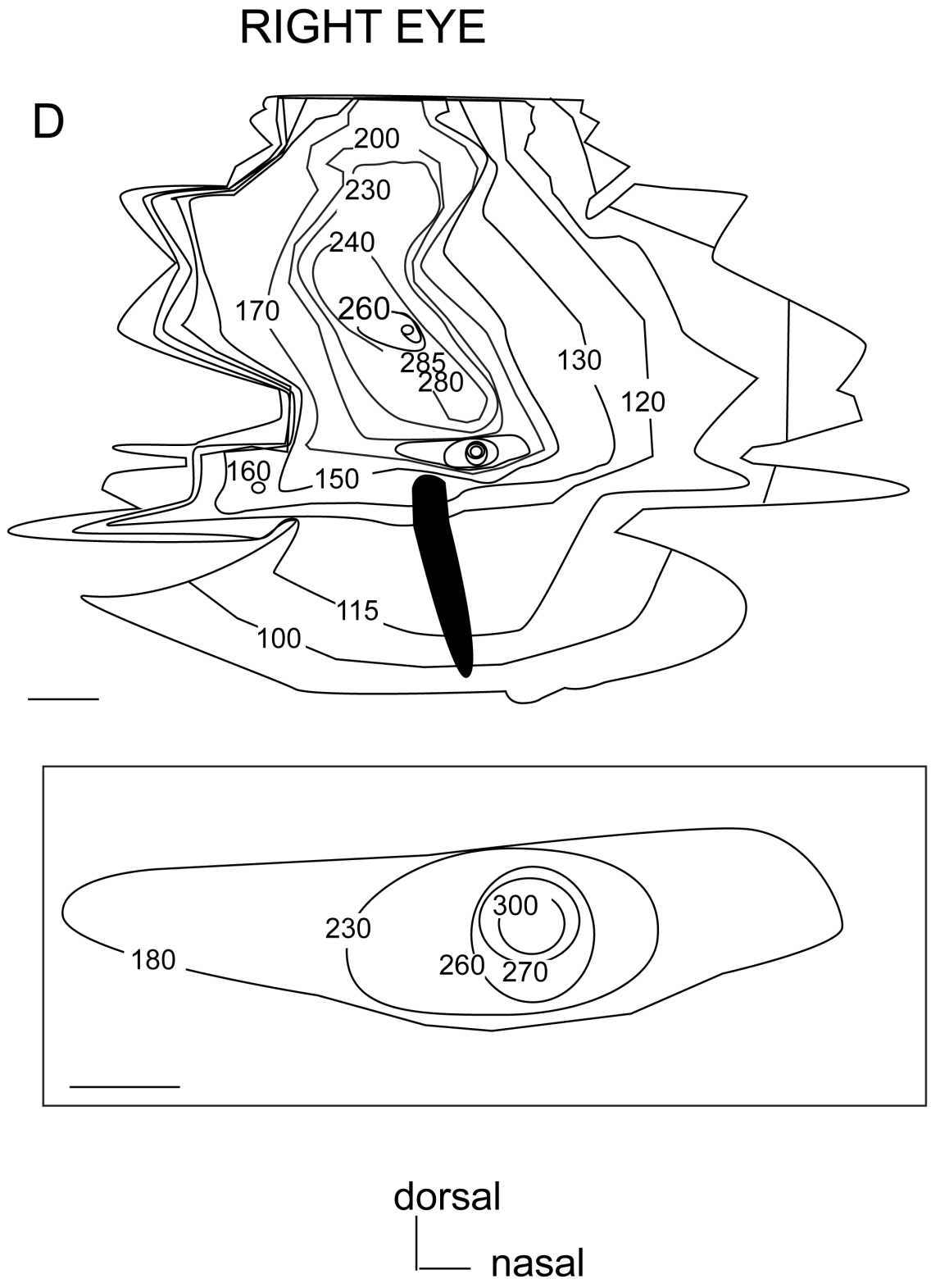
RIGHT EYE
D
200
230
240
170
260
285
280
130
120
160
150
115
100
300
230
180
260
270
dorsal
nasal

Figure 3.3D

Figure 3.3: Topographic maps showing the photoreceptor densities across the pigeon retina in four eyes from different pigeons (two left eyes (A, C) and two right eyes (B, D)). The isodensity lines below the map are enlarged views of the foveal region (A'-D'). Dorsal is oriented towards the top of the page, with the nasal and temporal orientation is indicated for each column. The numbers must be multiplied by 1000 to obtain cell density (cells/mm^2). The pecten is indicated by a black filled area in the ventral retina. Scale bars for A-D= 2 mm; A'-D' = 500 μm.

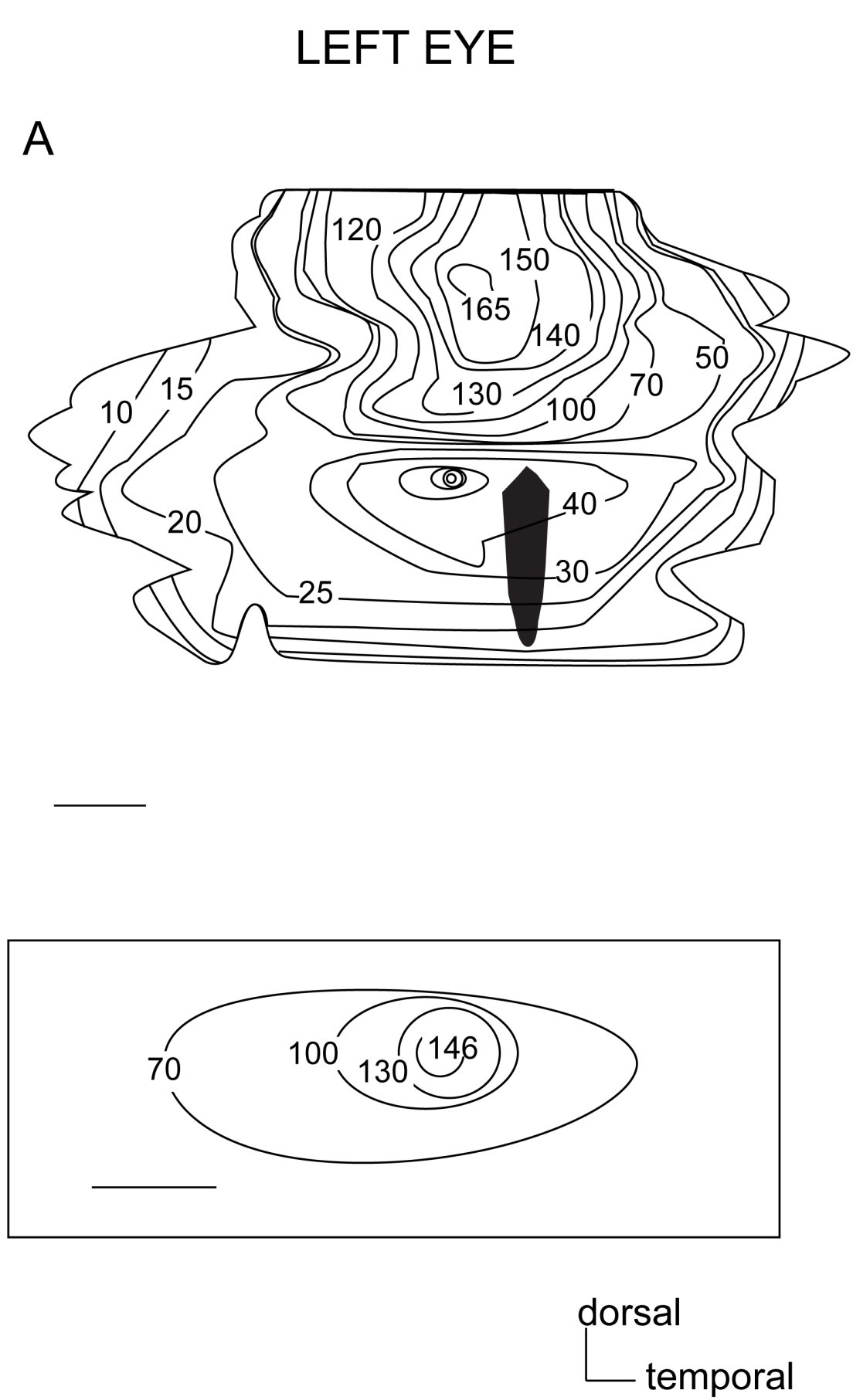
LEFT EYE
A
120
150
165
140
50
15
10
130
70
100
40
20
30
25
70
100
130
146
dorsal
temporal

Figure 3.4A.

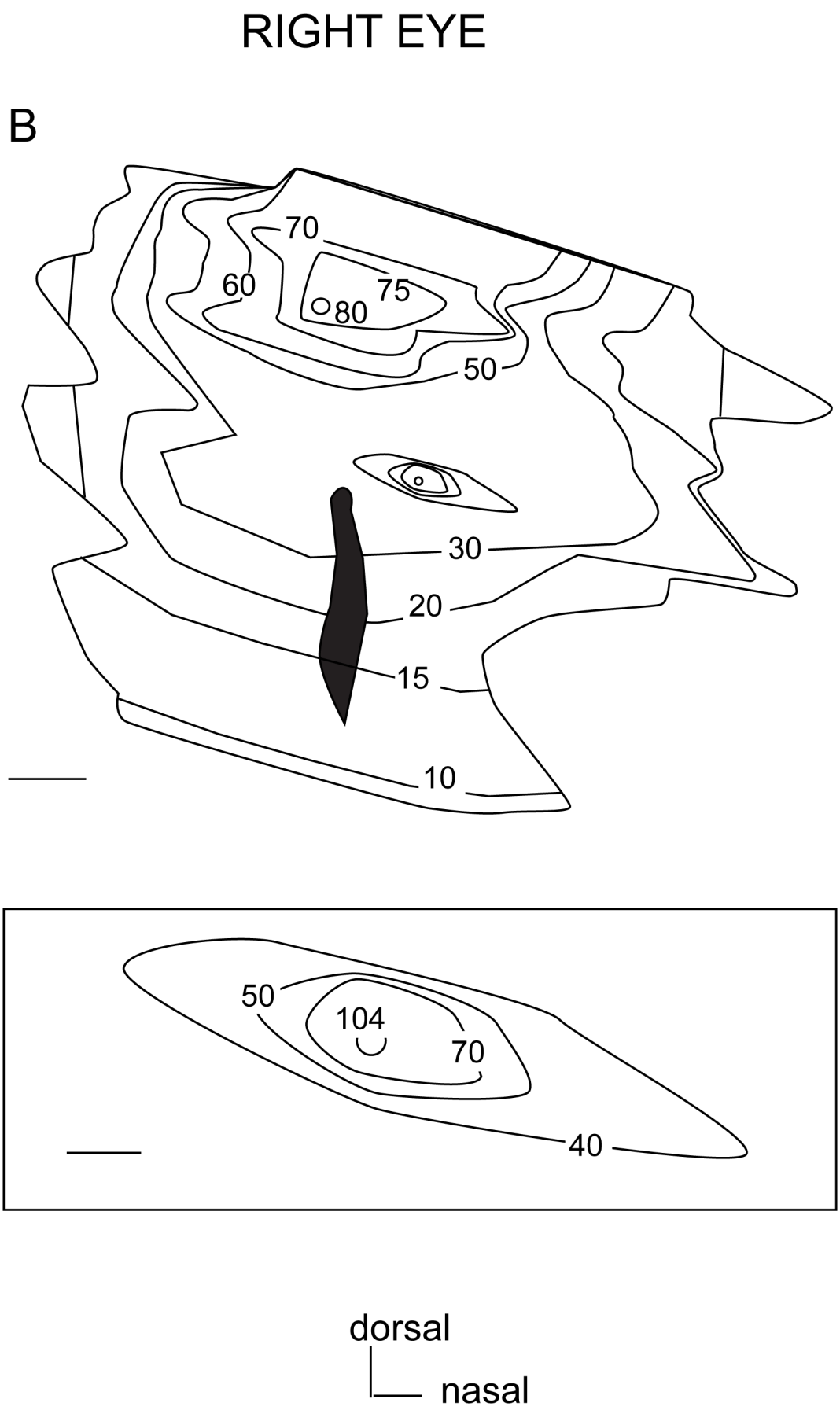

Figure 3.4B.

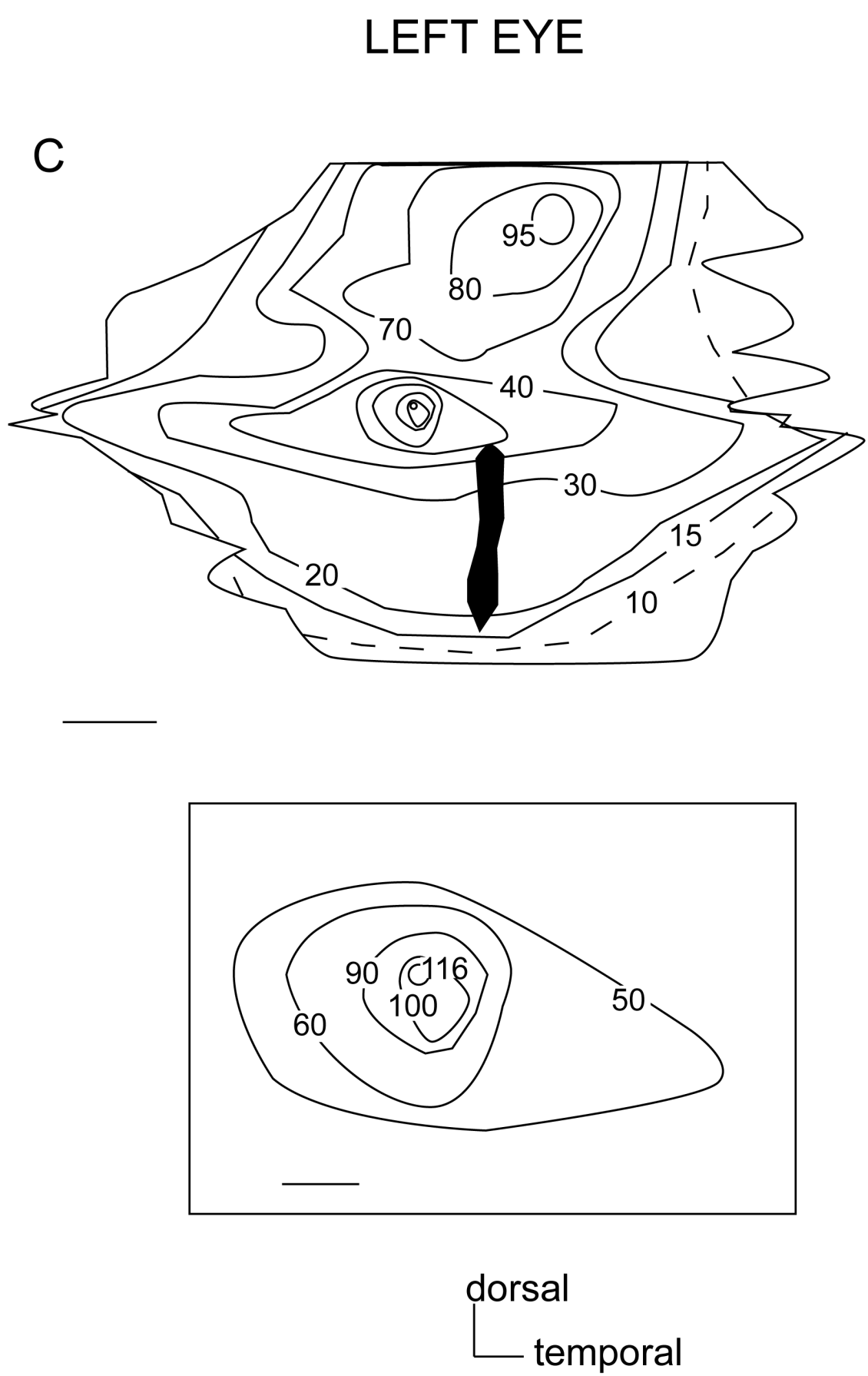
LEFT EYE
C
95
80
70
40
30
15
20
10
90
116
100
60
50
dorsal
temporal

Figure 3.4C.

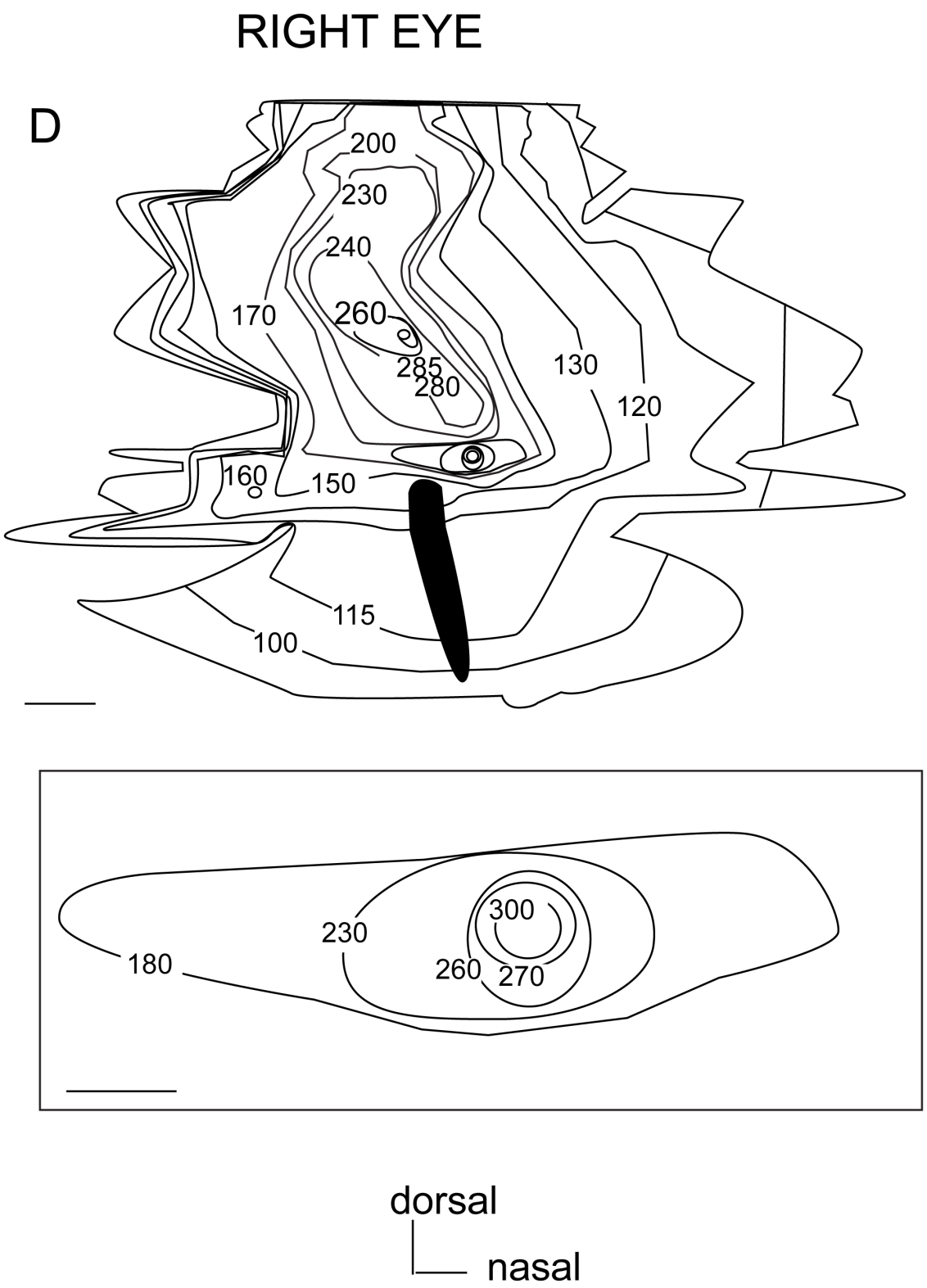
RIGHT EYE
D
200
230
240
170
260
285
280
130
120
160
150
115
100
300
230
180
260
270
dorsal
nasal

Figure 3.4D.

Figure 3.4: Topographic maps of ganglion cell densities in four pigeon retinas. The maps correspond to the photoreceptor maps in Figure 3.3. The isodensity lines below the maps are enlarged views of the foveal region showing a steep cell density gradient (A'-D'). The numbers must be multiplied by 1000 to obtain cell density (cells/mm^2). The pecten is indicated by a black filled area in the ventral retina. Dashed isodensity lines in C represent an estimate of where similar density would be found. Scale bars A-D = 2 mm; A'-D' = 500 μm.

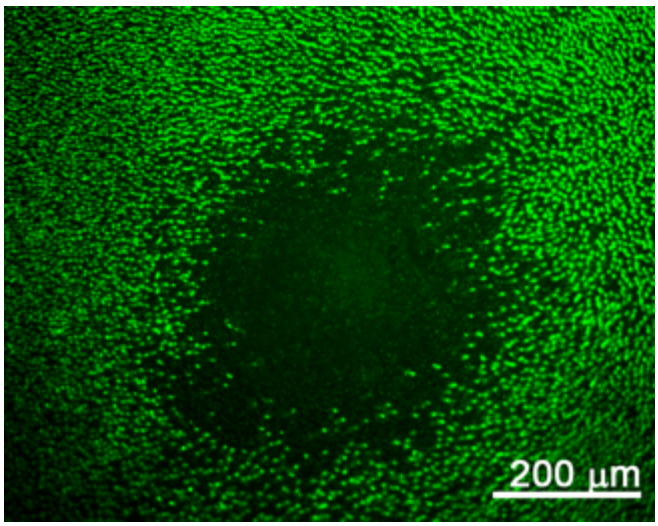

Figure 3.5. Rod photoreceptor outer segment distribution in the fovea of an isolated pigeon retina. Image of fovea stained with rod opsin antibody. Note rod-free area.

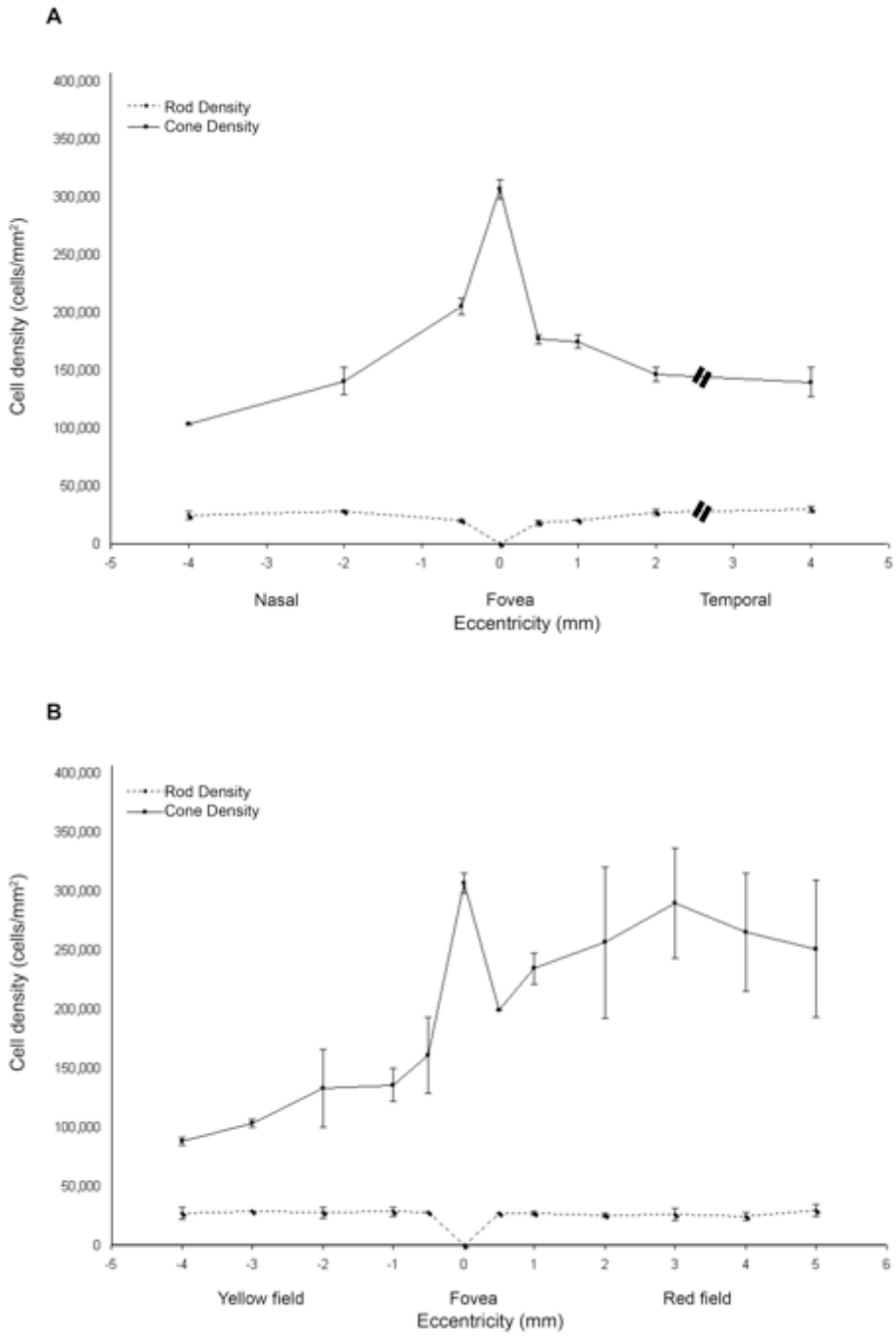

Figure 3.6: Graphs of cone and rod photoreceptor densities along the horizontal and vertical meridians. A) The mean densities of cones and rods +/- SEM were plotted along the horizontal meridian. The optic disc is temporal to the fovea (two black bars). B) The mean densities of cones and rods +/- SEM were plotted across the vertical meridian.

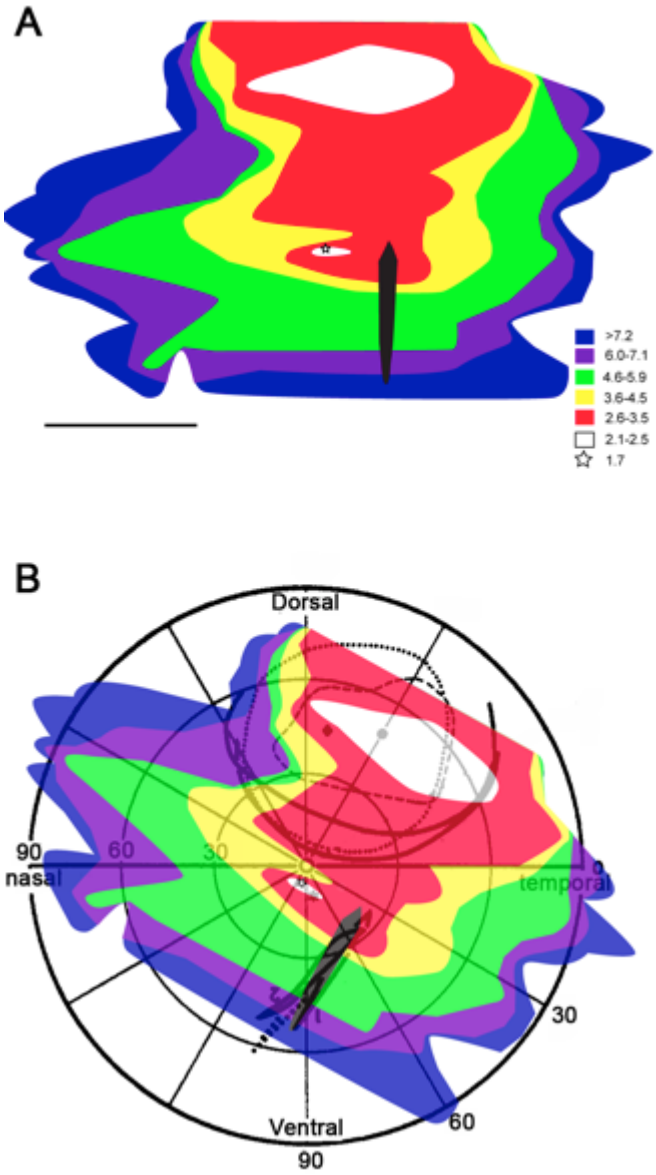

Figure 3.7. Summary of cone photoreceptor to ganglion cell convergence ratios. A). The ratio of cone photoreceptors to ganglion cells was colour-coded to show local difference in convergence. The white and coloured areas indicate the lowest convergence of photoreceptor to ganglion cells. The cooler colours, going towards blue, indicate a greater degree of convergence, leading to higher ratios. B) The colour-coded map was rotated 25 ° and overlaid on a map of visual space (adapted from (Nalbach *et al*., 1990)). Scale bar = 4 mm.

Table 3.1. Summary of Mean Cell Density (Mean ± SEM (cells/mm^2))

	PR (n^ = 10)	**RGC (n^ = 4)**	**Rods**	**Cones**
Fovea	326,961† ± 10,645	110,317 ± 7,872	0	302,541
Area dorsalis	312,807 ± 46,551	88,395 ± 20,434	26,245 ± 4,898	289,982
Red Field	238,693 ± 21,727	73,811 ± 15,657	26,694 ± 1133	214,750
Yellow Field	184,802 ± 5,953	38,692 ± 2,883	22,101 ± 1136	160,126

† PR densities in the fovea are statistically significantly higher compared to the red and yellow fields, but not the *area dorsalis*.

^ The number of eyes is denoted by n.

* RGC densities in the fovea are statistically significantly higher compared to the *area dorsalis*, red and yellow fields.

Table 3.2. Summary of PR to RGC Ratios in Different Species

Species	**Ratio in Central Fovea**	**Ratio in Temporal Fovea/*Area dorsalis***
Pigeon (*C. livia*) †	2.6:1	3.5:1
Red-tailed hawk (*B. jamaicensis*) ‡	3.4:1	3.5:1
Goshawk (*A. gentilis*) ‡	5.1:1	6.6:1
Sparrow hawk (*F. sparverius*) ‡	2.8:1	11.0:1
Blue jay (*C. cristata*) ‡	3.6:1	-
Least Tern (*S. albifrons*) ‡	5.9:1	2.4:1
Nuthatch (*S. carolinensis*) ‡	1.2:1	-
Sunbird (*N. chalypea*) ‡	2.0:1	-
Anolis cuvieri#	1.8:1	1.2:1
Anolis equestris#	3.0:1	1.3:1
Anolis cristatellus#	1.4:1	1.4:1
Anolis carolinensis#	1.1:1	1.5:1
Anolis distichus#	1.2:1	1.0:1
C. macroptera§	13:1	-
Rhesus (*M. mulatta*)‡	5.3:1	-
Human	1:3	-

† All photoreceptor densities, including rod density, were divided by the density of cells in the GCL without the correction factor.

‡ Some birds have central and temporal foveas, and others only have a central fovea.

Anolis lizards have central and temporal foveas. Ratios were calculated from the average cell densities/visual degrees^2 data.

§ Deep sea fish have a temporal fovea where the ganglion cells are displaced to the perifoveal region. The ratio of PR to RGC in this species is of the perifoveal region.

† Total foveal and *area dorsalis* PR densities (including rod density) were divided by GCL density (calculated without a correction factor).

‡ Bird foveas (Fite & Rosenfield-Wessels, 1975).

Anolis lizards (Fite & Lister, 1981).

§ Deep sea fish (Collin *et al*., 2000)

^ (Curcio and Allen, 1990)

Chapter 4 – Morphological Classification of Bipolar Cells in the Adult Pigeon Retina

Abstract

High acuity vision in primates is mediated by well-characterised midget bipolar and ganglion cells. It is an open question whether pigeons, which have two areas of high acuity, contain midget-like bipolar cells. Previous descriptions of pigeon bipolar cells identified 8 basic types, but the bipolar cells were only sampled from the red field. In this study, bipolar cells were classified in the fovea, the central red and central yellow fields and sought to identify a midget-like bipolar cell. Bipolar cells were labelled with DiO using the Diolistics delivery method. Eight bipolar cell types were classified in the retina using a modification of Mariani's (1987) classification scheme. Eight of these bipolar cell types (B1 – B8) had similar dendritic morphology to the ones described by Mariani. Two bipolar cell types, B7 and B8, had comparatively smaller dendritic fields than the other types in the fovea and the central red field respectively. Both B7 and B8 bipolar cell types were estimated to possibly receive input from at least one photoreceptor in the fovea and the central red field. Based on the dendritic field size and estimated lower information convergence from photoreceptors to bipolar cells, B7 and B8 may be good candidates for being the midget-like bipolar cells in the pigeon retina.

4.1 Introduction

The retina processes and transmits signals to the brain, which encodes various aspects of the visual scenery such as colour, motion, contrast, depth, distance, fine spatial detail, form and direction. Once the light is converted to an electrochemical signal by the photoreceptors, information is transmitted to the bipolar cells through a synapse. Depending on which glutamate receptor is expressed by the bipolar cells (Nakajima et al., 1993; Vardi et al., 1993; Nomura et al., 1994; Vardi, 1998; Qin and Pourcho, 1999), the different types of bipolar cells are able to respond differently to the output signals of photoreceptors (Slaughter and Miller, 1981; Masu et al., 1995; DeVries and Schwartz, 1999; DeVries, 2000; Awatramani and Slaughter, 2001).

Various morphological bipolar cell types have been classified in a number of retinas, such as the rabbit (Strettoi et al., 1990; Mills and Massey, 1992; Jeon and Masland, 1995; Strettoi and Masland, 1995; Brown and Masland, 1999; MacNeil et al., 2004), rat (Euler and Wässle, 1995); mouse (Ghosh et al., 2004; Pignatelli and Strettoi, 2004; Wässle et al., 2009); ground squirrel (Puller et al., 2011); cat (McGuire et al., 1984; Cohen and Sterling, 1990); zebrafish (Li et al., 2012) and primates (Boycott and Dowling, 1969; Kolb, 1970; Mariani, 1981; 1983a; Mariani, 1984; Boycott and Wässle, 1991; Chan et al., 2001a). Classification of bipolar cells in mammals was based on several morphological parameters, but the most common parameters used were dendritic branching pattern, dendritic field size, and axon stratification in the IPL. Knowledge of the various bipolar cell type morphologies has provided us with some insight into the way information is passed from photoreceptors to bipolar cells and then onto the RGCs in the mammalian retina. Given that there are several morphological types of neurons in the retina, it appears that parallel processing begins early in the visual neurocircuitry (Strettoi et al., 2010).

The number of photoreceptor inputs onto a bipolar cell is influenced partly by bipolar dendritic field size, with smaller fields receiving fewer inputs than wider fields. Indeed, there is a bipolar cell, termed the midget, which has small dendritic fields (~5 μm in diameter) narrow enough to receive input from one cone photoreceptor (Boycott and Dowling, 1969; Kolb, 1970). In turn, the midget bipolar contacts one midget ganglion cell (Polyak, 1941; Kolb and Dekorver, 1991; Calkins et al., 1994; Kolb and Marshak, 2003). Because a midget ganglion cell receives from one cone in the primate fovea, the visual information transmitted from the photoreceptors to the RGCs retains high spatial resolution.

It would be a useful starting point for determining the anatomical basis of a midget circuitry to characterise the morphology of a bipolar cell type and compare it with the primate midget cell. Previous studies have provided some evidence based on bipolar cell morphology to support the claim of a similar midget circuitry existence in birds (Lockhart, 1979; Quesada et al., 1986; Mariani, 1987; Quesada et al., 1988). In the chicken retina, a presumptive bipolar cell was classified with a dendritic field width of 3–5 μm (Quesada et al., 1986; Quesada et al., 1988), which is comparable to that of the primate midget bipolar cell. In the two areas of high cell densities, the fovea and the red field, in the pigeon retina, Lockhart (1979) and Mariani (1987) identified a 'midget-like' bipolar cell type with a dendritic field size similar to that found in the chicken and primate retinas. However, the number of photoreceptor inputs feeding into the midget-like bipolar cell in the avian retina was not determined.

Chapter 3 showed that the areas in the pigeon associated with high visual acuity have a much higher density of photoreceptors and RGCs compared with the peripheral retina (Galifret, 1968; Binggeli and Paule, 1969; Querubin et al., 2009). The high acuity regions were estimated to have the least convergence from photoreceptors to RGCs

(2.5:1) (Querubin *et al*., 2009). The amount of convergence or divergence in the visual processing pathway from the photoreceptors to the bipolar cells and then to the ganglion cells may be affected by a number of factors, including cell density, neuronal type, dendritic field size, axon terminal size, synaptic density, and so on. Galifret (1968) reported that the number of cells in the INL is about nine times the number of RGCs and about eight times the number of photoreceptors in the fovea and red field. From this data, one would expect that a large amount of information convergence may occur from the INL to the GCL.

Although the morphological bipolar cell types in the pigeon red field have been classified (Mariani, 1987), it is uncertain whether the bipolar cell types found in the red field were also distributed throughout the retina, particularly in the fovea and the central yellow field. The current study classified the bipolar cell types in the central red and yellow fields and in the fovea. Bipolar cells were morphologically characterised using a modification of the classification scheme of Mariani (1987) using the DiOlistics technique. A total of eight morphological bipolar cell types were classified similar to that reported by Mariani. In addition, the estimated amount of convergence between photoreceptors and bipolar cells has been calculated in the two high cell density areas to determine the degree of convergence. Based on the dendritic morphology of the bipolar cells and the number of photoreceptor inputs, not one, but two candidate midget bipolar cells were identified in the pigeon retina.

4.2 Methods and materials

Tissue collection and processing

Twelve adult pigeons (*Columba livia*) of both sexes were obtained from a pigeon farm in New South Wales, Australia. Ethical approval for the current study was obtained from The Australian National University Animal Ethics committee.

The pigeons were euthanized by an intraperitoneal injection of 2-3 mL of Lethabarb (33 mg/kg) with Lignocaine (20 mg/mL). Once corneal and pain reflexes were lost, the pigeon was decapitated and the eyes enucleated. The eyes (n = 16) were dissected in Dulbecco's Modified Eagle Medium (1x DMEM) with high D-glucose and L-glutamine (GIBCO, Cat # 11995065) bubbled with carbogen (95% O_2/5% CO_2). Dissection involved removal of the anterior chamber, vitreous, sclera, choroid, and retinal pigment epithelium. The pecten was trimmed to ease flattening the tissue. Two punch biopsies were taken from each retina: one containing the fovea and the central yellow field surrounding the fovea; and another from the centre of the red field. The punch biopsy was 5 mm in diameter. The retina was immersed in DMEM, which was bubbled continuously with carbogen.

A 20 mL solution of 2% agar was dissolved in 18 mL DMEM and 2 mL deionised water (dH_2O), heated to 40°C while stirring, and poured into a small Petri dish (~ 2 mm diameter). The punched retinas were then immediately placed within the molten agar and arranged vertically straight as possible by holding the edges of the retina with forceps before it solidifies. Two to three retinas could be aligned straight adjacent to each other in the agar. After the agar had solidified, the excess agar was trimmed off with a razor to form the remaining agar into a cube. This cube was affixed with a strong adhesive onto the vibratome stage in which the retinas were aligned

perpendicular to the blade. The stage was filled with DMEM and surrounded with ice. The retinas were sliced at a thickness of 200 μm that showed the cross-section of the retina. Each slice was placed on top of a filter paper and immersed in DMEM until Diolistics bombardment. Only the retinal slices were used in the Diolistics labelling of bipolar cells. Wholemount retinas were not used in the bipolar cell type investigation.

Diolistics labelling

The Diolistics labelling procedure was modified from Sun and co-investigators' (2002) protocol. Dye-coated tungsten particles were prepared as follows. Thirty mg of tungsten particles (M-17, Bio-Rad, 75054) were spread evenly onto a microscope slide with a few drops of methylene chloride. Approximately 3 mg of DiO (Invitrogen, D275) crystals were dissolved in 100 μL of methylene chloride and applied to the tungsten particles. Once dried, the DiO-coated tungsten particles were scraped into a 13 mL falcon tube using a razor blade and suspended in 5 mL of dH_2O. The tungsten solution was vortexed at maximum speed for 10 minutes. Between 3 and 10 μL of the dye-coated tungsten solution was applied on macrocarrier discs and air-dried in the dark for a day. The tube and macrocarrier discs containing dye-coated tungsten solution were stored in the dark at 21-25 °C.

Macrocarrier discs containing tungsten particles were placed 2 cm away from a 450 psi (Bio-Rad, 165-2326) rupture disc in a PDS-1000/He System, BIORAD gene gun chamber. The retina slices were removed from DMEM by using forceps to hold the filter paper and laid flat in a Petri dish with the retina facing up. The chamber was vacuumized (20–25 Hg/mm) before Helium gas was released at a pressure of 450 psi to propel tungsten particles onto the retina. After disc rupture, the vacuum was released. Each slice of retina was bombarded once. After the bombardment, live retinas were

incubated in DMEM for a further hour at 40°C with 5% CO_2. Afterwards, the retina was fixed in 4% paraformaldehyde (PFA in 0.1M PBS pH ~ 7.4) for 60 minutes, followed by two washes in PBS for 5 minutes each.

To label the cell nuclei, all retinas were placed in Propidium iodide (diluted 1:1000 in 0.1 M PBS, Sigma) for 2 minutes, and then washed in PBS twice for 5 minutes each. No dehydration steps were carried out. An overlying coverslip with glycerol or Aqua Poly/Mount (Polysciences Inc, 18606) mounting medium was used.

Bipolar cell image acquisition and cell location recording

The cross-section of retinal slices showing all the layers was visualized with a fluorescent confocal microscope to identify DiO-labelled bipolar cells. DiO-labelled bipolar cells were scanned using both a HeNe and argon laser using a 488 nm excitation filter and a BP 505-530 nm emission filter on a confocal microscope (LSM 5, Carl Zeiss). For each cell, a Z scan using a 40x water-immersion objective was taken from the level of the uppermost to the deepest extent of the processes. Each optical slice was 1.0 μm thick. Only completely filled and minimal overlapping cells that spanned the OPL, INL and IPL were analysed and classified. Occasionally the DiO-coated tungsten particle obscured the processes. In these cases, the cells were still scanned but the number of axonal stratifications was not counted.

For each cell scanned, the retinal location, i.e. central red field, central yellow field or fovea was recorded. The colour of the photoreceptor oil droplets over the cell was used as an indicator of whether the cell was located in the central red or the central yellow fields. A cell was recorded as being in the fovea if it was located within 0–300 μm of the foveal centre. The location of the centre of the fovea was found by the presence of the pit. Cells sampled from the central yellow field were those located

around 2 – 3 mm outside the fovea. The central yellow field was punch biopsied from the centre of the retina, which also contained the fovea. The punch biopsy from the central red field would have also included the *area dorsalis*.

Measurements of the bipolar cell parameters

After the labelled bipolar cells were scanned by the confocal microscope, a number of structural features of the bipolar cell were measured and qualitatively recorded. Measurements of the soma diameter, dendritic field width and axon branch width and axon stratification depth were carried out from the saved images of each cell using the Zeiss LSM Image Browser (version 4, 2, 0, 121). The soma diameter was measured by manually drawing a line across the widest part of the soma using the measuring line tool in the Zeiss software. The width of the dendritic field was measured by drawing a line across two tips on opposite ends of the dendrite that appears to be the widest aspect. The number of lateral axon branches in the IPL for each bipolar cell was counted and recorded. The bipolar cells were recorded as mono-, bi-, tri- or tetra-stratified depending on the number of axon branches it possessed. To measure the depth of stratification of each axon branch, the measured thickness of the IPL and the distance of the axon branch with respect to the INL/IPL boundary were recorded for each bipolar cell. From these measurements, the percentage in which the axon ramified was calculated and analysed for each bipolar cell type. A percentage close to 0% represents a depth of where the INL/IPL border is located and 100% represents a depth of the IPL/GCL boundary. The presence or absence of the Landolt's club was also recorded. The level at which the bipolar cell's soma was located in the INL was recorded by indicating whether the soma was in the outer (near the OPL), middle, or inner third of the INL.

4.3 Results

Due to the randomness of particle impact on the retinal slice, multiple types of cells including photoreceptors, horizontal cells, amacrine cells, bipolar cells, RGCs and glial cells in retinal slices were labelled with DiO (data not shown). Labelled bipolar cells could be distinguished from Müller cells, whose cell bodies are also located in the INL, by the cell body shape and morphology of the Müller processes. In the current study, only bipolar cells were categorized and analysed.

Classification criteria

Labelled bipolar cells were sampled from cross-sections through the fovea, the central red field and central yellow field. A total of 317 bipolar cells (n = 11 in fovea; 209 in central red field; 98 in central yellow field) have been classified into eight morphological bipolar cell types (B1 – B8) in the pigeon retina (Figs. 4.1 and 4.2). Mariani's (1987) nomenclature for naming each bipolar cell type was adopted in the current study and corresponds to each of his eight bipolar cell types. Our bipolar cells were categorized based on one or two of the parameters for classifying the eight bipolar cell types described by Mariani (1987). Mariani's parameters for classifying the bipolar cells were: dendritic field branching pattern; dendritic field width, the presence of Landolt's club; the level in which the cell body was located in the INL; the number of the axon branches; and stratification level in the IPL. However, our analysis of the bipolar cells in our data revealed that each bipolar cell type can vary considerably in these parameters, as presented below. Therefore, not all the parameters used by Mariani were applied in our classification of bipolar cells in our sample, hence the classification scheme has been modified slightly. First, bipolar cells were classified based on the similarity of the cell's dendritic branching pattern with any one of Mariani's eight

bipolar cell types. In our classification scheme, a bipolar cell type is primarily considered distinct from the other types if the dendritic branching pattern differs. If two bipolar cell types share a very similar dendritic branching pattern, then a distinction is made based on another parameter – the presence or absence of a Landolt's club, in addition to the dendritic branching pattern. The other parameters such as soma location in the INL, number of axon branches and stratification depth were not used to classify the bipolar cells into distinct types and therefore were not used to distinguish between the bipolar cell types. The characteristics of the eight bipolar cell types are described below.

The eight bipolar cell types characteristics

B1 - At their apical ends, B1 bipolar cells (n=14) had three to four long dendrites, which curved towards the ONL (Fig. 4.3A, white arrow). Their dendritic field width average was the widest out of all the bipolar types spanning about 24.8 ± 6.5 μm (mean ± SD). The average soma diameter of B1 bipolar cells was about 2.8 ± 0.7 μm.

The majority of the B1 cells had a Landolt's club (12 out of 14), which is a long process that extends from the primary dendritic branch in the OPL to the level of the inner segment of the photoreceptors (Fig. 4.3A white arrowhead). Most of the B1 bipolar cells (13 out of 14) had somas located in the outer third of the INL. Only one of the B1 bipolar cells had a soma located in the middle third of the INL.

Two axon stratification varieties of B1 bipolar cells were found in the pigeon retina – the monostratified and the bistratified. The monostratified B1 bipolar cells had their axon terminal stratifying in the middle at about 46% of the IPL thickness. The bistratified B1 bipolar cells had one of their first axon branch ramifying at 20% of the

IPL (near the INL/IPL border), while the second axon ramified at 43% of the IPL (near the middle of the IPL).

B2 bipolar cells (n=10) had dendrites which curved toward the ONL, similar to the B1 bipolar cells (Fig. 4.3B, white arrow). B2 differed from B1 in that none of the B2 bipolar cells had a Landolt's club. The mean dendritic field width of B2 bipolar cells was 16.8 ± 4.8 μm and their soma diameter was about 3.1 ± 0.4 μm. Their somas were located in either the outer (6 out of 10) or middle (4 out of 10) third of the INL.

Most of the B2 cells were bistratified, with only one monostratified B2 cell found. The two axon branches of the bistratified B2 bipolar cells stratified at 39% and 72% of the IPL thickness. The monostratified B2 bipolar cells ramified at 68% of the IPL thickness.

B3 bipolar cells' (n = 76) dendrites extended horizontally straight along the OPL (Fig. 4.3C white triangle) compared to the B1 and B2 cell processes. B3 bipolar cells had a mean dendritic field width of about 15.8 ± 5.5 μm and a mean soma diameter of 2.8 ± 0.5 μm.

The Landolt's club emanated from the centre of its dendritic field. The majority of B3 bipolar cells observed had a Landolt's club (59 out of 76), while only a small proportion (17 out of 76) of the B3 bipolar cells were not observed with a Landolt's club. It is possible that the Landolt's club may have been excluded from the sliced retina. The somas of B3 bipolar cells were located either in the middle third of the INL (43 out of 76), or in the outer third of the INL (33 out of 76).

Four axon stratification varieties were found for B3 bipolar cells: monostratified, bistratified, tristratified and tetrastratified. The axon terminal of monostratified B3 bipolar cells stratified at about 45% of the IPL thickness. The bistratified B3 bipolar cell's axon branches ramified at 21% and 54% of the IPL

thickness. The axon branches of the tristratified B3 bipolar cells stratified at 5%, 59% and 86% of the IPL thickness. The tetrastatified B3 bipolar cell ramified at 7%, 50%, 85% and 98% of the IPL thickness.

B4 bipolar cells (n=37) were characterised by two to three dendritic branches, each one containing several tiny, fine fibres pointing toward the ONL (Fig. 4.3D, curved arrow). The mean dendritic field width of B4 bipolar cells was about 10.9 ± 3.0 μm, and their soma diameter was about 2.9 ± 0.5 μm.

Almost all the B4 bipolar cells had a Landolt's club emanating at the centre of the dendritic field, except for one which did not have a Landolt's club. This cell's Landolt's club may been cut during sectioning of the retina. B4 somas were observed in either the outer (15 out of 37) or middle (22 out of 37) third of the INL.

The number of axon branches of B4 bipolar cells ranged from monostratified to tetrastratified. The monostratified B4 bipolar cell stratified at 51% of the IPL thickness. The bistratified B4 bipolar cells ramified at 34% and 50% of the IPL thickness. The tristratified B4 cells stratified at 20%, 39% and 55% of the IPL thickness. The tetrastratified B4 bipolar cells ramified at 3%, 25%, 40% and 54% of the IPL thickness.

B5 bipolar cells (n=29) had a mixture of straight and slightly wavy dendrites (Fig. 4.3E). B5 bipolar cells had an average dendritic field width of about 17.8 ± 5.3 μm and a mean soma diameter of about 2.6 ± 0.5 μm.

The Landolt's club extended from the centre of the dendritic field. Most of the B5 bipolar cells were observed to have a Landolt's club (24 out of 29), and a small proportion of the B5 cells did not (5 out of 29). The majority of B5 cells had their somas located in the outer third (22 out of 29), while a few were in the middle third (7 out of 29) of the INL.

The monostratified, bistratified, tristratified and pentastratified varieties of B5 bipolar cells were found. The monostratified B5 bipolar cells ramified at about 69% of the IPL thickness. The axon branches of the B5 bistratified cells ramified at 17% and 70% of the IPL thickness. B5 tristratified cells had axon branches at about 20%, 44% and 55% of the IPL thickness. The pentastratified B5 bipolar cell stratified at 28%, 39%, 76%, 82% and 90% of the IPL thickness.

B6 bipolar cells (n=55) were characterised by very wavy dendrites with tips that point toward the ONL (Fig. 4.3F). All the B6 cells lacked a Landolt's club. The mean dendritic field width of B6 cells was 21.2 ± 5.7 μm, the second widest out of all the bipolar cell types. The mean soma diameter was 2.9 ± 0.6 μm. Their somas were located mostly in the outer third (49 out of 55) of the INL, while only a small proportion of the B6 cells had somas in the middle third (6 out of 55).

Three different stratifications were found for B6: monostratified, bistratified and tristratified. The monostratified B6 bipolar cell ramified at 28% of the IPL thickness. The bistratified B6 cell stratified at 22% and 50% of the IPL thickness. B6 tristratified cells ramified at about 14%, 56% and 71% of the IPL thickness.

B7 bipolar cells (n=63) were characterised by numerous curved, highly branched and intertwined dendrites (Fig. 4.3G). The mean dendritic field width of B7 cells was 12.7 ± 3.9 μm and soma diameter of about 3.0 ± 0.6 μm.

The Landolt's club was observed in a majority of B7 bipolar cells (53 out of 63). The soma was located mostly in the outer third (45 out of 63) and a small proportion was in the middle third (18 out of 63) of the INL.

All the different axon stratification varieties were found for B7 bipolar cells: monostratified, bistratified, tristratified, tetrastratified and pentastratified. The monostratified B7 bipolar cell ramified at 57% of the IPL thickness. The bistratified B7

bipolar cell had axon branches at 32% and 76% of the IPL thickness. Tristratified B7 cells ramified at 21%, 59% and 87% of the IPL thickness. The tetrastratified B7 bipolar cell ramified at 48%, 75%, 86% and 100% of the IPL thickness. Pentastratified B7 bipolar cells ramified at 8%, 26%, 54%, 91% and 100% of the IPL thickness.

B8 bipolar cells (n=34) were characterised by a narrow dendritic branch extending horizontally in the OPL and on the branch were numerous smaller fine fibres that projected towards the ONL from a side branch (Fig. 4.3H, white star). The B8 cells' mean dendritic field width was the narrowest out of all the bipolar cell types (6.8 ± 2.1 μm). Their soma diameter was 2.8 ± 0.5 μm. The B8 bipolar cell was observed as a bistratified only which stratified at 37% and 56% of the IPL thickness.

Almost all the B8 bipolar cells had a Landolt's club (33 out of 34). Their somas were located in either in the middle third (24 out of 34) or in the outer third (10 out of 24) of the INL.

Number of bipolar cell types sampled in different retinal regions

The chances of labelling bipolar cells were not the same across the pigeon retina depending on the retinal location as shown by the various number of cells obtained in the fovea, central red and yellow fields (Table 4.1). Due to the difficulty targeting a small area like the fovea, only eleven bipolar cells in total were labelled by the Diolistics technique, which were classified as belonging to the following three bipolar cell types: B2, B5 and B7. Most of the bipolar cells in the fovea were classified as B7.

The large area of the central red and yellow fields allowed greater numbers of bipolar cells to be labelled by the Diolistics technique. More bipolar cells were labelled in the central red field than in the central yellow field due to the higher density of cells in the INL in the central red field. Bipolar cells in the central red and yellow fields were

classified as belonging to all eight types. The B3, B6 and B7 bipolar cell types formed the majority of our bipolar cell sample obtained from the central red field. In the central yellow field, B3, B4 and B6 bipolar cells formed the majority of our bipolar cell sample taken from the central yellow field.

Differences in dendritic filed size in the retinal regions

In the fovea, the minimum dendritic field width measured was 4.8 μm and the maximum was 15.1 μm. In the central yellow field, the dendritic field widths ranged from 6.2 μm to 36 μm. The smallest dendritic field width measured was 3.1 and the widest was 37 μm, which were in the central red field.

Out of the three bipolar cell types in the fovea, B7 had the narrowest average dendritic field of 9.8 μm (Table 4.2). In the central red field, B8 had a smaller dendritic field width compared with the other bipolar cell types. In the central yellow field, B8's dendritic field width was still comparatively smaller than the other bipolar cell types.

4.4 Discussion

We have classified eight morphological bipolar cell types in the pigeon retina using a modification of Mariani's (1987) bipolar cell classification criteria. Each type of bipolar cell differed mainly in the pattern of dendritic branching. B8 had the smallest dendritic field width, while B1 had the widest. Unlike the previous study by Mariani (1987), each bipolar cell type was analysed in greater detail using Mariani's parameters for classifying the bipolar cells in order to reveal the intricate variations in characteristics within each type and how the cell types' dendritic field widths differed in

the fovea and the central red and yellow fields. The implications of these findings will be discussed in the following sections.

Distribution of bipolar cell types in the retina

As has been hypothesised by Wässle and Boycott (1991), in order for a local region on the retina to be able to process various aspects of the visual image that falls on it, all the RGC types must be distributed across the retina. If this hypothesis is applied to the distribution of bipolar cells, then all the bipolar cell types identified in the present study would be distributed throughout the retina. In support of this hypothesis, all eight bipolar cell types were found in the central red and yellow fields. However, only three types were identified in the fovea. There may be several reasons for not finding all the subtypes in the fovea. One could be due to the possibility that certain types were distributed at a low frequency in the fovea, and thus the chances of encountering these cells were also low. Another reason may be due to the sampling bias of the Diolistics technique as well as the difficulty with sampling a small area like the fovea. The possibility that all the bipolar cell types are distributed in all regions of the retina cannot be ruled out based on the current data.

Bipolar cell dendritic field size and density relationship with high visual acuity

In order for the retinal neurons to resolve high spatial frequency, cells with narrow dendritic fields and high density are thought to be an essential component for high visual acuity (Wässle and Boycott, 1991). The two areas associated with high visual acuity, the fovea and the *area dorsalis*, have been shown to contain high cell densities in the pigeon retina (Galifret, 1968; Binggeli & Paule, 1969; Querubin *et al*.,

2009). If the bipolar cells formed the majority of cells in the INL, then small dendritic fields in the two high density areas would be very useful in enabling these cells to resolve fine detail. As the cell density decreases away from the centre of the peak density areas, the bipolar cell dendritic fields would widen. Dendritic field sizes of bipolar cells were indeed reported to be wider in the peripheral yellow field than the pigeon fovea (Lockhart, 1979). In the rabbit retina, Mills and Massey (1992) observed an increase in bipolar cell dendritic field size with respect to the visual streak (which is equivalent to the pigeon's high density areas). Given that the INL cell densities in the central red field is five times higher than the peripheral yellow field (Galifret, 1968), one would expect that dendritic field sizes would be much smaller in the central red field than in the peripheral yellow field. However, as our study could not sample the peripheral yellow field, this is, at present, is open to speculation.

An inverse relationship between higher percentage of a bipolar cell type in one high cell density region over a less dense area and a narrow bipolar cell dendritic field size has been reported in the rabbit retina (Mills & Massey, 1992). The bipolar cell type, with a greater density in the rabbit visual streak, also had narrower dendritic fields in the streak than the peripheral retina. Having a greater percentage of bipolar cell types with narrower dendritic fields in the high cell density areas may enable the cells to resolve high spatial frequency.

The resolution of fine spatial vision not only requires a high density of bipolar cells with narrow dendritic fields, but also that the dendritic fields overlap only a small amount at the perimeter of the dendritic field. Since a specific marker for each bipolar cell type was not available, labelling and quantifying each type to determine the density and percentage of each bipolar cell was not possible. Even if we could use the percentage frequency with which each bipolar cell type was found, it would not be

accurate to use it to calculate the density of each cell by multiplying it with the INL cell densities reported by Galifret (1968), as it is not the density of the bipolar cell population. Therefore, a specific labelling technique for all the bipolar cell types in the pigeon would help determine the extent in which each type efficiently provides coverage.

Convergence between photoreceptors and bipolar cells

The number of photoreceptor inputs into a bipolar cell partly depends on the densities of these neurons at specific locations in the retina. Photoreceptor density in the fovea and the central red field (*area dorsalis*) were reported to be about 300,000 cells/mm^2 (Querubin *et al*, 2009). Galifret (1968) found that the number of cells in the INL was about four times the number of photoreceptors in the fovea and red field. Based on these figures, it would be estimated that there would be about one photoreceptor to four cells in the INL. However, it is far from an accurate estimation of the number of photoreceptors contacting bipolar cells since the INL comprises of bipolar cells, horizontal cells, amacrine cells, IPCs, Müller cells and displaced RGCs (Uga and Smelser, 1973; Mariani and Leure-DuPree, 1977; Mariani, 1983b; Hayes, 1984; Mariani, 1987). Another way to estimate the amount of convergence would be to calculate the ratio between the size of the dendrites and axon terminals in the OPL.

Estimating the number of photoreceptors providing input into each bipolar cell type has been done previously by Boycott and Dowling (1969). They estimated the number of cone input onto midget bipolar cells based on the size of the cone pedicles and bipolar cell dendritic fields. Lockhart (1979) measured the photoreceptor axon terminals from the fovea and red field, and reported that the width of the photoreceptor axon terminals ranged between 6 and 18 μm in the pigeon fovea and between 6 and 17

μm in the red field (Lockhart, 1979). By using Lockhart's (1979) published measurements of photoreceptor axon terminal sizes and dendritic field sizes from the present analysis, it is possible to estimate the number of photoreceptor inputs into a bipolar cell type (Table 4.3). Such an analysis suggests that bipolar cell types with smaller dendritic fields such as B7 (in the fovea) and B8 (in the central red field) could contact between 0.4 and 1.6 photoreceptors. These estimates of cone input are similar to that found in the primate fovea, where a midget bipolar cell is connected to one cone photoreceptor (Polyak, 1941; Boycott & Dowling, 1969; Kolb, 1970; Calkins *et al*., 1994). In comparison, bipolar cell types in the pigeon retina with the widest dendritic field width (the B1 bipolar cell) may receive up to 3.8 photoreceptor inputs. This is broadly comparable to a diffuse cone bipolar of primate retina which contacts at least six cones, within its dendritic field (Boycott and Dowling, 1969; Kolb, 1970; Mariani, 1981; 1983a; Boycott and Hopkins, 1993). These figures are only rough estimates but serve to indicate greater convergence onto BC outside the pigeon fovea.

In the pigeon fovea, it is possible that the number of bipolar cells a photoreceptor can synapse with may be more than one, due to the exceedingly high density of cells in the foveal INL (Galifret, 1968). Based on Lockhart's (1979) study, photoreceptors in the fovea can have a wide axon terminal (18 μm diameter). This type of photoreceptor may be able to contact about two or more bipolar cells in the fovea if the bipolar cell's dendritic field is 9 μm. If a cone photoreceptor type, with a wide axon terminal, predominates in the fovea, which is connected to several small dendritic field bipolar cell types such as B7, it is possible that a great deal of divergent (1:2 cone:bipolar cell) processing occurs in this area. Similarly in the red field, a photoreceptor with a 17 μm wide axon terminal may be able to contact at least 2.6 B8 bipolar cells, theoretically. Although it is also possible that each photoreceptor contacts

different bipolar cell types similarly to the primate retina, where a cone can contact a mixture of different cone bipolar cell types (eg. Midget and S-cone bipolar contacting a S-cone (Klug et al., 2003)).

Caution must be observed when interpreting these estimates, for it assumes that a bipolar cell's dendritic field directly lay underneath the photoreceptors' axon terminals, and that the close hexagonal packing of the photoreceptors are constant throughout the retina, with negligible space between them. When Leeper (1978) analysed the photoreceptor contacting the horizontal cells in the turtle retina, it was observed that two horizontal cells with different dendritic field size and shape can contact the same subset of photoreceptors. Therefore, cells with different dendritic field size and shape can contact the same number of photoreceptors if the inter-photoreceptor distance and packing differs proportionately as well.

It is also possible that a bipolar cell's dendritic field may be situated between the outer edges of several photoreceptor axon terminals (Boycott & Dowling, 1969). Consequently, more than one photoreceptor may be contacting a B7 or a B8 bipolar cell type. If this is the case then the present study's estimates could underestimate the number of inputs a photoreceptor can make into a bipolar cell. A more direct confirmation of the connectivity between the different types of photoreceptors and bipolar cells is required using electron microscopic reconstruction to determine the number of cells connected to each other.

A possible midget circuitry in the pigeon fovea and central red field

In the primate fovea, the circuitry thought to subserve high acuity vision is the midget pathway. It consists of each midget bipolar cell contacting one cone photoreceptor and conveying the output to one midget ganglion cell (Polyak, 1941;

Boycott & Dowling, 1969; Kolb, 1970; Calkins *et al*., 1994). Finding the midget cell types in the pigeon retina with similar morphology and neuronal interconnectivity as the primate's at the anatomical level is a useful starting point. There is evidence that the pigeon also has a midget-like bipolar cell type which had a very small dendritic field (2.5–6 μm diameter (Lockhart, 1979; Mariani, 1987). Even though Mariani (1987) has proposed that B8 was the candidate midget bipolar cell due to its small dendritic field, the amount of photoreceptors it contacts was not reported. Our study supports the claim that B8 may be the candidate midget-like bipolar cell based on its small dendritic field. Another bipolar cell type, B7, is also a good candidate for being a midget-like bipolar cell type. The reason for this is that B7 bipolar cell type had a much narrower dendritic field width compared with the other types in the fovea. It is possible that these cell types can receive input from at least one photoreceptor. The dendritic field sizes of the two candidate midget bipolar cells and the estimated low convergence from photoreceptors to these cell types suggest that a circuitry similar to the primate midget may exist in the pigeon. However, further investigation is required to support this hypothesis by various means including electrophysiological and anatomical methods to elucidate the properties of the pigeon 'midget-like' neuronal types.

The IPL sublamina in the pigeon retina

Determining the number of IPL substrata in the pigeon retina was difficult and therefore, assigning the bipolar axon stratification in a particular IPL sublamina was avoided. Instead, the stratification depth of the axon branches was reported as a percentage of the IPL thickness. Ideally, it would have been useful if a consensus exists on exactly the number of sublaminas present in the pigeon retina. Cajal (1972) has subdivided the vertebrate IPL into five sublaminas, which has been widely used in

studies of the retina. However, Cajal (1889; 1972) also found that in certain areas of the avian retina, more than five sublaminas were present. Immunohistochemical analyses of calbindin and calretinin labelled pigeon retinas have indicated that there may be additional sublaminas within the traditional five layer subdivisions (Pasteels et al., 1987; Pochet et al., 1991). Another way would be to subdivide the IPL into ON and OFF sublamina, as it has been determined using electrophysiology and anatomical methods in some vertebrate retinas (Nelson et al., 1978; Kolb, 1979; Nelson and Kolb, 1983; Bloomfield and Miller, 1986; Ammermüller and Kolb, 1995; Euler et al., 1996). Since the ON and OFF physiological properties of the various bipolar cell types have not yet been defined in the pigeon retina using electrophysiological techniques, it was not appropriate to subdivide the pigeon IPL into ON and OFF sublamina.

Interspecies comparison of bipolar cell types: ON and OFF bipolar cells possibility

The subdivision of the IPL into ON and OFF sublamina requires electrophysiological recordings of bipolar cells and determining their stratification in the IPL. However, in the pigeon, recordings from bipolar cells are lacking and therefore, it is not possible to identify which bipolar cells have ON or OFF properties based on the stratification pattern of their axon. The physiological properties of the multiple bipolar cell types in the pigeon retina can only be speculated upon at this time. Although, the present study did not investigate the physiological properties of the bipolar cells in the pigeon retina, there is a strong chance that ON or OFF bipolar cell types may also exist in this species. Bipolar cell types with ON or OFF properties have been electrophysiologically demonstrated in various species such as the mudpuppy (Werblin and Dowling, 1969), goldfish (Kaneko, 1970), turtle (Ammermüller and Kolb, 1995),

teleost (Grant and Dowling, 1996), white perch (Grant and Dowling, 1995) and zebrafish (Connaughton and Nelson, 2000). Indirect evidence recorded from the pigeon optic tract and chiasm - that demonstrated an ON or OFF centre-surround receptive field organization was present - may lend support to the speculation that ON and OFF bipolar cells exist (Pearlman and Hughes, 1976).

A question raised in the current study was whether the multistratified axon of some bipolar cells would follow the ON and OFF stratification boundaries if they existed in the pigeon, similar to what has been demonstrated in the cat and human retinas (Kolb 1979; Kolb & Dekorver, 1991). The bipolar cells in these species, which were reconstructed from electron microscopy images, had their axon terminals stretching either a third or two-thirds of the IPL thickness, but were restricted to either the ON or OFF sublamina.

It would be interesting to determine whether the pigeon bipolar cells exhibit similar electrophysiological properties as those reported in the turtle retina and whether the ON/OFF subdivision in the IPL are the same in both species. Ammermuller and Kolb (1995) recorded the electrophysiological properties of bipolar cells in the turtle retina. They found that the functional organization of the turtle IPL into OFF (strata 1 and 2) and ON sublaminae (strata 3, 4 and 5) was clear for certain varieties of OFF-centre and ON-centre bipolar cells. However, there were exceptions to this, they found a few varieties of sustained OFF-centre bipolar cells having axon terminals in strata 3-5 (the ON sublamina) in addition to their terminations in strata 1 or 2 (the OFF sublamina) (Ammermüller & Kolb, 1995). Multistratified bipolar cells which had axon branches in both the ON and OFF sublamina have been shown to exhibit either ON or OFF physiology in the goldfish retina (Connaughton & Nelson, 2000). If this were also the case in the pigeon retina, then multistratified bipolar cells may also exhibit ON or

OFF or both physiologies. Electrophysiological recordings would be necessary to test the extent to which the ON and OFF stratification boundaries apply to birds.

Dendritic morphology similarities with other species

The pigeon retina contains similar bipolar cell types to the chicken. There were seven morphological bipolar cell types (B1–B7) identified in the chicken retina (Quesada *et al*., 1988). Within three chicken bipolar cell types, further subtypes were defined – three subtypes for B1 ($B1_a$, $B1_b$, and $B1_c$); two B2 subtypes ($B2_a$, $B2_b$); and two B4 subtypes ($B4_a$, $B4_b$). The pigeon B1 and B2 bipolar cell types correspond to the chicken $B1_c$ bipolar cell or 'candelabra-shaped' cell, in terms of the shape and branching pattern of the dendrites. Quesada and co-investigators (1988) considered the chicken B1 type to be similar to what Polyak (1941) called the 'mop bipolar cell' in the primate retina. The mop bipolar cell is now termed the rod bipolar cell for it was found to exclusively contact only rod spherules and not cone pedicles (Boycott & Dowling, 1969; Kolb, 1970). Although there are some similarities in the dendritic structure between the avian B1 bipolar cell type and the mammalian rod bipolar cell, a thorough reconstruction of the B1 bipolar cell connectivity with a rod photoreceptor is required to demonstrate it as the rod bipolar cell. It is possible that the B1 bipolar cell can synapse with both rod and cone photoreceptors.

The dendritic shape of the pigeon B3 and B5 appears similar to the chicken $B2_a$, $B2_b$ and B3 in that their dendrites travel parallel to the OPL. The B6 bipolar cell type in the pigeon may correspond to the $B1_b$ of the chicken retina. The chicken B7 has been considered as the midget bipolar cell in the chicken retina, which also has a very small dendritic field ranging from 3-5 μm in diameter. However, unlike that of the pigeon B8 bipolar cell type, the B7 in the chicken retina may not have a Landolt's club present.

Consequently, the chicken B7 lacking a Landolt's club appears similar to our B7 bipolar cell type in the pigeon retina. Similar to our observations in the pigeon retina bipolar cell types, the presence or absence of Landolt's club varied greatly within each bipolar cell type, as well as the location of the soma and the length and number of axon branches in the IPL. Overall, the pigeon bipolar cell types show similarities with that of the chicken bipolar cell types. It is possible that not all the pigeon bipolar cell types have been found by the current study due to sampling issues.

A few pigeon bipolar cell types have similar dendritic branching pattern as the bipolar cell types in the primate, which Polyak (1941) identified termed as diffuse, brush and flat bipolar cells. These primate cell types resemble the dendritic morphology of the B3, B5 and B6, except that in the primate retina, a Landolt's club is not as common as in the avian bipolar cells. For a more complete comparison of the bipolar cell types between the primate and pigeon, it is necessary to investigate the physiology of the pigeon bipolar cell types in order to understand the extent in which the bipolar cell types differ from the primate bipolar cells.

Advantages and disadvantages of the Diolistics technique

The advantage of the Diolistics technique used in the current study was that it allowed the labelling of a large number of cells per retina, thus allowing a more efficient use of the equipment and retinas and at a shorter time frame compared with other methods like the Golgi impregnation. However, Diolistics labelling can be difficult to control as too many cells within close proximity can be densely labelled at once, which prevents the resolution of dendritic or axonal detail. Using this technique was also troublesome for trying to label neurons in a small area like the fovea as mentioned above. There is the possibility that too little DiI or DiO could prevent the

complete labelling of the entire dendritic or axonal structure. However, care was taken to ensure that only completely labelled bipolar cells were scanned. The tips of the dendrites and axon branches were inspected for clear, bright labelling. Nevertheless, Diolistics is an efficient way of labelling neurons and obtaining a large sample for analysis.

4.5 Conclusions

The study has identified eight morphological bipolar cell types which bear similarities to Mariani's bipolar cell types in terms of dendritic branching pattern. Out of the eight bipolar cell types, B7 and B8 are possible good candidate midget-like bipolar cells because of their smaller dendritic field sizes. B7 and B8 bipolar cell types were estimated to have lower photoreceptor input and may possibly contact one photoreceptor in the two high acuity regions. Although the current study has only estimated the number of photoreceptor inputs into the bipolar cell types, a more direct method of determining the number and type of photoreceptor input is required to confirm the present estimates. Further work into the differential distribution of the different bipolar cell types in the pigeon retina would contribute into our understanding of the neuronal circuitry of the pigeon retina.

Chapter 4 figures & tables

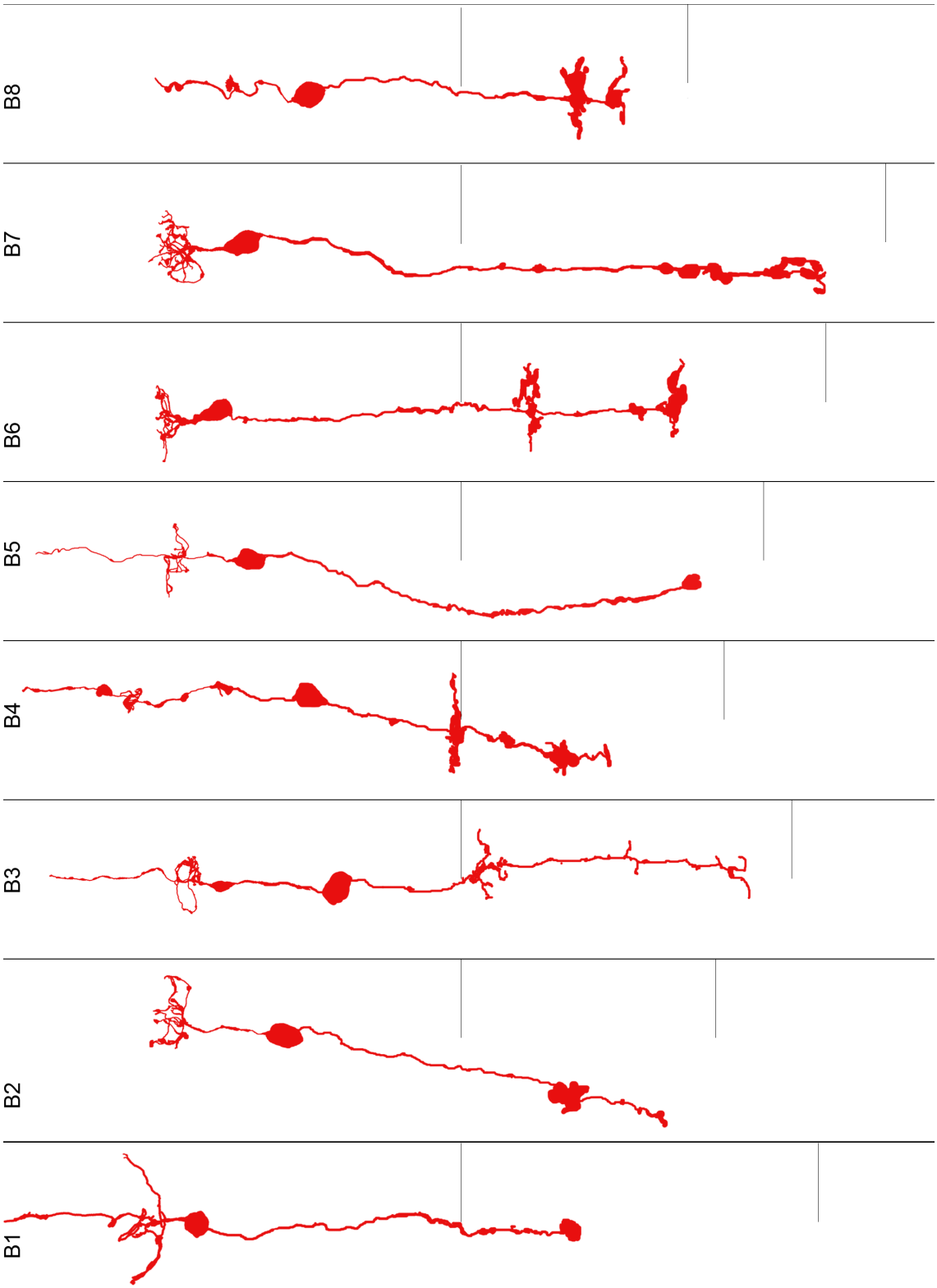

Figure 4.1. Drawings of representative bipolar cell types B1 – B8. Hand-drawn in Adobe Photoshop CS5. The horizontal lines indicate the IPL thickness.

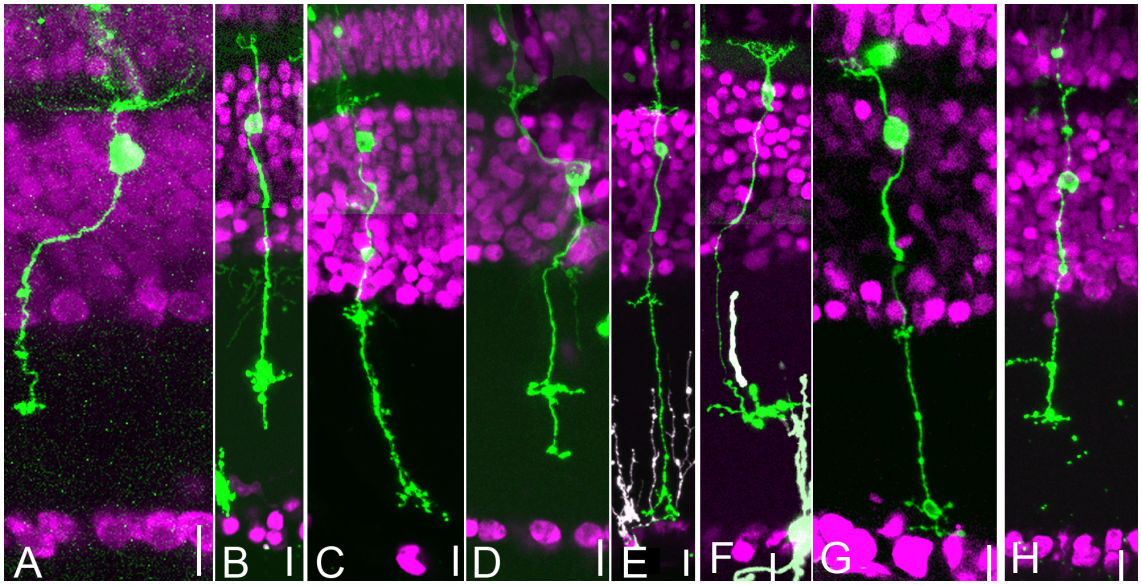

Figure 4.2. Micrographs showing the ranges of bipolar cell morphologies in DiO-labelled retinas (green labelled cells). (A) B1. (B) B2. (C) B3. (D) B4. (E) B5. (F) B6. (G) B7. (H) B8. The micrographs were cropped, the colours and contrast modified from the original scanned image using Adobe Photoshop CS5. (F-G) The white cells and processes belong to neighbouring non-bipolar cells. All white scale bars on the bottom of each image are equal to 10 μm.

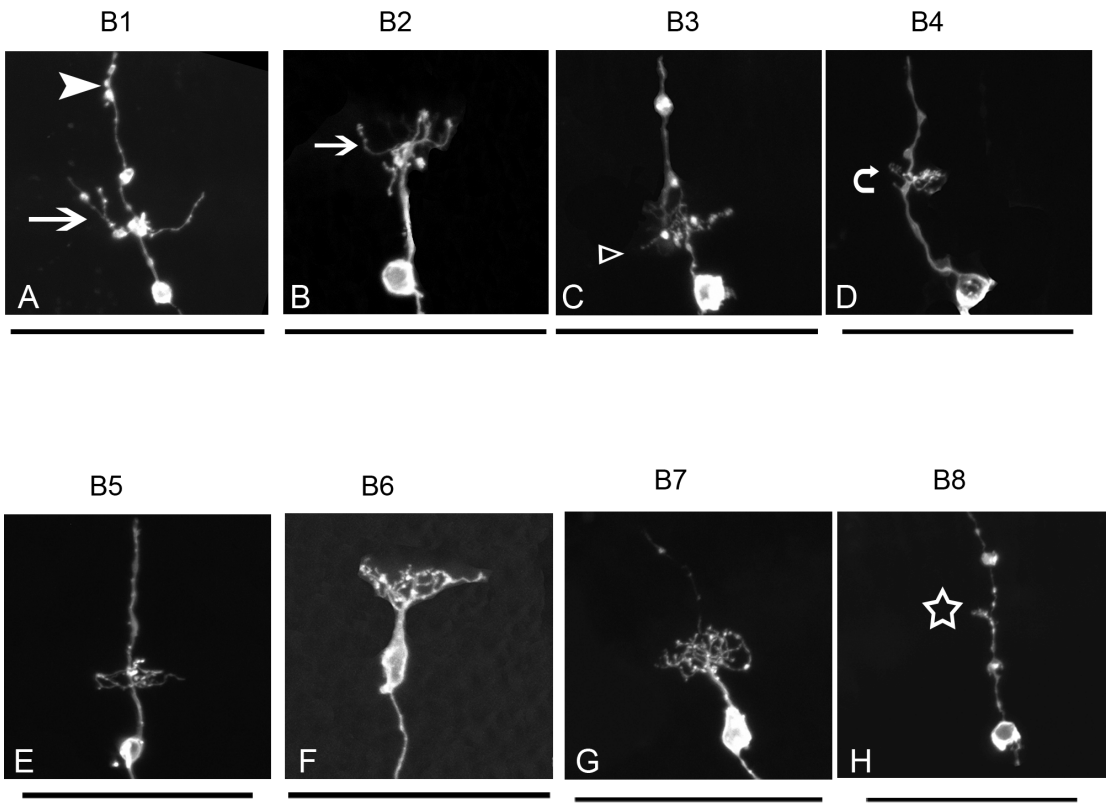

Figure 4.3. Micrographs showing the different morphologies of the dendrites. The micrographs were cropped and the contrast modified from the original scanned image using Adobe Photoshop CS5. All black scale bars on the bottom of each image are equal to 50 μm.

Table 4.1. Number of bipolar cell types sampled in different retinal locations

Bipolar cell type	Number of cells sampled		
	Fovea	Central Yellow Field	Central Red Field
B1	0	2	12
B2	1	4	5
B3	0	24	52
B4	0	19	18
B5	1	14	14
B6	0	22	33
B7	9	9	45
B8	0	4	34
Total	11	98	209

Table 4.2. Dendritic field widths in the fovea, central red and yellow fields

Bipolar cell type	Average dendritic field width (± SD μm)		
	Fovea	Central Yellow Field	Central Red Field
B1	-	31.1 ± 3.1	23.8 ± 6.4
B2	12.1	19.9 ± 4.9	15.3 ± 4.0
B3	-	16.6 ± 7.1	15.4 ± 4.6
B4	-	12.0 ± 3.3	9.8 ± 2.3
B5	10.5	17.7 ± 6.7	18.5 ± 3.4
B6	-	18.5 ± 5.7	23.1 ± 5.0
B7	9.8 ± 3.4	12.3 ± 4.4	13.3 ± 3.7
B8	-	9.7 ± 1.9	6.4 ± 1.8

Table 4.3. Estimated number of photoreceptor inputs into each bipolar cell type in the fovea and red field

Bipolar Cell Types		Number of photoreceptor input into a bipolar cell type*						
		Fovea			Red field			
	Mean dendritic field width in fovea^	Photoreceptor 1 (diameter = 6.00 μm)#	Photoreceptor 2 (diameter = 15.72 μm)#	Photoreceptor 3 (diameter = 17.94 μm)#	Mean dendritic field width in red field^	Photoreceptor 1 (diameter = 6.32 μm)#	Photoreceptor 2 (diameter = 15.30 μm)#	Photoreceptor 3 (diameter = 16.88 μm)#
B1	-	-	-	-	23.8	3.8	1.6	1.4
B2	12.1	2.0	0.8	0.7	15.3	2.4	1.0	0.9
B3	-	-	-	-	15.4	2.4	1.0	0.9
B4	-	-	-	-	9.8	1.5	0.6	0.6
B5	10.5	1.8	0.7	0.6	18.5	2.9	1.2	1.1
B6	-	-	-	-	23.1	3.7	1.5	1.4
B7	9.8	1.6	0.6	0.5	13.3	2.1	0.9	0.8
B8	-	-	-	-	6.4	1.0	0.4	0.4

^ mean dendritic field widths from our data (refer to Table 4.2)

Photoreceptor diameter was calculated from the photoreceptor measurements in the fovea and the red field reported by Lockhart (1979). Photoreceptor 1, 2, 3 refer to three different photoreceptor types, which Lockhart (1979) identified in the fovea and red field. Each photoreceptor type in the fovea and red field had different axon terminal diameters as shown in the brackets.

* The number of photoreceptor inputs into a bipolar cell type was calculated by dividing the mean dendritic field width by the photoreceptor axon terminal diameter.

Chapter 5 – Morphological Classification of Ganglion Cells in the Pigeon Retina

Abstract

This study sought to classify the RGCs into groups and identify whether a midget ganglion cell exists in the pigeon retina. Classification of the RGCs in the pigeon retina was based on the number of dendritic arbours or whether the dendrites do not stratify in a distinct layer. Five morphological RGC groups were identified, based on the pattern of stratification, the unstratified, monostratified, bistratified, tristratified and tetrastratified. The unstratified RGC had dendrites extending vertically over a thick portion of the IPL whereas the other stratified groups had horizontal dendritic arbours stratifying at a narrow portion of the IPL. The unstratified RGC had the smallest dendritic field out of the other groups. Based on the unstratified RGC's small dendritic field size, it may be a a good candidate for being a 'midget-like' ganglion cell in the pigeon retina; however its morphology differs considerably from the primate midget ganglion cell. The evidence suggest that the pigeon has a different circuitry involved in processing high acuity information in the two specialised areas. Further work is required to determine the physiology, differential distribution and coverage of the different RGC groups in the pigeon retina.

5.1 Introduction

In order to represent the complex visual world accurately, the retina has many different types of ganglion cells. The RGC types are defined by their morphological and physiological parameters (Masland, 2001). Various morphological RGC types with distinct dendritic morphologies, stratification patterns in the inner plexiform layer (IPL) and projection targets in the brain have already been identified in several species (Kolb et al., 1981; Amthor et al., 1983; Amthor et al., 1989b; Dacey, 1993a; Doi and Uji, 1995; Berson et al., 1998; Berson et al., 1999; Isayama et al., 2000; Mangrum et al., 2002; Sun et al., 2002; Kong et al., 2005; Isayama et al., 2009).

My hypothesis is that the distribution of each RGC type in the retina is constant and that each type is present across the retina. Full coverage of the retina by all RGC types would ensure that any location on the retina would be able to respond to an appropriate stimulus and process its individual components (review Wässle & Boycott, 1991). This is one of underlying principles of parallel processing in the retina.

For a RGC to be able to resolve fine spatial detail, RGC density must be high and their dendritic field should be narrow in the specialized retinal areas (Wässle & Boycott, 1991). High RGC density areas on the retina are present in the *area* or *fovea centralis* (Walls, 1942; Stone, 1965; Provis, 1979; Curcio and Allen, 1990; Salinas-Navarro et al., 2009). However, only a few RGC types have been known to have a narrow dendritic field in the high RGC density areas. The best characterised is the 'midget' ganglion cell, which has a small dendritic field that receives input from only one cone photoreceptor via a midget bipolar cell in the primate fovea (Polyak, 1941; Boycott & Dowling, 1969; Kolb, 1970; Calkins *et al*., 1994). This circuitry is thought to preserve the high spatial sampling limit set by the cone photoreceptors in the primate

fovea (Wässle & Boycott, 1991). In other mammalian species, the beta cell also has a small dendritic field in the *area centralis,* which has been implicated in contributing to high acuity vision (Boycott and Wässle, 1974; Kolb, 1979; Stein *et al*., 1996; Isayama *et al.,* 2009). For vertebrate animals that possess both an *area dorsalis* and a fovea, such as the pigeon (Galifret, 1968; Binggeli & Paule, 1969; Querubin *et al.,* 2009), it raises the question of whether a midget or beta RGC exists in this animal.

The sparse evidence to support a morphological counterpart of a midget ganglion cell in the pigeon has raised doubts over this issue. A 'midget-like' ganglion cell impregnated by the Golgi method was found in the pigeon retina; however, its characteristics were morphologically different from those of the primate midget ganglion cell (Lockhart, 1979). The pigeon midget-like RGC found by Lockhart (1979) has a slightly wider dendritic field and a distinct dendritic pattern compared with that of the primate. Since the morphology of the midget-like RGC did not share the same characteristics as that of the primate, it may suggest a different midget circuitry is in place in the pigeon retina.

In addition, a correlation between the dendritic field size of beta and midget RGCs and their density has been observed in mammalian retinas (Watanabe and Rodieck, 1989; Dacey and Petersen, 1992; Dacey, 1993b; Stein et al., 1996). These studies reported a proportional increase in the dendritic field size of certain RGC types with distance from the high cell density areas. The issue of whether avian species with two high cell density areas also exhibit an inverse relationship between RGC dendritic fields and density remains to be characterised.

Differentiating between various RGC types often requires a comparison of their morphology at a particular eccentricity. Boycott and Wässle (1974) observed that three morphological RGC types in the cat - the alpha, beta and gamma cells - were

distinguishable from one another by their cellular dimensions. These dimensions included soma and dendritic field sizes at various eccentricities from the *area centralis*. Similar studies in the primate retina found that the two main RGC types, the midget and parasol ganglion cells, have different cell sizes at various eccentricities from the fovea (Watanabe & Rodieck, 1989; Dacey & Petersen, 1992; Kolb & Marshak, 2003). A relationship between eccentricity and cell size allowed the identification of distinct RGC groups in the chick retina (Naito & Chen, 2004a). Although Lockhart (1979) has reported that the dendritic field sizes of ganglion cells in the fovea and red field were narrower compared with the peripheral retina in the pigeon, it was yet to be demonstrated how the various RGC types change at various eccentricities.

The aim of this study was to classify the pigeon RGCs into groups and identify the best candidate midget-like RGC. Classification of the RGCs was based on the number of dendritic stratification in the IPL. Five RGC groups were identified, including a likely candidate for a pigeon midget-like RGC, with the smallest dendritic field size.

5.2 Materials and methods

Tissue collection and processing

Twenty-three adult pigeons (*Columba livia*) of both sexes were obtained from a pigeon farm in New South Wales, Australia. Ethical approval for the current study was obtained from The Australian National University Animal Ethics committee.

The pigeons were euthanized by an intraperitoneal injection of 2-3 mL of lethabarb with ~ 2% lignocaine (20 mg/mL). Once corneal and pain reflexes were lost, the pigeon was decapitated and the eyes enucleated. A small proportion of eyes (n=6) were fixed by an injection of 4% paraformaldehyde (PFA) in 0.1 M PBS (pH 7.4) into the globe followed by immersion fixation in PFA at 4 °C until used in the diolistics protocol (see below). The majority of eyes (n=31) were dissected in Dulbecco's Modified Eagle Medium (1x DMEM) with high D-glucose and L-glutamine (GIBCO, Cat # 11995065 and 10313021) bubbled with carbogen. Dissection of both fixed and live tissue involved removal of the anterior chamber, vitreous, sclera, choroid, and retinal pigment epithelium. The pecten was trimmed. The retinas were flattened by making relaxing cuts and placed onto a filter paper with the GCL facing upwards. Prior to and after diolistics bombardment (see below), non-fixed retinas were maintained in DMEM inside a tissue incubator (37° C, 5% CO_2).

Diolistics labelling

The diolistics labelling technique was modified from Sun and co-investigators (2002). Dye-coated tungsten particles were prepared as follows. Tungsten particles (30 mg, M-17, Bio-Rad, 75054) were spread evenly onto a microscope slide with a few

drops of methylene chloride. About 3 mg of DiI (Invitrogen, D282) or DiO (Invitrogen, D275) crystals were dissolved in 100 μL of methylene chloride and applied to the tungsten particles. Once dried, the DiI/O-coated tungsten particles were scraped into a 13 mL falcon tube using a razor blade and suspended in 5-10 mL of deionised water. The tungsten solution was vortexed at maximum speed for 10 minutes prior to its application onto macrocarrier discs (20 μL) and air-dried in the dark for a day. The tube and macrocarrier discs containing dye-coated tungsten solution were stored in the dark at room temperature (21-25° C).

Macrocarrier discs containing tungsten particles were placed 6 cm away from a 650 psi (Bio-Rad, 165-2327) or 450 psi (Bio-Rad, 165-2326) rupture disc in a PDS-1000/He System BIORAD gene gun chamber. The retina was removed from DMEM or PFA including excess liquid on the retinal surface and laid flat in a Petri dish with the GCL side up. As quickly as possible, the tungsten particles were propelled at a vacuum of 20–25 Hg/mm with a pressure of 650 or 450 psi. After disc rupture, the vacuum was released. Each retina was bombarded with particles 2-4 times, with each bombardment targeting different areas.

After the bombardment, fixed retinas were placed in 0.1 M PBS in the dark for 1-3 weeks until DiI was visualized throughout the entire cell from axon to dendrite. Live retinas were incubated in DMEM for a further 3 hours at 37°C with 5% CO_2. After 60 minutes of incubation in DMEM, the retina was examined with a fluorescence microscope to see if the dendrites were completely labelled. If the dendrites had not yet been completely filled, the retina was returned to DMEM for another 60-120 minutes. Once the cells were completely filled, the retina was fixed in 4% PFA for 60 minutes, followed by two washes in PBS for 5 minutes each.

To label cell nuclei, all retinas were placed in Propidium iodide (diluted 1:1000 in 0.1 M PBS, Sigma) for 5 minutes, and then washed in PBS twice for 5 minutes each. The retina was flatmounted onto superfrost plus slides and coverslipped with Aqua Poly/Mount (Polysciences Inc, 18606).

RGC image acquisition and mapping

A confocal fluorescence microscope (PASCAL, Carl Zeiss) was used to view the DiI or DiO labelled cells. DiI-labelled RGCs were scanned using a HeNe laser using an excitation filter set at 543 nm and an emission filter set at LP 560 nm. DiO labelled cells were scanned using both a HeNe and argon laser using a 488 nm excitation filter and a BP 505-530 nm emission filter. For each RGC, a Z scan using either a 20x dry or 40x water-immersion objective was taken from the level of the axon, through the soma, the most distal end of the dendrites, ending at the border of the IPL and INL. Each optical slice was 0.9–1.0 μm thick.

Only completely filled and minimal overlapping RGCs in the GCL were analysed and classified. RGCs were considered to be completely filled if the tips of the dendrites could be brightly resolved under the microscope. If the tips of the dendrites were not very clear or were too faint to resolve, then these were not analysed further and excluded from classification. RGCs in the GCL were identified by the presence of a labelled axon extending from the soma and travelling to the nerve fibre layer, which differentiates them from displaced amacrine and glial cells. RGCs whose dendrites overlapped greater than 50% with a nearby cell were not included in the data due to difficulty analyzing the dendritic arborization pattern. Cells with very large dendritic fields were reconstructed from montages using Image J (1.42k, National Institutes of Health) software.

For each RGC scanned, the X, Y coordinates within the retina and the cell's location were recorded. Four different retinal locations, the *area dorsalis*, fovea, red field and yellow field, were identified in the pigeon retina using the following criteria. The ganglion cell was recorded as being in the fovea if it was located within a 300 μm diameter of the fovea. The location of the centre of the fovea was found by the presence of the pit nasal to the optic disc and has the highest ganglion cell density within the depression. If the ganglion cell was located within the *area dorsalis*, it was recorded as being in that location. The *area dorsalis* was identified within the red field as a region of highest ganglion cell density compared with the surrounding red field. The colour of the photoreceptor oil droplets surrounding the ganglion cell was used as an indicator of whether the cell is located in the red or yellow fields. A ganglion cell located in an area with red oil droplets was recorded as being in the surrounding red field, but not in the *area dorsalis* if the cell density was less than that in the *area dorsalis*. A ganglion cell located in an area with yellow oil droplets was recorded as being in the surrounding yellow field, which is outside the fovea.

Measurements of the soma and dendritic field areas were carried out using either the Zeiss LSM Image Browser (version 4, 2, 0, 121) or Image J software. To view the cell in various axes, the same Zeiss program was used to generate X, Y, and Z projections.

Measurement of RGC morphology

The following morphological parameters were measured for the RGCs:

a) Soma area. A closed free shape curve tool was used to trace around the largest soma area out of a series of Z optical images.

b) Dendritic field area. A convex polygon was drawn joining the outermost tips of the dendrites. If the RGC had more than one dendritic arbor, ie, it was either bi-, tri-, tetra- or penta-stratified, then a convex polygon was drawn for each dendritic arbor and the maximum area or diameter was used in our analysis.

c) Stratification in the IPL. Since the IPL thickness changes across the retina, IPL stratification of each cell was expressed as a percentage of the IPL thickness in which a particular cell was found. IPL thickness was calculated from the actual difference in the Z slice height of the outermost boundary of the GCL (defined as 100 %) to the innermost boundary of the INL (defined as 0 %). To determine the percentage of the IPL at which the RGCs stratify, the distance from where the dendritic arbor stratifies to the INL boundary was measured and divided by the IPL thickness. For multi-stratified RGCs (bi- to tetra-stratified) the depth of IPL stratification of each arbor was measured. The IPL percentage was calculated for each of the arbors of multi-stratified RGCs.

Retinal region recording

The distance of the RGC from the fovea was calculated from the X, Y coordinates using the microscope stage ruler. The fovea's X, Y coordinates, located nasal of the pecten tip, were determined from wholemount by finding the area of highest ganglion cell density visible from Propidium Iodide staining of the GCL. The *area dorsalis* was identified by finding the area of highest RGC density within the red field.

5.3 Results

DiI- or DiO-coated tungsten particles penetrated into the RGC side of the retinal flatmounts as deep as the INL, which resulted in labelling of RGCs, displaced amacrine cells in the GCL as well as Müller and amacrine cells in the INL (n = 904 cells; data not shown for non-RGCs). Displaced RGCs were not identified in any of the retinal preparations. When non-RGC cell types were excluded, a total of 765 RGCs were analysed.

The frequency histogram of the RGC soma area show that the soma size is skewed to the left (range = 14-364 μm^2; mode = 50 μm) and the large majority of soma areas are between 20 and 100 μm^2 (Fig. 5.1A). The dendritic field area histogram showed a range of areas from 269 to 203,300 μm^2 in which a majority of RGC field areas are below 2000 μm^2 (Fig. 5.1B).

Nomenclature and classification scheme of the RGCs

The pigeon RGCs were grouped together if the dendritic stratification patterns in the IPL were similar. If the RGC's dendrites made a well-defined lateral arbourization, which extended horizontally along an IPL stratum, then we termed this dendritic arbour as being 'stratified'. The number of dendritic arbours was counted and the following prefixes were used: mono-, bi-, tri- and tetra-stratified. If the RGC's dendrites did not form a well-defined dendritic stratification in the IPL, but instead appear to extend vertically in the IPL without stratifying, then the term 'unstratified' was used. In total, five RGC groups were identified from the sample of labelled RGCs, which could be distinguished from the other groups by the number or lack of stratifications. The other

parameters such as soma area, dendritic field area and dendritic branching pattern were recorded for each RGC group, but were not used to distinguish between the groups due to the great degree of overlap. Although that a RGC group had several variations for different parameters, these variations were not used to further classify them into subgroups due to the large number of variations. The characteristics of the five RGC groups are described below.

Morphological characteristics of the 5 RGC groups

Unstratified

RGCs in the unstratified group were distinctly characterised by dendrites that extended vertically in the IPL (Fig. 5.2). The percent stratification depth of 462 unstratified RGCs was measured from where the dendrites depart the GCL/IPL boundary to the dendritic terminals. RGCs in this group occupied various IPL thicknesses (between 0% and 97% of the IPL thickness) (Fig. 5.2A-C).

The unstratified group had a mean soma area of 49 ± 25 μm^2 (± SD, n = 475). The soma area of the unstratified group ranged from 14 to 364 μm^2. The smallest soma of the unstratified group was found in the fovea, while the largest soma was in the yellow field.

The mean dendritic field area of the unstratified group was 2,853 ± 7,961 μm^2. The unstratified group's dendritic field area ranged from 269 – 121,730 μm^2. The smallest dendritic field area was found in the *area dorsalis* and the largest in the yellow field.

The unstratified group exhibited various degrees of dendritic branching pattern frequency – a mixture of high and low (Fig. 5.3). The RGCs with high frequency

branching pattern possessed thin crooked dendrites, which often appear chaotic (n = 289) (Fig. 5.3A). The dendrites of the unstratified RGCs had numerous varicosities (Fig. 5.20B straight arrow). RGCs with low frequency branching pattern (n = 196) appeared less chaotic than the highly branched unstratified RGCs (Fig. 5.2B).

Monostratified

RGCs belonging to monostratified group were characterised by having their primary dendrites branching off multiple times at a single IPL sublamina where they travelled horizontally (Fig. 5.4A-B). The depth of the terminal stratification zone in the IPL was measured in 80 monostratified RGCs. They stratified at various depths ranging from 0% - 97% of the IPL thickness.

The monostratified group had a mean soma area of 52 ± 18 μm^2 (n = 81; range = 16 – 94 μm^2). Both the smallest and the largest cells of this group were found in the yellow field. The mean dendritic field area of the monostratified group was 7,165 ± 5,412 μm^2 (range = 1,044 – 24,696 μm^2). The smallest and largest dendritic field areas were found in the yellow field.

Three varieties of monostratified RGCs were found which differed in the degree of dendritic branching frequency (Fig. 5.5). The majority (n = 79) of monostratified RGCs possessed high frequency dendritic branching patterns (Fig. 5.5A). At a certain level of the IPL, the dendrites branched multiple times producing short, crooked processes that pointed in various directions (Fig. 5.5A curved arrow). They also had a coarse overall appearance due to the presence of numerous varicosities and high degree of branching frequency with minimal space between the dendrites (Fig. 5.5A). The second variety of monostratified RGC had a slightly less frequent dendritic branching (Fig. 5.5B). One of the features of this monostratified RGC was the recursive dendritic

tips (Fig. 5.5B straight arrow). The third variety of monostratified RGC had a low frequency branching pattern, fewer varicosities, spines (Fig. 5.5C squiggly arrow), and short branches (Fig. 5.5C arrow head) along the primary and secondary dendrites.

Bistratified

The bistratified RGCs were characterised by two dendritic arbours stratifying at two substrata in the IPL (Fig. 5.6). The IPL stratification depths of both dendritic arbours were analysed in 122 RGCs. The proximal arbour (closest to the GCL) stratified at mean of about 84% of the IPL thickness, with a range of 59% - 100%. The distal arbour stratified at a mean of about 34% of the IPL thickness, with a range of 9% - 88%.

The bistratified group had a mean soma area of 75 ± 38 μm^2 (n = 122; range = 25 – 273 μm^2). The smallest and largest soma areas of the bistratified group were found in the yellow field. The mean dendritic field area of the bistratified group was 14,579 ± 9,656 μm^2 (range =1,557 – 44,065 μm^2). The smallest and largest dendritic field areas were found in the yellow field.

Bistratified RGCs were observed with six different combinations of low and high frequency branched arbours (Figs. 5.7, 5.8). One combination consisted of a high frequency branching pattern in both the proximal and distal arbours (Fig. 5.7A-B). The dendrites had numerous coarse varicosities and spines. Although there were numerous branches in the proximal arbour, there was some space in between the dendrites (Fig. 5.7A).

The second variety of bistratified RGCs had a combination of low frequency dendritic branching in the proximal arbour and a very high frequency branching in the distal arbour (n=31) (Fig. 5.7C-D). The proximal dendrites had some varicosities and

few spines (Fig. 5.7C). Their distal dendrites branched extensively from the centre and spread radially with very little space between the dendritic processes (Fig. 5.7D). Varicosities were abundantly present along the distal dendrites. The entire distal dendritic arbour had an oval shape and a tangled appearance. Often, the distal tips of the dendrites pointed away from the soma.

The third variety of bistratified RGCs (n = 30) had a low frequency branching pattern in the proximal dendrites and an even lower frequency branched distal arbour (Fig. 5.7E-F). Its proximal dendrites pointed away from the soma (Fig. 5.7E). The primary dendrites extending from the soma were widely spaced apart, and branched only a few times. The dendrites were slightly wavy with very few spines and varicosities. The shape of the proximal arbour was eccentric relative to the soma. From the proximal arbour, several secondary or tertiary dendrites descended further into the IPL, then terminated with or without lateral processes (Fig. 5.7F).

The fourth variety had a combination of high frequency branching in the proximal arbour and a very low frequency branching in the distal arbour (n=2) (Fig. 5.8A-B). Although there were numerous branches in the proximal arbour, the dendrites had some space between them. Some of the dendritic tips were recursive. Varicosities and spines were present in both arbours.

The fifth variety of bistratified RGC had a low frequency branched proximal and a high frequency branched distal arbours (n = 2) (Fig. 5.8C - D). Its proximal arbour had long, wavy secondary and tertiary dendrites, with a great amount of space between the dendrites (Fig. 5.8C). Compared to the proximal arbour, the distal abour had a higher number of branching and dendritic processes travelling radially (Fig. 5.8D). The dendritic processes had less space between them compared to the proximal arbour. Both arbours had varicosities, spines and recursive dendritic tips.

The sixth combination observed was that both proximal and distal arbours had high frequency branching (Fig. 5.8E-F). Varicosities, spines and recursive dendritic tips were occasionally found. There was some space between the dendrites in both the proximal and distal arbours. The size of the proximal's dendritic field was slightly wider than the distal arbour's.

Tristratified

The tristratified RGCs had dendritic arbours stratifying at three substrata in the IPL (Fig. 5.9). The stratification depths of 40 tristratified RGCs were analysed. The three dendritic arbours stratified at mean depths of about 23%, 56% and 88% of the IPL thickness. The range of stratification depths for the first arbour (closest to the GCL) was 57% - 100%. For the second arbour, the range of stratification depths was 25% - 90%, and for the third arbour it was 0% - 67% of the IPL thickness.

The tristratified group had a mean soma area of 72 ± 56 μm^2 (n = 49; range = 24 – 268 μm^2). The smallest and largest soma areas of the tristratified group were found in the yellow field. The mean dendritic field area of the tristratified group was 33,056 ± 45,827 μm^2 (range = 2,414 – 203,300 μm^2). The smallest and largest dendritic field areas were found in the red field outside the *area dorsalis*.

Four combinations of frequency branching patterns were observed for the tristratified group (Figs. 5.10, 5.11). The first combination had low frequency branching in the first and second arbours and high frequency branching in the third arbour (n = 21) (Fig. 5.10A-C). In the first and second arbour, there was some space between the dendrites, but in the third arbour, there was little space between the dendrites. This minimal spacing between processes gave the third arbour a chaotic appearance. All arbours had varicosities along their dendrites.

The second combination had much lower frequency branching in the second and third arbours compared to the first arbour (n = 5) (Fig. 5.10D-F). The dendrites of the first arbour were not highly branched. The first arbour's dendrites were widely spaced apart, with some spines and varicosities. The dendritic tips pointed away from the soma. The second and third arbours rarely branched many times.

The third combination had high frequency branching in the first and second arbours and an unbranched third arbour (n = 3) (Fig. 5.11A-C). The dendrites in the first and second arbour were filled with varicosities and spines, which gave a coarse appearance. Only a few dendritic processes were present in the third arbour (Fig. 5.11C).

The fourth combination had low frequency branching in all the arbours (n = 13) (Fig. 5.11D-F). The primary, secondary and tertiary dendritic processes were longer in the first arbour compared with the second and third arbours. The dendrites in all three arbours had varicosities, few spines and were widely spaced apart. A few dendritic tips were recursive in all three arbours.

Tetrastratified

The tetrastratified group had dendritic arbours stratifying in four sublamina of the IPL (Fig. 5.12). An analysis of the stratification depths of 15 tetrastratified RGCs was conducted. The four dendritic arbours stratified at mean depths of about 11%, 33%, 55% and 85% of the IPL thickness. The range of stratification depths for the first arbour (closest to the GCL) was 62% - 100%. For the second arbour, the range of stratification depths was 37% - 80%, for the third arbour it was 18% - 65%, and for the fourth it was 0% - 41% of the IPL thickness.

The tetrastratified group had a mean soma area of 47 ± 19 μm^2 (n = 17; range = from 31 – 100 μm^2). The smallest and largest soma areas of the tetrastratified group were found in the yellow field. The mean dendritic field area of the tetrastratified group was 6,680 ± 5,326 μm^2 (range = 1,920 – 19,706 μm^2). The smallest dendritic field area was found in the red field, while the largest was found in the yellow field.

Two combinations of branching patterns were observed for the tetrastratified group. The majority of RGCs had high frequency branching in all four arbours (n = 14) (Fig. 5.13A-D). The dendrites were crooked with spines and varicosities. Within each arbour, there was a small amount of space between the dendrites.

The second combination had progressively decreasing amount of branching frequency from the first to the fourth arbour (n = 3) (Fig. 5.13E-H). The dendrites in the first and second arbours were long with a few spines and varicosities. In the third and fourth arbour, branching rarely occurred and only very short lateral processes were present (Fig. 5.13G-H).

Number of RGCs sampled in different retinal regions

Certain RGC groups were more frequently sampled than other groups out of the total number of RGCs in our sample (n = 765). The unstratified made up the highest proportion of the sample (64%, n = 489). The other groups formed lower proportions of the sample: the bistratified group at 17% (n = 128), the monostratified group at 11% (n = 82), the tristratified group at 6% (n = 49), and the tetratratified group made up the least at 2% (n = 17).

The chances of labelling bipolar cells were not the same depending on the retinal location as shown by the various number of cells obtained in the fovea, central red and yellow fields (Table 5.1). The number of labelled RGCs was much higher in the red

field and *area dorsalis*, and lower in the fovea and yellow fields. Due to the small area of the fovea, it was difficult to target and obtain an abundant number of labelled RGCs in this area. Given the larger area of the red and yellow fields, this allowed greater numbers of RGCs to be labelled by the Diolistics technique. In addition, more RGCs were labelled in the red field, including the *area dorsalis*, than in the yellow field due to the higher RGC density in the red field.

When the numbers of RGC groups were analysed in detail within a region, certain RGC groups were sampled more frequently in a particular retinal region(s) than the other (Table 5.1). The unstratified group was the most frequently sampled out of the other groups in the *area dorsalis*, red field, fovea and yellow field. The least frequently sampled group in the *area dorsalis*, red and yellow fields was the tetrastratified group. In the red and yellow fields, the bistratified group was the second most frequently sampled group. In the *area dorsalis*, the monostratified group was the second most frequently sampled. In the fovea, the mono- and bi-stratified groups were the next most frequently sampled after the unstratified group.

Relationship between the dendritic field areas and eccentricity from the fovea

Due to their greater RGC numbers in the sample, only the unstratified, monostratified and bistratified groups were further analysed separately in terms of how its dendritic field areas changed as its distance from the fovea increases. The tristratified and tetrastratified groups were not further analysed as the RGC numbers were too low for meaningful interpretation. RGCs sampled in the fovea and the yellow field were plotted in the graphs. These yellow field RGCs were outside the fovea and the red field, and whose eccentricity from the fovea ranged between ≤ 1 mm – 16 mm. The dendritic

field area was also analysed to determine how it changed as it enters the *area dorsalis*. The following sections describe the differences in dendritic field areas at different eccentricities for each group.

Unstratified

The dendritic field areas of the unstratified RGCs located in the yellow field did not exhibit a sharp increase as the distance from the fovea increases (Fig. 5.14A). However, a subtle relationship between eccentricity and dendritic field size is evident in that (a) within 1 mm of the fovea, there are no unstratified cells with dendritic fields > 7,000 μm^2, and (b) the largest dendritic field diameters in the yellow field are seen at > 6 mm eccentricity. In the *area dorsalis*, unstratified cells with the largest dendritic fields were > 5 mm from the fovea (Fig. 5.14B).

Monostratified

With respect to the fovea, the dendritic field areas of the monostratified RGCs located in the yellow field exhibited a trend towards increasing dendritic field size as the distance from the fovea increases (Fig. 5.15A). At eccentricities of less than 1 mm from the fovea, monostratified RGCs in this region of the yellow field had similar dendritic field areas of < 8000 μm^2 as those in the fovea. The maximum dendritic field area of 23,960 μm^2 was reached at about 4 mm eccentricity from the fovea, however, the majority of dendritic field areas were below 20,000 μm^2.

Most of the monostratified RGCs in the *area dorsalis* had similar dendritic fields as those in the fovea (Fig. 5.15B). Although a few monostratified RGCs in the *area dorsalis* had dendritic field areas above 8,000 μm^2.

Bistratified

The dendritic field areas of the bistratified RGCs in the yellow field exhibited no clear relationship between size and eccentricity from the fovea (Fig. 5.16A). The dendritic field areas of bistratified RGCs in the yellow field, within 2 mm eccentricity from the fovea, was similar to those in the fovea. At eccentricities greater than 2 mm from the fovea, the dendritic fields of the majority of bistratified RGCs in the yellow fields were in the same range as in the fovea. A similar result is seen in the cells sampled in the *area dorsalis* (Fig. 5.16B).

5.4 Discussion

Our study, the first large scale survey of RGCs in the pigeon retina, classified five morphological RGC groups distinguished by their dendritic stratification pattern in the IPL (Fig. 5.17). The number of RGC groups in the pigeon retina is similar to that classified in the chick retina by Naito and Chen (2004a), which had six RGC groups. Each group in the pigeon retina was characterised in terms of the depth at which the dendritic arbour stratified in the IPL, the soma and dendritic field areas, and the frequency of dendritic branching. The unstratified group was sampled the most frequently in the all regions of the retina. The analysis of the dendritic field area versus eccentricity from the fovea revealed that the unstratified and bistratified RGCs did not exhibit a clear increase in dendritic field area with increasing eccentricity in the yellow field, only the monostratified did. The dendritic field areas of the unstratified, monostratified and bistratified RGCs in the fovea and the *area dorsalis* were similar. The implications of the study's findings will be discussed below.

Distribution and coverage of RGC groups in the pigeon retina

It has been hypothesized that when a spot of illumination hits the retina, all RGC types should be present in that illuminated region. In other words, each RGC type must be distributed so as to provide complete coverage across the retina (Wässle & Boycott, 1991). For the purpose of this study, if the RGC groups classified in the pigeon retina were considered to be equivalent to different types, then the hypothesis would be that all the groups would be distributed throughout the retina. Counter to this argument would be that not all the RGC types are distributed uniformly throughout the pigeon retina. What the current study was unable to determine was how each of the RGC groups cover

or tile the retina: ie, does the dendritic fields of each group provide a complete and efficient coverage with sufficient overlap and no gaps across the retina? Future investigation involving quantifying the densities of each RGC type using methods that can specifically label these cells in the pigeon retina would be useful in determining the degree of dendritic coverage across the retina and which groups provide significant contribution to the circuitry in a specific area.

Our grouping of RGCs into five groups has certainly missed some RGC types in the pigeon retina, one of which is the displaced RGCs, as a result of the limitation of the Diolistics technique used. Displaced RGCs in the pigeon retina have been counted and mapped in a previous study by Hayes and Holden (1983), revealing that the numbers of displaced RGCs are concentrated in the central yellow field (near the fovea) and in the mid-temporal yellow field. Displaced RGCs were sparsely distributed in the red field and only one was found in the fovea (Hayes & Holden, 1983). Given that the displaced RGCs are not evenly distributed in the pigeon retina, it is possible that other types of RGCs are also distributed unevenly. This uneven distribution of certain retinal neurons is not surprising as it has been shown in Chapter 3 that the pigeon fovea is rod-free (Querubin et al., 2009). Furthermore, previous studies have shown that certain regions in the pigeon retina contain different quantities of synaptic units in terms of the ratio of amacrine and bipolar synapses, amacrine synaptic density, and the ratio of bipolar to amacrine and ganglion cell synapses (Dubin, 1970; Yazulla, 1974). The red field was found to contain higher amacrine to bipolar cell synaptic ratio and amacrine synaptic density than the yellow field and *area centralis* (fovea) (Yazulla, 1974). Thus, there is growing evidence that the circuitry, the interconnections and the pathways for transmission of information between various types of neurons are different in the two specialized areas.

Dendritic field variation in different retinal regions

In the mammalian retina, it has been shown that certain types of RGCs, eg, the alpha and beta cells, dendritic field size increase with increasing eccentricity from the *area centralis* and/or visual streak (Boycott & Wässle, 1974; Stein *et al*., 1996; Isayama *et al*., 2009). A similar analysis was conducted for the unstratified, monostratified and bistratified groups to investigate whether dendritic field areas become larger as the distance from the pigeon fovea increases and enters the peripheral retina outside the specialized areas. However, such analyses were restricted to RGCs sampled in the fovea and the yellow field, where dendritic fields were expected to be larger as the RGC density in the yellow field is lower. This expectation was met: the monostratified RGCs exhibited greater dendritic field area as they are located further from the fovea and reach the peripheral yellow field. Contrary to the expectation, the bistratified RGCs did not show enlargement of dendritic field areas as their location reaches the peripheral yellow field. The unstratified RGCs showed only a subtle increase at greater eccentricities. When the dendritic fields of these three RGC groups were compared between the fovea and the *area dorsalis*, no differences were found. It would be interesting to determine how the coverage between the different regions change as the dendritic field sizes vary and how much overlap exists between the dendrites of different RGC types. Future studies are required to answer these questions.

Connectivity between RGCs and bipolar cell types

If a particular bipolar cell type co-stratifies in the same IPL sublamina as a RGC group, it is possible that the two neurons are connected. We have reported the depths of at which the bipolar cell types and RGC groups stratify in the IPL. However, RGC groups co-stratifying in the same sublamina as a bipolar cell type do not necessarily

mean that synaptic connections exist between them. A more thorough detailed analysis will be required to establish that certain types of bipolar and ganglion cells form synapses with each other. This may involve specific labelling of either the bipolar cell or RGC types using immunohistochemistry to identify synaptic proteins on the processes of these cells, similar to the experiments conducted in the marmoset retina (Percival *et al*., 2009; Percival *et al*., 2011). A more direct way would be to identify the synaptic ribbons in the axon terminals of a bipolar cell type in contact with a RGC type using electron microscopic reconstruction (Kolb, 1970; Kolb, 1979; Kolb & Dekorver, 1991; Calkins *et al*., 1994).

Possible midget-like RGC type in the pigeon retina

The primate fovea contains midget bipolar cells and midget ganglion cell types (Polyak, 1941; Boycott & Dowling, 1969; Kolb, 1970; Calkins *et al*., 1994; Kolb & Marshak, 2003). The 1:2 ratio between a cone photoreceptor and midget ganglion cells ensures that it preserves the high spatial resolving limit set by the cone photoreceptors (Wässle & Boycott, 1991). The dendritic diameter in the primate fovea of a midget RGC is so small (5–10 μm diameter (Boycott & Dowling, 1969; Kolb, 1970; Dacey, 1993b; Kolb & Marshak, 2003)) that it only contacts one midget bipolar cell. Identifying a type of bipolar cell and RGC in the pigeon fovea with a dendritic morphology the same as that in the primate fovea would suggest that the existence of a midget circuitry in the pigeon retina may be possible. The results of the study in Chapter 4 indicated that at the level of bipolar cell and photoreceptor connectivity, a midget circuitry appeared to have some similarity with that of the primate. A similar midget-like bipolar cell type identified by Mariani (1987) and Lockhart (1979) were proposed as possible midget-like bipolar cells in the pigeon retina (see Chapter 4).

These bipolar cells were estimated to receive input from only one photoreceptor and had narrow dendritic field widths in the fovea and red field (Lockhart, 1979; Mariani, 1987). However, a pigeon RGC with a dendritic morphology similar to the primate midget RGC was not found in our study. The RGC group in the pigeon retina that contained ganglion cells with the smallest dendritic fields was the unstratified group. The unstratified RGCs' minimum dendritic field area was 269 μm^2 (diameter ~ 18.5 μm) located in the *area dorsalis*. If the definition of a midget RGC is that its dendritic field size is the smallest out of all the other RGC types, then the best candidate midget-like RGC in the pigeon would be the unstratified RGC.

The pigeon unstratified RGC has several differences with the primate midget RGC. Firstly, the primate midget ganglion cell has a single primary dendrite emanating from the soma, and the primary dendrite branches into a narrow arbour (Polyak, 1941; Boycott & Dowling, 1969; Kolb, 1970; Kolb & Marshak, 2003). In contrast, our pigeon midget-like unstratified RGC had a dendritic branching pattern very distinct from the primate cell in that the unstratified cell has several dendritic processes. Second, the diameter of the unstratified RGC dendritic field was wider compared with the primate midget ganglion cell. Unlike the primate midget ganglion cell which monostratifies at either the ON or OFF sublamina of the IPL (Polyak, 1941; Boycott & Dowling, 1969; Kolb, 1970; Dacey, 1993b; Kolb & Marshak, 2003), the pigeon unstratified group RGCs stratified broadly at different depths in the IPL. Considering the pigeon unstratified group RGCs have vertically oriented dendrites and occupy a thick portion in the IPL, its morphology suggests that it may receive input from several bipolar cells. The high amount of convergence from photoreceptors to RGCs via bipolar cells does not resemble the single cone input feeding into primate midget pathway observed in the fovea. The true number of bipolar cells contacting the unstratified group RGCs in the

IPL would need to be examined using electron microscopy reconstruction similar to that done in the primate retina (Kolb, 1970; Kolb & Dekorver, 1991; Calkins *et al*., 1994).

Correlation between the morphological and physiological RGC types in the pigeon

According to Dubin (1970), the pigeon retina is thought to be more 'complex' than the primate, cat and rat retinas based on the ganglion cell receptive field properties. The ganglion cell receptive fields in the cat and monkey are organized in simple, concentric, antagonistic and centre-surround pattern (Kuffler, 1953; Hubel and Wiesel, 1960; Wiesel, 1960; Rodieck and Stone, 1965a; b). These receptive fields are well organized to send a message about local intensity differences but pass on a relatively untransformed picture of the retinal image to the higher visual centres. In the pigeon, most receptive field units are complex as there are a greater percentage of ganglion cells with directional selective and motion sensitive properties. Direction selective RGCs respond only to specific directions in movement (Maturana and Frenk, 1963). These directional movement RGCs were reported to form 30% of the accessible cell population of the pigeon optic nerve. Their five fundamental characteristics include: small receptive fields; an exclusive response to the movement of an edge in one direction but not in the reverse; an absence of response to phasic changes of ambient light; and a uniformly on-off receptive field.

Maturana and Frenk (1963) found another type of RGCs, the horizontal edge detectors, which respond maximally to a horizontal edge moving vertically up or down across the receptive field, or to the tip of a bar, or to the corner of a rectangle if the horizontal edge extends for some distance in the surroundings.

Other investigators reported similar findings to Maturana and Frenk (1963) (Pearlman and Hughes, 1976). Pearlman and Hughes (1976) reported that the most common type of RGC receptive field unit in the pigeon is the direction selective units, which comprise about 38% of the recorded units. The direction selective units have the basic ON-OFF inhibitory surround cells. The second type respond to ON and OFF stationary spots of light. These RGCs comprise 25% of the recorded population. All of the receptive fields have inhibitory surrounds of varying strength that do not produce a response when illuminated alone, but antagonize responses from the central region. The third type were motion sensitive units, comprising 15% of the recorded population. The motion sensitive units have similar responses to the ON-OFF centre type. The fourth type respond only to ON or OFF stationary stimuli in their receptive field centres with antagonistic but unresponsive receptive field surrounds. These cells comprise about (11%) of the units studied. It would have been interesting to know what the morphology of these recorded RGCs in order to compare it with the morphology of the RGCs in our data.

Grouping the pigeon RGCs according to the number of dendritic arbours may be useful in presumptively associating this morphological parameter with known physiologies of ganglion cells in other species. Direction selective RGCs have been well characterised in the mammalian retinas (Barlow and Levick, 1965; Amthor et al., 1984b; Famiglietti, 1992b; a; Yang and Masland, 1992). The morphology of the direction selective RGCs in the mammalian retina is that of a bistratified RGC: one arbour narrowly stratifies within sublamina a of the IPL, and the other ramifies narrowly in sublamina b, hence it is called the ON-OFF direction-selective ganglion cell. In the pigeon retina, our study has identified the bistratified RGC, which has similar dendritic morphology as those direction-selective ganglion cells described in the

mammalian retinas (see Figs. 5.7-5.8). It is possible that some of the pigeon bistratified RGCs we have identified could have direction selective properties that previous investigators have recorded in the pigeon. The presence of a high proportion of direction selective RGCs in the pigeon may be useful for detecting rapidly approaching predators attacking the pigeon. Another property of the ganglion cell that may be useful for the pigeon's daily activities, such as searching for food on the ground, is light adaptation to changes in the light intensity during the day. Smirnakis and collaborators (1997) reported that RGCs in the tiger salamander and rabbit adapt gradually to abrupt or quick changes in both image contrast and spatial correlations within a scene even at constant mean intensity. It would be interesting to determine the physiological properties of the other RGC groups in the pigeon retina and how this relates to some of their visual capabilities.

What factors in the retinal circuitry other than the type of RGCs may contribute to the pigeon's 'complex' ganglion cell receptive field properties? There is evidence showing that the ratio of the number of amacrine cell synapses to bipolar cell synapses may be correlated with the ganglion cell receptive field complexity (Dubin, 1970). The pigeon red field contains a greater ratio of amacrine cell synapses (conventional synapses) to bipolar cell (ribbon) synapses compared with that in the human parafovea, monkey fovea, cat and rat. These ratios have been correlated with the ganglion cell receptive field complexity, with the pigeon being the most complex, while the primate, cat and rat being the least complex as discussed above. Furthermore, the pigeon red field has been found to have a higher amacrine cell synapse density, lower bipolar cell synapse density, and a greater involvement of amacrine cells in the IPL circuitry compared with the primate, cat and rat. If amacrine cells are more involved in modifying the information process than the bipolar cells providing input into the RGCs

in the pigeon red field, this could suggest that the circuitry or the visual information pathway signaling is different. It might be better adapted for a different form of visual stimuli compared with the primate or the cat or rat. The primate relies greatly on its central vision to resolve fine details mediated by the fovea, while the pigeon on direction and motion sensitivity. Determining the mechanisms in which the amacrine cell, bipolar cell and ganglion cell modify the responses to different forms of visual stimuli would provide invaluable information into the visual processing in the pigeon retina.

Pigeon RGC types compared with other avian RGC types

There have been a few studies, which have morphologically classified the RGC types in the pigeon retina using a distinct classification scheme from ours. Unlike previous studies, our classification system was based solely on the dendritic stratification pattern of the RGCs in the pigeon retina. Other parameters of classification such as dendritic field and soma sizes did not allow a clear distinction of the different RGC groups in our study. Hayes and Holden (1980) classified RGC types based on soma size in the pigeon retina, and revealed the presence of only a single size class in the central yellow field. Hayes (1982) reported preliminary findings of a few morphological RGC types in the peripheral nasal yellow field labelled by HRP, including small bushy, monostratified, bistratified and wide-field RGCs, but the detailed morphological characteristics of these RGCs have not been reported. The dendritic morphology, size and stratification pattern of these ganglion cell types may correspond to some of our groups.

Compared with previous studies in the chick and quail retinas, most of our morphological RGC groups are similar to the groups defined by different investigators

(Ikushima et al., 1986; Thanos et al., 1992; Chen and Naito, 1999; Naito and Chen, 2004a; Chen and Naito, 2009). Thanos and co-investigators (1992) classified eight groups of RGCs, including displaced ganglion cells in the chick retina, a slightly greater number of groups than ours. Their groups 1 and 2 showed similar dendritic morphology to our subgroups unstratified group, in terms of dendritic size and stratification patterns. Thanos and collaborators' (1992) unistratified and bistratified RGCs may be comparable to our monostratified and bistratified groups in the pigeon retina. Unlike Thanos and colleagues' (1992) study, we were not able to label displaced ganglion cells in our study. In the quail retina, seven types were identified by HRP labelling, some of which had similar flatmount dendritic branching pattern and field size to our unstratified, monostratified and tristratified groups (Ikushima *et al*., 1986). Naito and Chen (2004a) classified six RGC groups in the chick retina based on soma and dendritic field size changes with respect to eccentricity from the central area (or *area centralis*) and further subdividing them into complex and sparse dendritic branching pattern. Although our classification scheme differed from Naito and Chen's (2004a), all of the groups in our study have comparable flatmount dendritic field morphology with their six groups. In terms of the high frequency branching pattern of the pigeon RGC groups: the unstratified, bistratified, tristratified and tetrastratified groups may correspond to Naito and Chen's (2004a) complex groups I, 2 and 4. The low frequency branching pattern of RGCs in the pigeon unstratified, monostratified, bistratified and tristratified groups was similar to Naito and Chen's (2004a) simple subgroup 1 and 2. The unstratified and tristratified groups in our study showed comparable dendritic field branching pattern and very wide dendritic field areas as the group 3 RGCs (Naito & Chen, 2004a). The number of RGC groups classified depends on the classification system used, the data and the methods used to analyse the data. Regardless of the

classification scheme used and the method used to label the cells, the number and morphology of the different types/groups of RGCs in the pigeon retina are very similar between those classified previously in other avian species.

The advantages and limitations of the Diolistics technique

The Diolistics technique has allowed us to label hundreds of neurons in the retina and collect an abundant data on the various morphological characteristics of different RGCs. Unlike previous studies in the pigeon retina, which used the Golgi impregnation method, our study has revealed five RGC groups with distinct dendritic stratification pattern and number of arbours, and within each group several varieties exist with a wide range of stratification depths and dendritic branching patterns. The fluorescently labelled RGCs displayed the dendritic branches with so much clarity, it revealed some RGC groups, such as the unstratified, that have not been described in some mammalian retinas.

Although the Diolistics technique allowed faster and more efficient collection of a large number of RGCs per retina, there are some limitations to this method. It was not as successful in labelling a large number of RGCs in a small area like the fovea and was therefore undersampled compared with the larger areas like the red and yellow fields. Having a large area to target did not always result in a greater number of labelled RGCs. We found a much greater number of labelled RGCs in the red field than in the yellow field, despite ensuring that both areas received the same amount of 'shots'. The reason for this unequal sampling might be due to the higher density of RGCs in the red field than in the yellow field. As for the unequal proportion of RGC groups in the sample, it is likely that certain RGC groups were more easily labelled by DiI/DiO and that not all the RGC types have been labelled. Therefore, it should be borne in mind that the

numbers of RGC groups sampled in the different retinal regions do not equate to the true proportion of the groups in the RGC population.

5.5 Conclusions

The pigeon retina contains approximately five main RGC groups, which differ in stratification patterns. One RGC group, the unstratified, had the smallest dendritic field size and might be a good candidate midget-like ganglion cell in the pigeon retina. However, in terms of the dendritic morphology and stratification pattern of the unstratified RGCs, it is not the same as the primate midget ganglion cell. Because of its dendritic field size and thick stratification in the IPL, it is unlikely to contact only one bipolar cell. Therefore, these data suggest that pigeon may not have the same midget circuitry as the primate. The evidence suggests that the pigeon has a different circuitry from the midget circuitry involved in processing high acuity information in the two specialised areas. Further characterization of the pigeon RGC groups is necessary to determine its physiological properties, differential distribution, coverage, connectivity between other neurons in the IPL. This would increase our understanding of how physiologically different or similar it is from the primate midget RGC. Taken together, the pigeon retina may process high acuity information using an uncharacterised pathway, which when fully identified may provide another avenue of study to recapitulate high acuity vision.

Chapter 5 figures and tables

Figure 5.1. Frequency histograms of soma and dendritic field areas sampled in the retina (opposite page). A. = 10 μm^2 soma area intervals (n = 765). B. 500 μm^2 dendritic field area intervals (n = 755).

Frequency histograms of soma and dendritic field areas in the sample

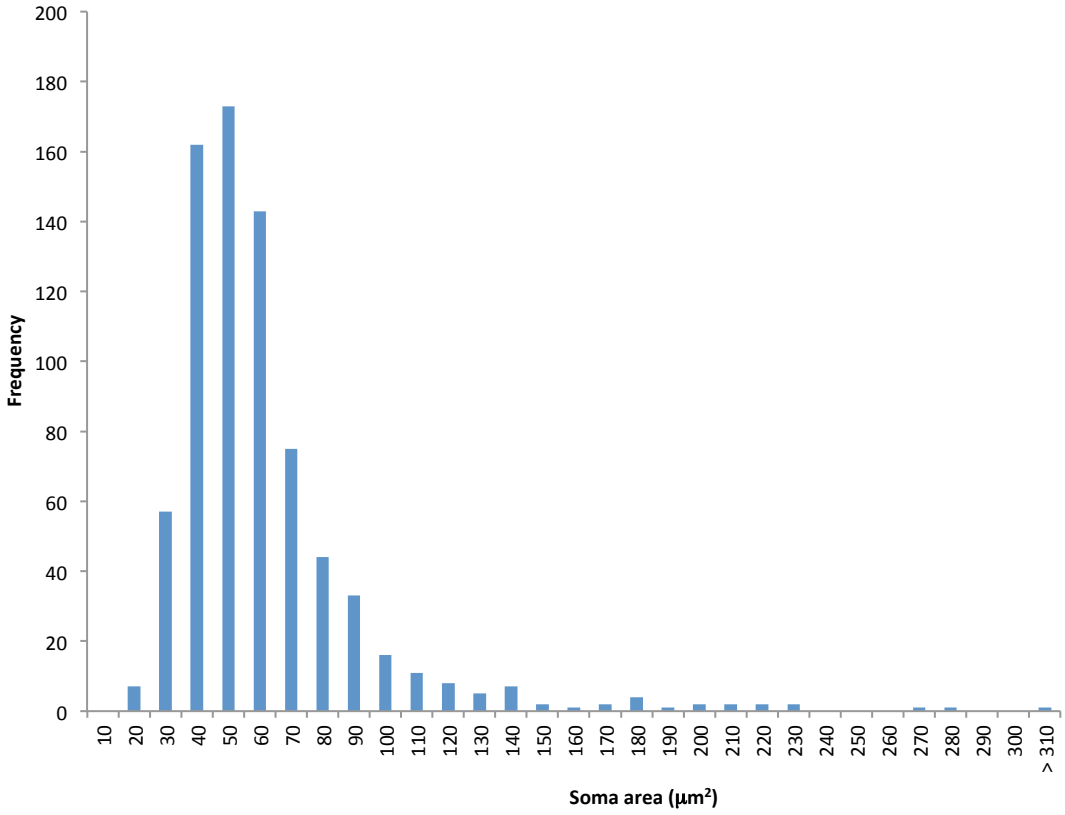

A.

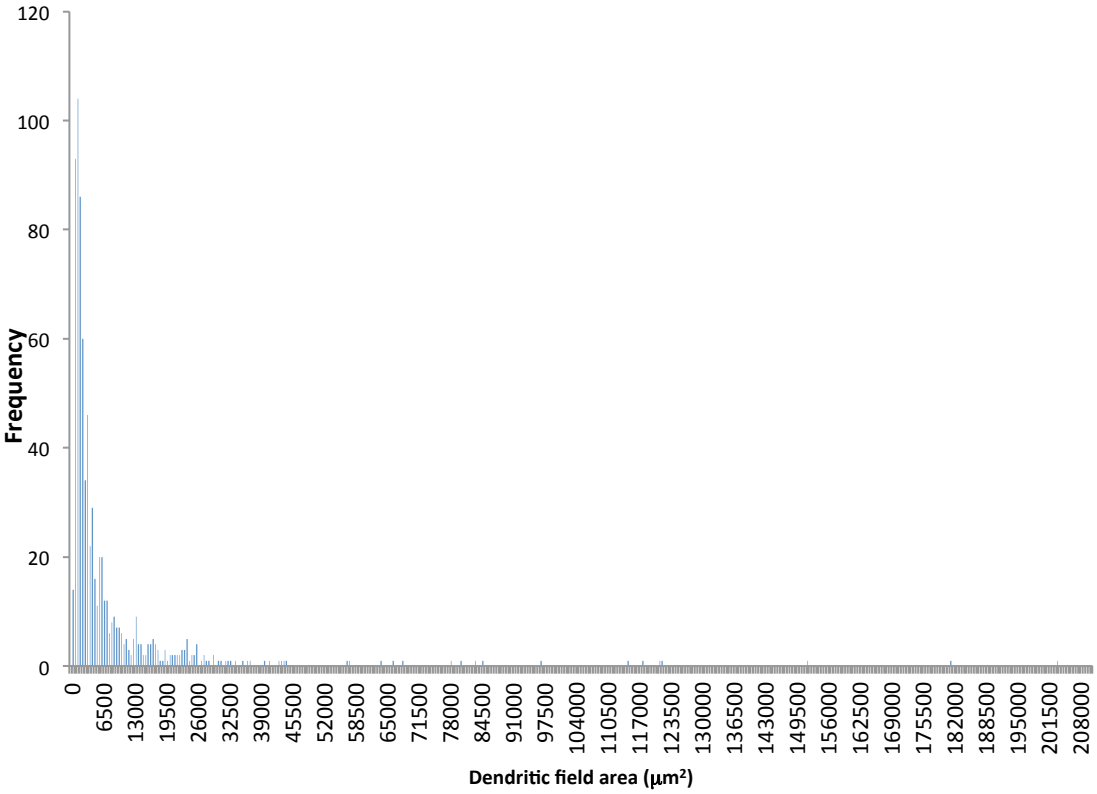

B.

Figure 5.1.

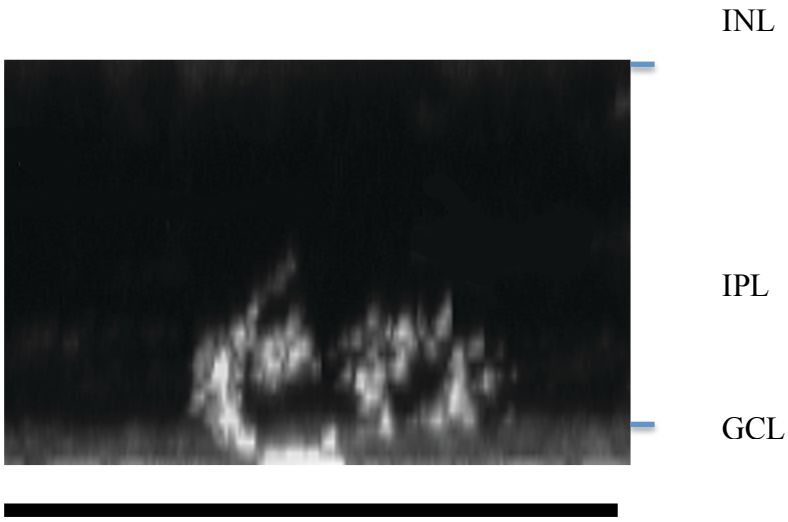

A. An unstratified RGC occupying in the inner half of the IPL.

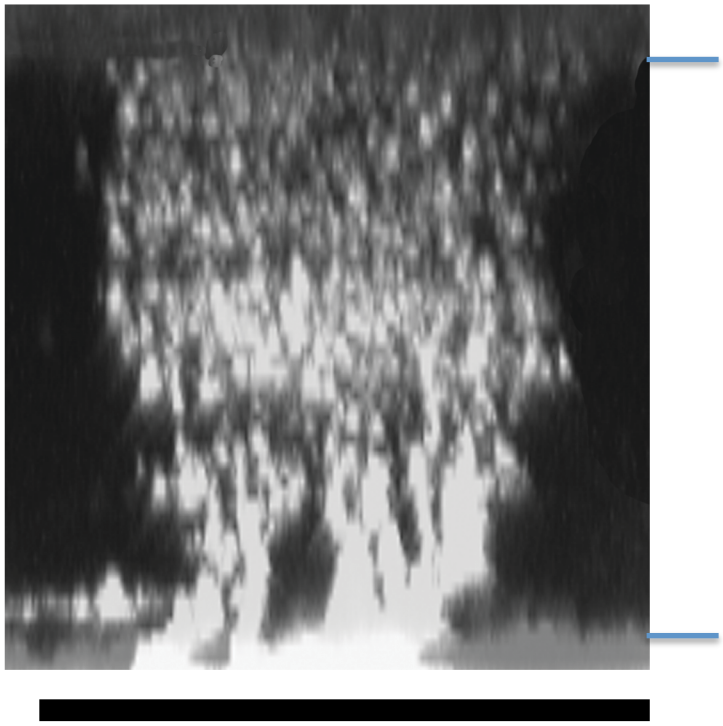

B. An unstratified RGC occupying the entire thickness of the IPL.

Figure 5.2 A-B. Z projection micrographs of the unstratified group. The ganglion cell body is at the bottom of the image in the GCL. The INL/IPL boundary is near the top of the image. The lines on the right hand side indicate the thickness of the IPL. Scale bar = 50 μm.

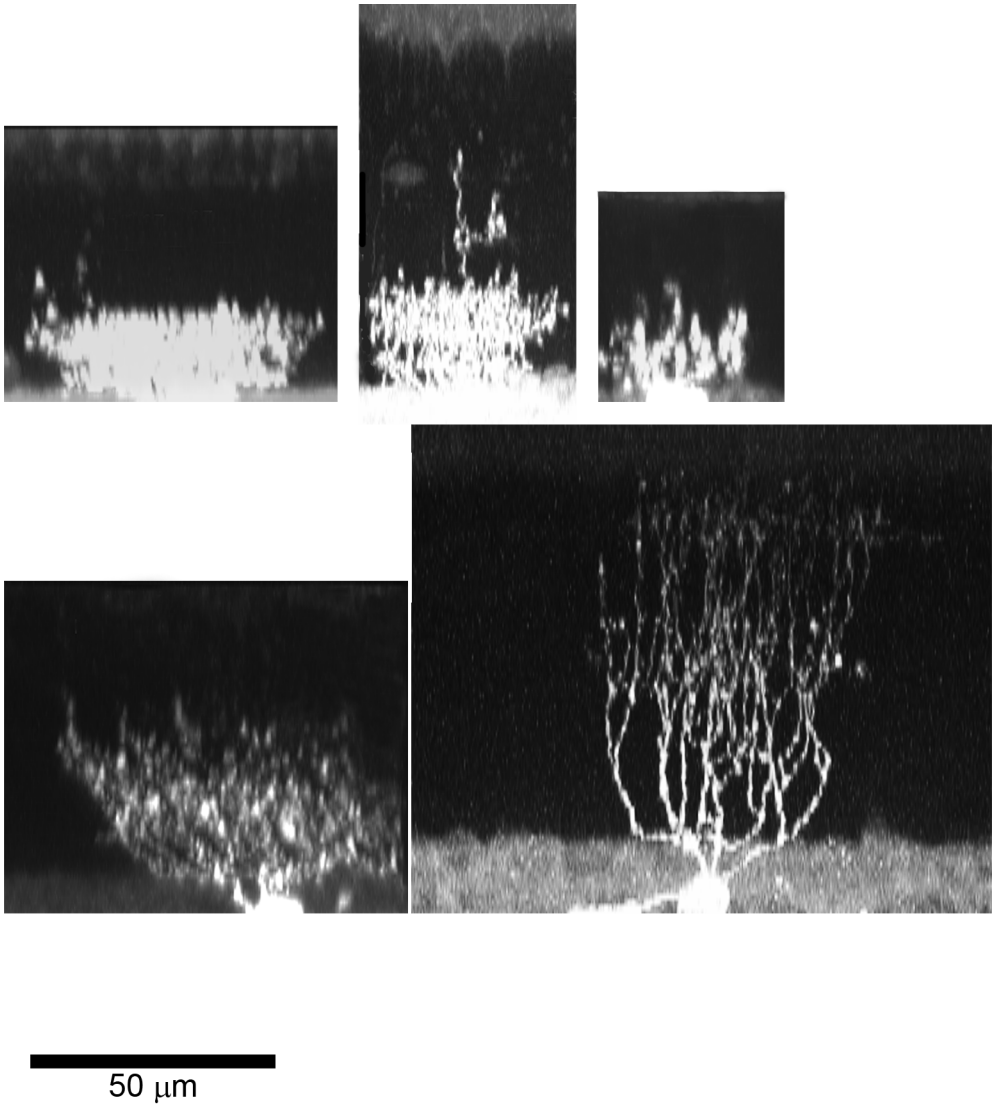

Figure 5.2 C. Z projection micrographs of the unstratified group. The unstratified RGCs above occupy various thicknesses of the IPL. The ganglion cell body is at the bottom of the image in the GCL. The INL/IPL boundary is near the top of the image.

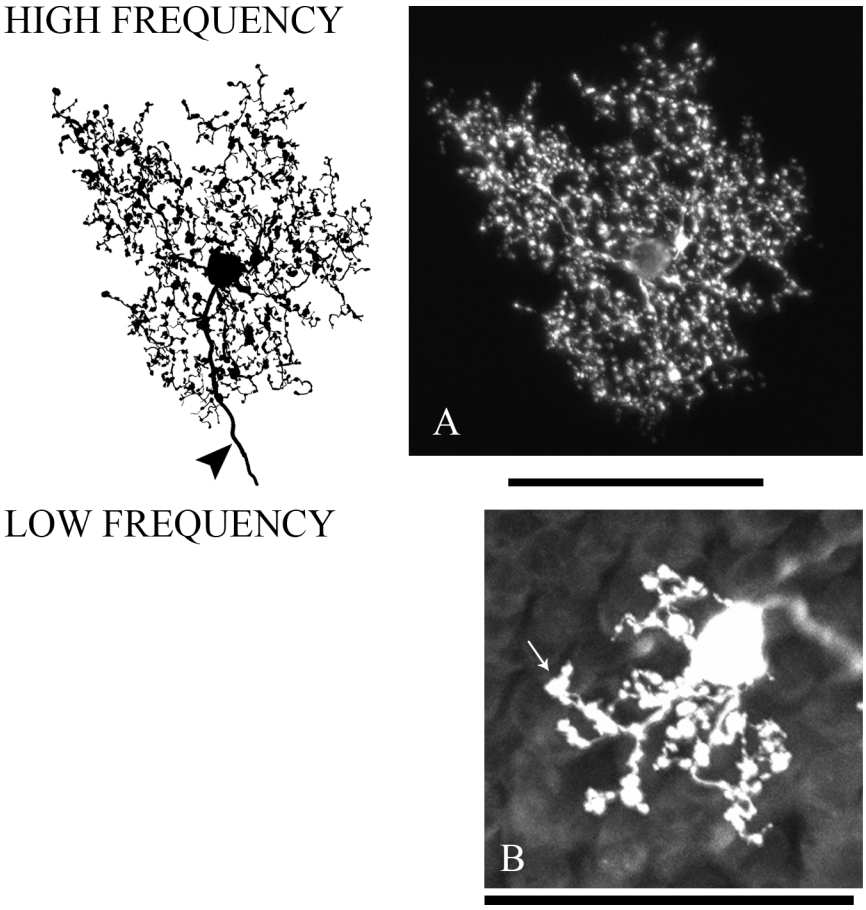

Figure 5.3. X/Y projection micrographs of the unstratified group exhibiting high and low dendritic branching frequency. A. High frequency dendritic branching RGC. To show the branching pattern more clearly, on the left of the micrograph of a high frequency RGC is a drawing of the same cell done in Adobe Photoshop CS5. The arrowhead points to its axon labelled. B. Low frequency dendritic branching RGC. The straight arrow points to a varicosity. The scale bars in A – B = 50 μm.

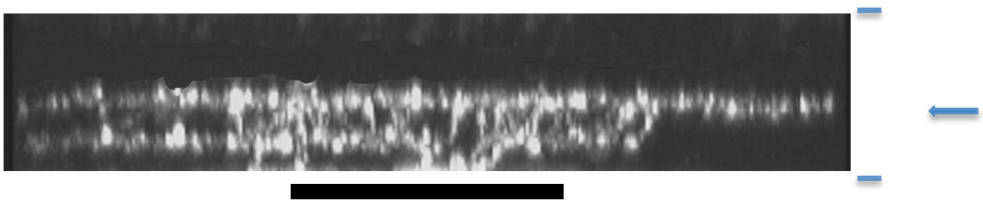

A.

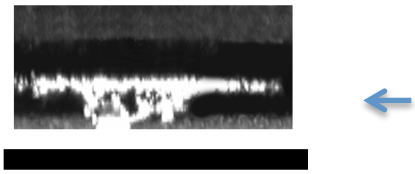

B.

Figure 5.4. Z projection micrographs of the monostratified group. A. A monostratified RGC. The ganglion cell body (not visible) is at the bottom of the image in the GCL. The INL/IPL boundary is at the top of the image. B. Another monostratified RGC. The arrows point to the horizontally stratifying dendritic arbour. The lines on the right hand side indicate the IPL thickness. A. Scale bar = 50 μm.

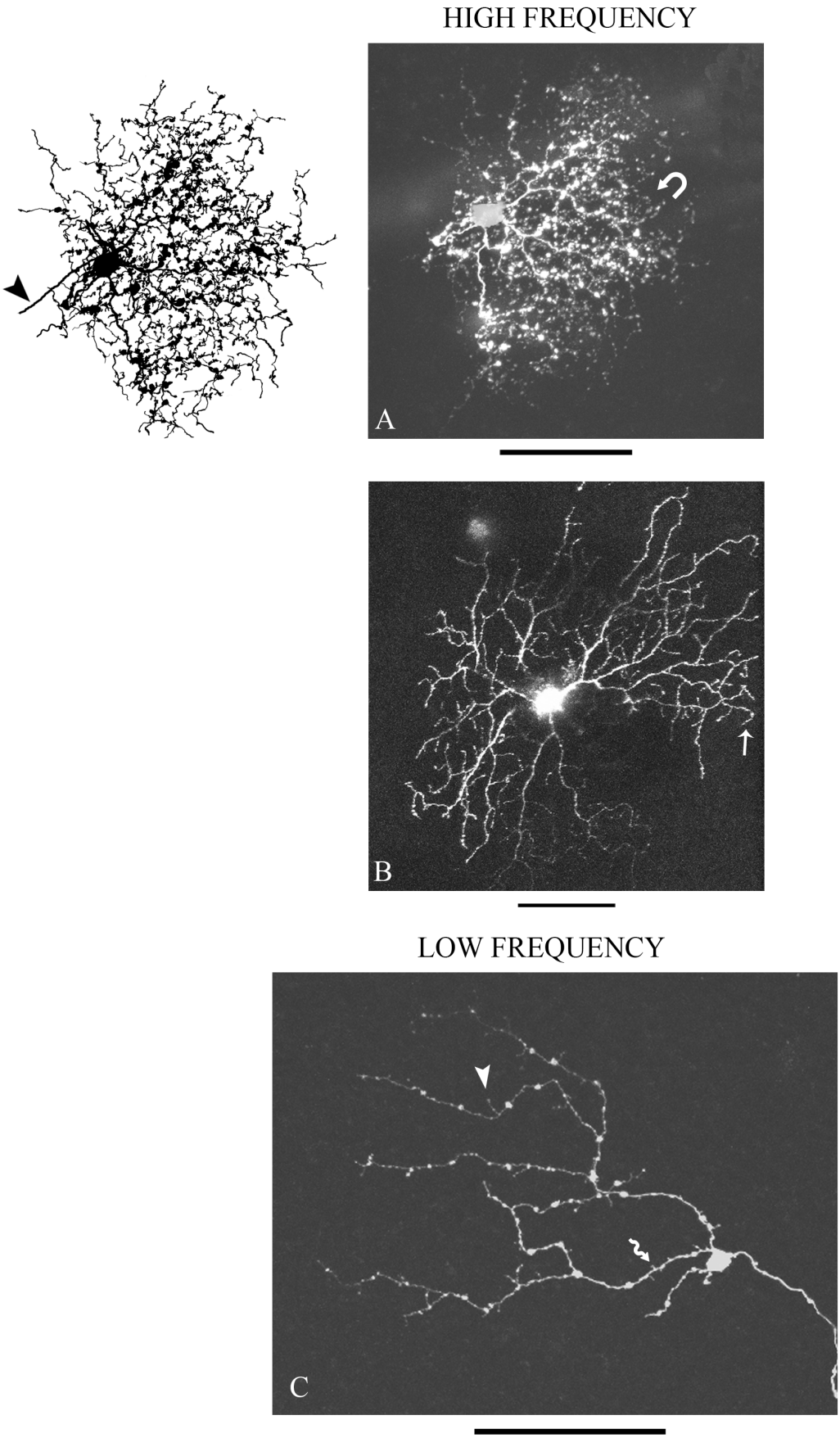

Figure 5.5

Figure 5.5. X/Y projection micrographs of the monostratified group exhibiting high and low dendritic branching frequency. A. A monostratified RGC with high frequency dendritic branching. The curved arrow points to the crooked processes. To show the branching pattern more clearly, on the left of the micrograph of a high frequency RGC is a drawing of the same cell done in Adobe Photoshop CS5. The arrowhead points to its axon labelled. B. Another RGC with high frequency dendritic branching. The straight arrow points to recursive tips. C. A monostratified RGC with low frequency dendritic branching. The arrowhead points to a short branch and the squiggly arrow points to spine. The scale bars in A = 50 μm; B - C = 100 μm.

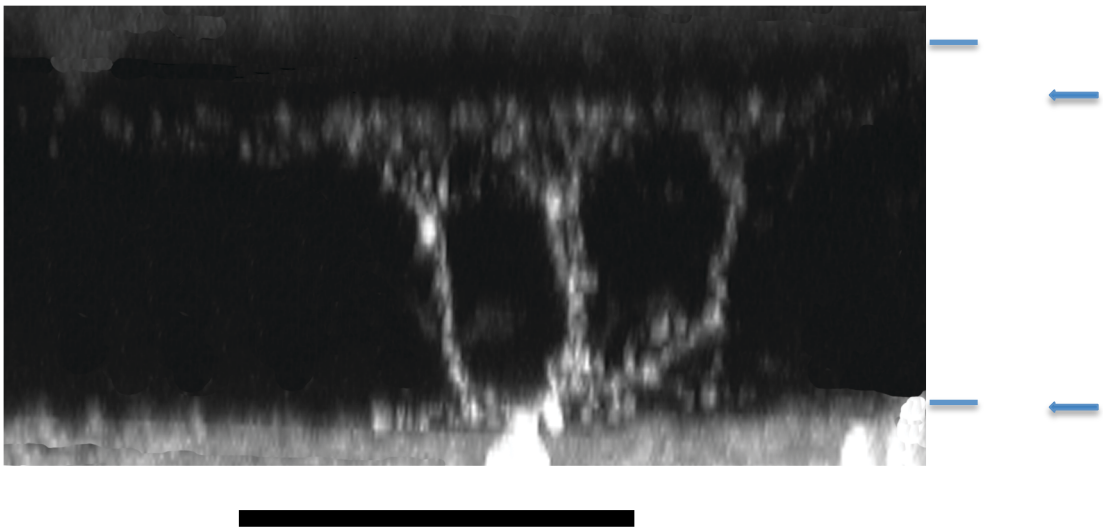

Figure 5.6. Z projection micrograph of a bistratified RGC. The ganglion cell body is at the bottom of the image in the GCL. The INL/IPL boundary is near the top of the image. The arrows point to the two dendritic arbours. The proximal arbour is close to the GCL and the distal arbour is close to the INL/IPL boundary. The lines on the right hand side indicate the thickness of the IPL. Scale bar = 50 μm.

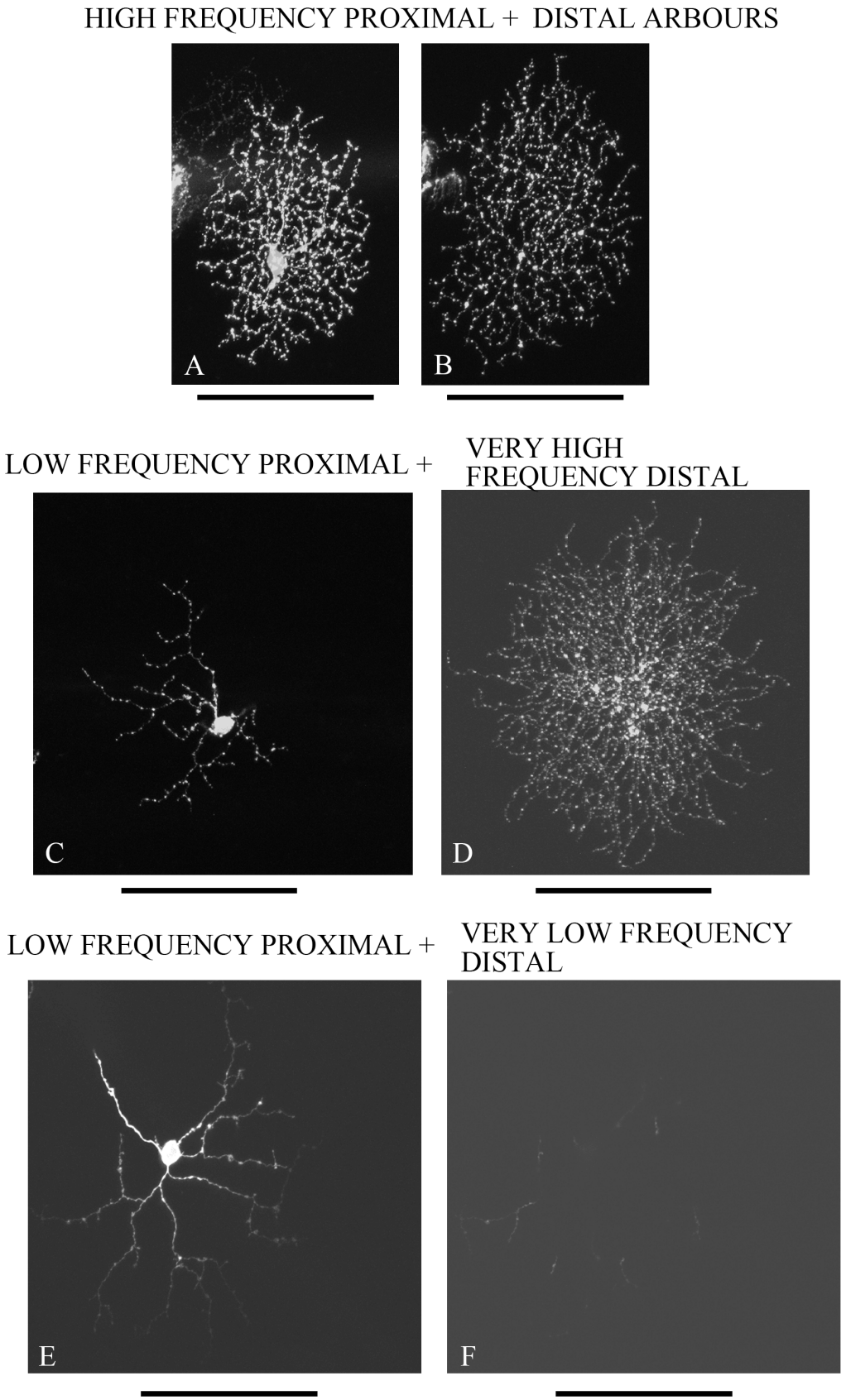
HIGH FREQUENCY PROXIMAL + DISTAL ARBOURS
A
B
LOW FREQUENCY PROXIMAL +
VERY HIGH FREQUENCY DISTAL
C
D
LOW FREQUENCY PROXIMAL +
VERY LOW FREQUENCY DISTAL
E
F

Figure 5.7

Figure 5.7. X/Y projection micrographs of the bistratified group exhibiting combinations of high and low dendritic branching frequency. A – B. A bistratified RGC with a high frequency dendritic branching in both the proximal and distal arbours. The bright white object in the left side of the RGC was a densely labelled spot. C - D. Another bistratified RGC exhibiting low frequency branching in the proximal arbour and a very high frequency branching in the distal arbour. E - F. A bistratified RGC with low frequency branching in the proximal arbour and a much lower frequency in the distal arbour. The scale bars in A - F = 100 μm.

HIGH FREQUENCY PROXIMAL + VERY LOW FREQUENCY DISTAL

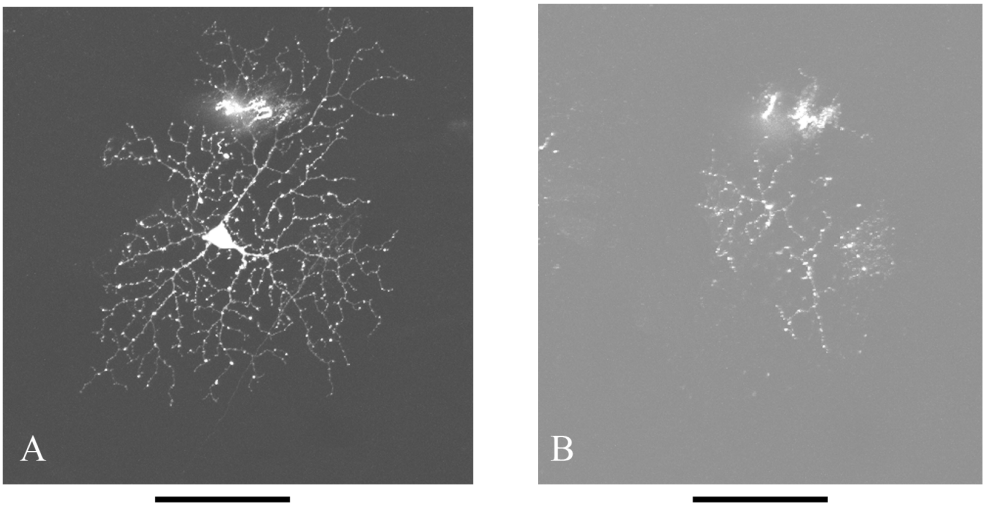

LOW FREQUENCY PROXIMAL + HIGH FREQUENCY DISTAL

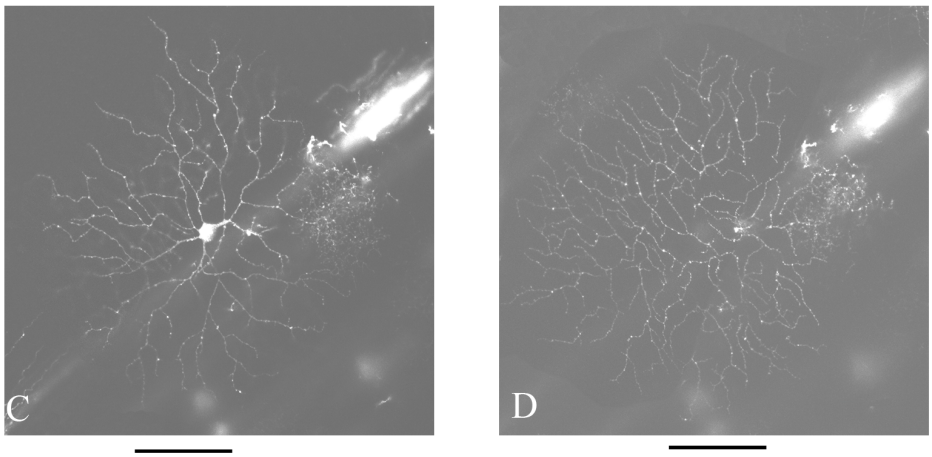

HIGH FREQUENCY PROXIMAL + HIGH FREQUENCY DISTAL

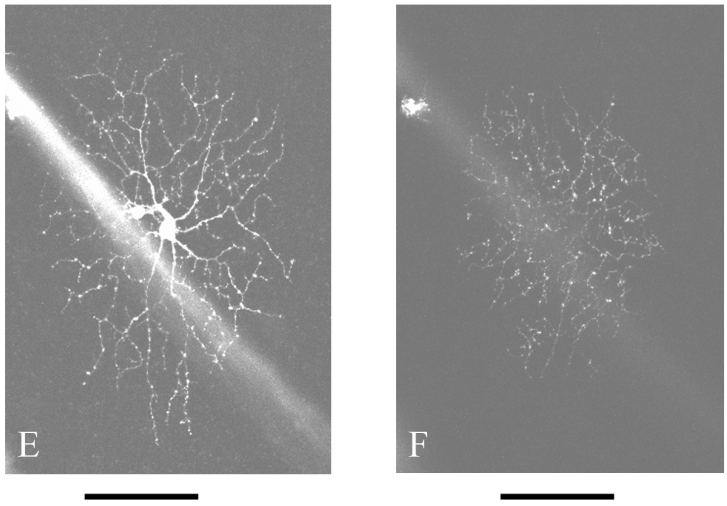

Figure 5.8

Figure 5.8. X/Y projection micrographs of the bistratified group exhibiting more combinations of high and low dendritic branching frequency. A – B. A bistratified RGC with a combination of high frequency dendritic branching in the proximal and very low dendritic branching frequency in the distal arbour. C - D. Another bistratified RGC exhibiting low frequency branching in the proximal arbour and a high frequency branching in the distal arbour. E - F. A bistratified RGC with a low frequency branching in the proximal arbour and an even lower frequency in the distal arbour. The bright white spots and lines near the RGCs were the densely labelled processes of adjacent cells. The scale bars in A - F = 100 μm.

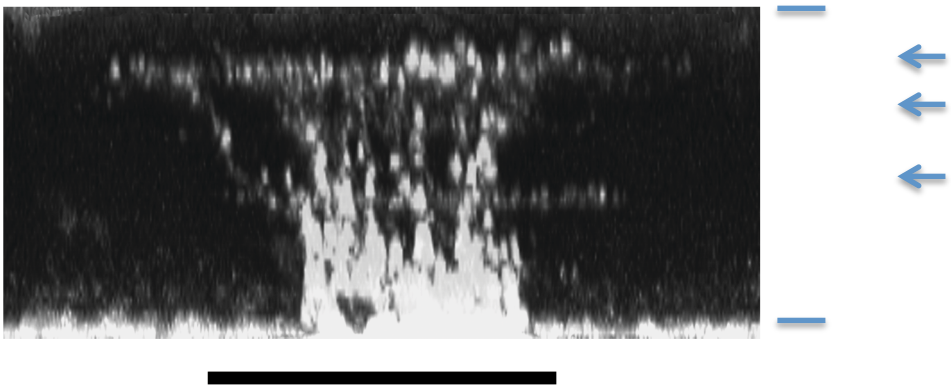

Figure 5.9. A Z projection micrograph of a tristratified RGC. The ganglion cell body is at the bottom of the image in the GCL. The INL/IPL boundary is near the top of the image. The arrows point to the three dendritic arbours. The lines on the right hand side indicate the thickness of the IPL. Scale bar = 50 μm.

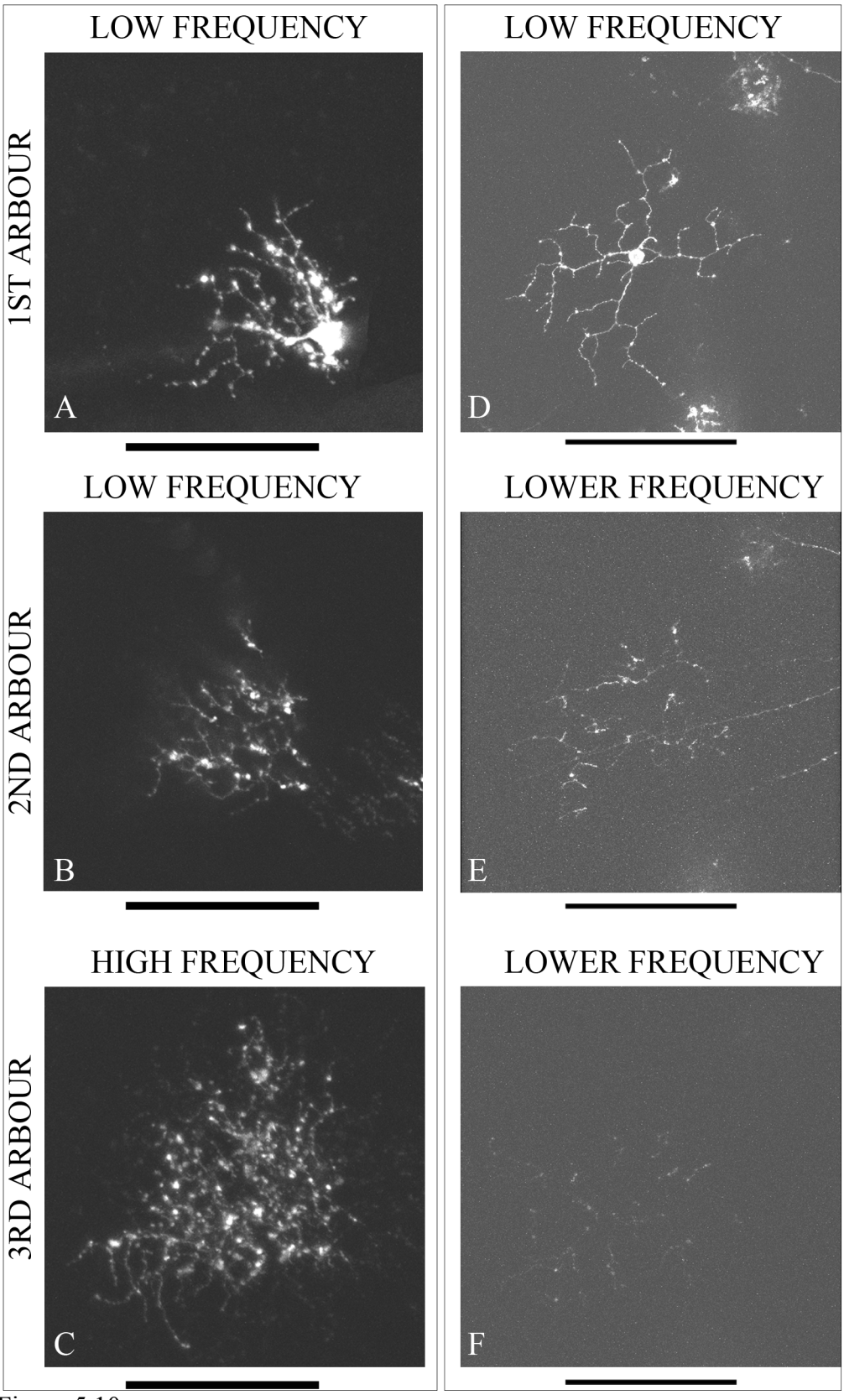
LOW FREQUENCY
LOW FREQUENCY
1ST ARBOUR
A
D
LOW FREQUENCY
LOWER FREQUENCY
2ND ARBOUR
B
E
HIGH FREQUENCY
LOWER FREQUENCY
3RD ARBOUR
C
F

Figure 5.10

Figure 5.10: X/Y projection micrographs of the tristratified group exhibiting combinations of high/low dendritic branching frequency in the first, second and third dendritic arbours. A – C. A tristratified RGC with a combination of low frequency dendritic branching in the first and second arbours and a high frequency in the third arbour. D - F. Another tristratified RGC exhibiting low frequency branching in the first arbour and even lower frequency branching in the second and third arbours. E. The labelled processes travelling across horizontally were from a different labelled cell. The scale bars in A – C = 50 μm; D - F = 100 μm.

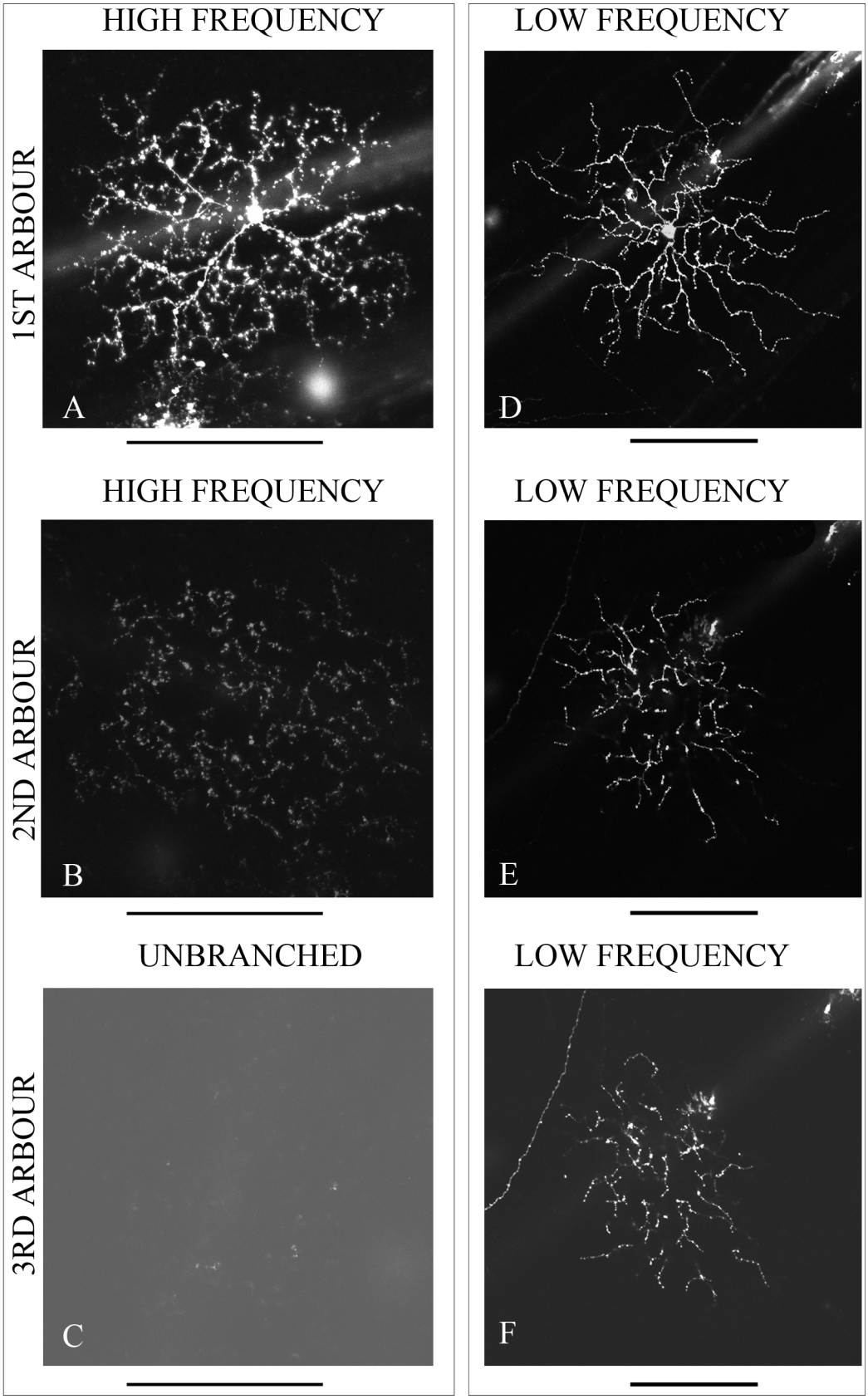
HIGH FREQUENCY
LOW FREQUENCY
1ST ARBOUR
A
D
HIGH FREQUENCY
LOW FREQUENCY
2ND ARBOUR
B
E
UNBRANCHED
LOW FREQUENCY
3RD ARBOUR
C
F

Figure 5.11

Figure 5.11: X/Y projection micrographs of the tristratified group exhibiting more combinations of high/low dendritic branching frequency. A – C. A tristratified RGC with a combination of high frequency dendritic branching in the first and second arbours. The third arbour is unbranched. A. The lines near the RGCs were the densely labelled processes of adjacent cells. D - F. Another tristratified RGC exhibiting low frequency branching in the first, second and third arbours. E - F. The labelled processes travelling diagonally on the top left corner were from a different labelled cell. The scale bars in A - F = 100 μm.

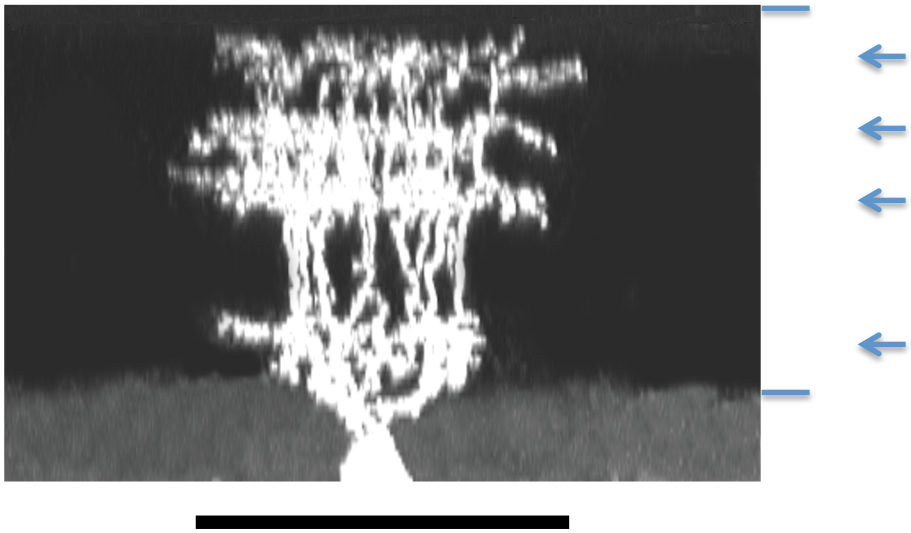

Figure 5.12. A Z projection micrograph of a tetrastratified RGC. The ganglion cell body is at the bottom of the image in the GCL. The INL/IPL boundary is near the top of the image. The arrows point to the four dendritic arbours. The lines on the right hand side indicate the thickness of the IPL. Scale bar = 50 μm.

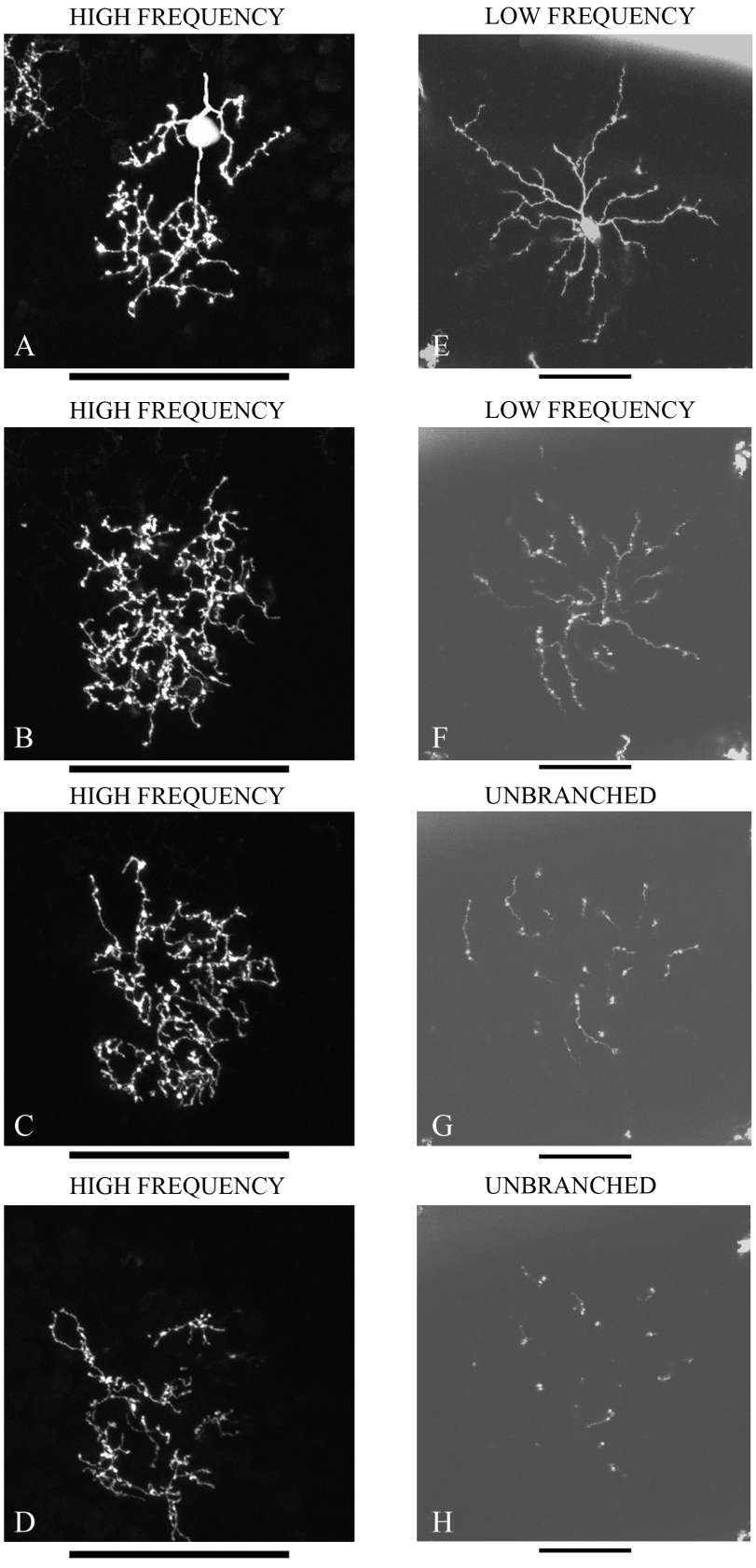
HIGH FREQUENCY
LOW FREQUENCY
A
E
HIGH FREQUENCY
LOW FREQUENCY
B
F
HIGH FREQUENCY
UNBRANCHED
C
G
HIGH FREQUENCY
UNBRANCHED
D
H

Figure 5.13.

Figure 5.13. X/Y projection micrographs of tetrastratified group exhibiting combinations of high/low dendritic branching frequency. A – D. A tetrastratified RGC exhibiting high frequency dendritic branching in the first, second, third and fourth arbours. E - H. Another tetrastratified RGC exhibiting low frequency branching in the first and second arbours. The third and fourth arbours had unbranched dendrites. The brightly labelled processes around the edges of the image were from different labelled cells. A – H. The scale bars = 50 μm.

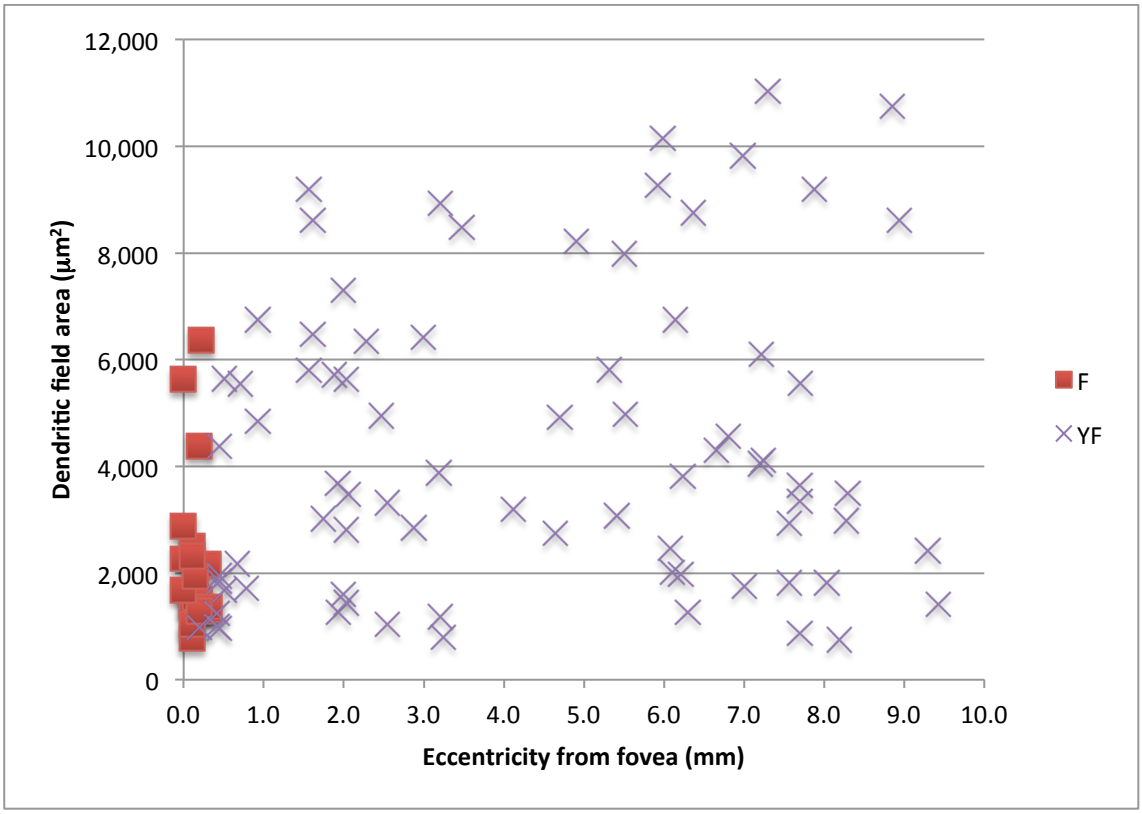

A.

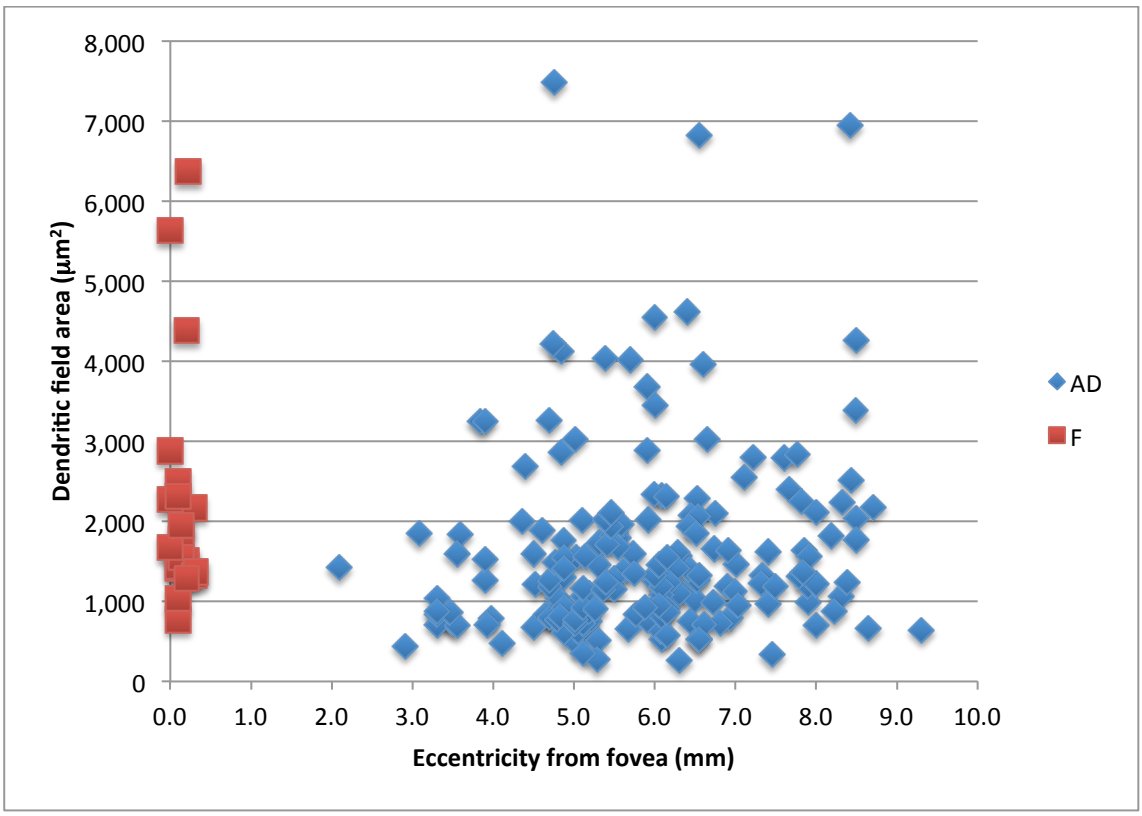

B.

Figure 5.14.

Figure 5.14. The dendritic field areas (μm^2) of unstratified RGCs plotted against eccentricity from the fovea (mm). A. The dendritic field areas of the unstratified RGCs located in the fovea (F) and the yellow field (YF) as the distance (eccentricity) from the fovea changes. B. The dendritic field areas of the unstratified RGCs located in the fovea and the *area dorsalis* (AD).

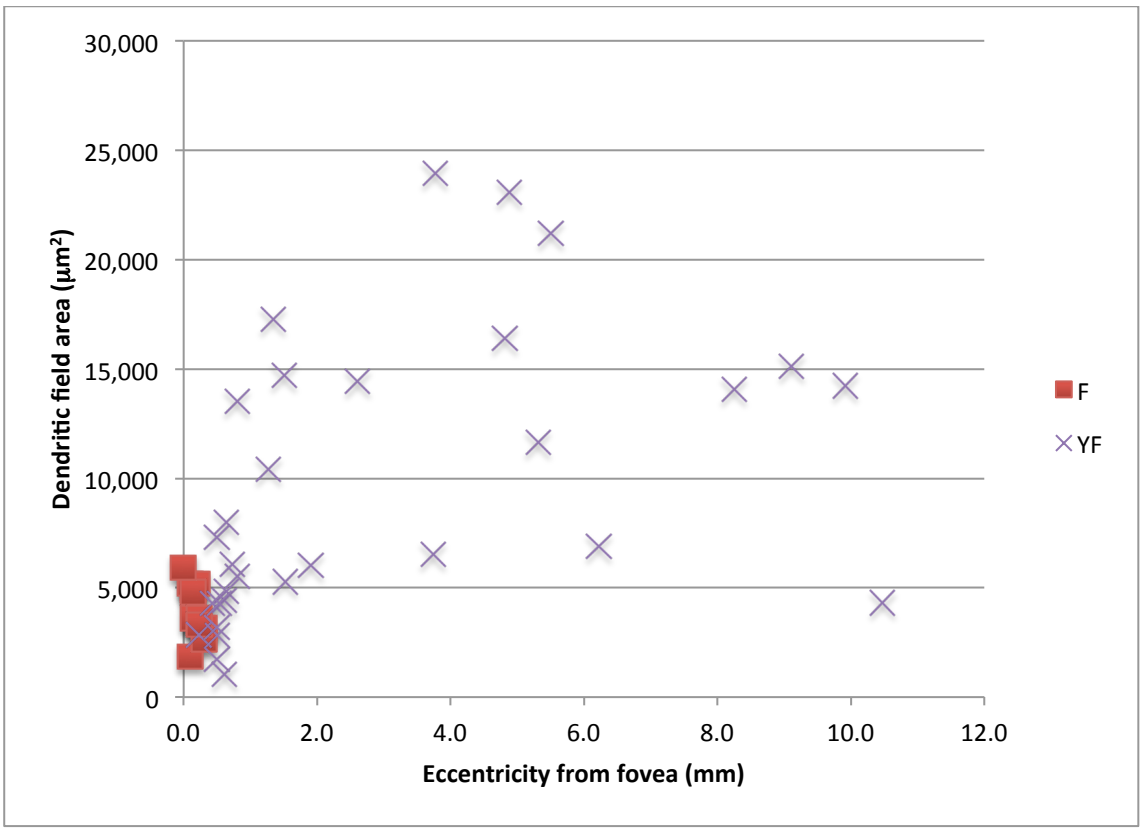

A.

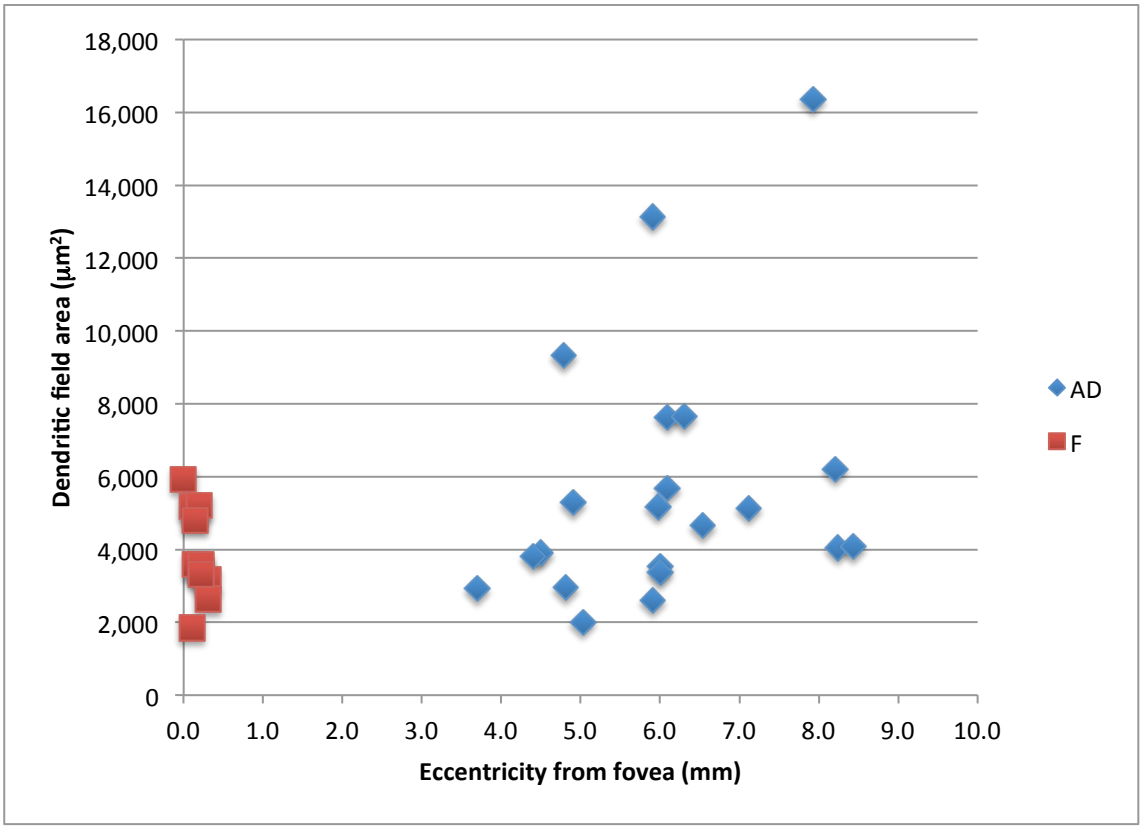

B.

Figure 5.15.

Figure 5.15. The dendritic field areas (μm^2) of monostratified RGCs plotted against eccentricity from the fovea (mm). A. The dendritic field areas of the monostratified RGCs located in the fovea (F) and the yellow field (YF) as the distance (eccentricity) from the fovea changes. B. The dendritic field areas of the monostratified RGCs located in the fovea and the *area dorsalis* (AD).

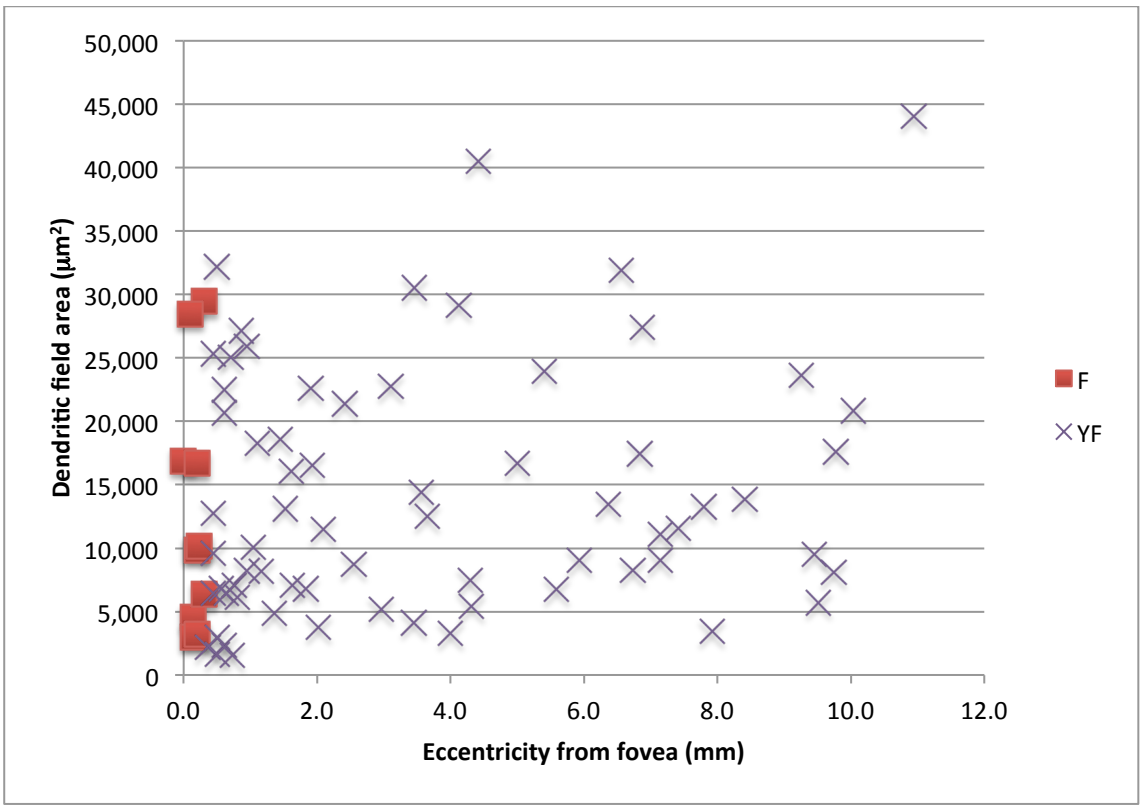

A.

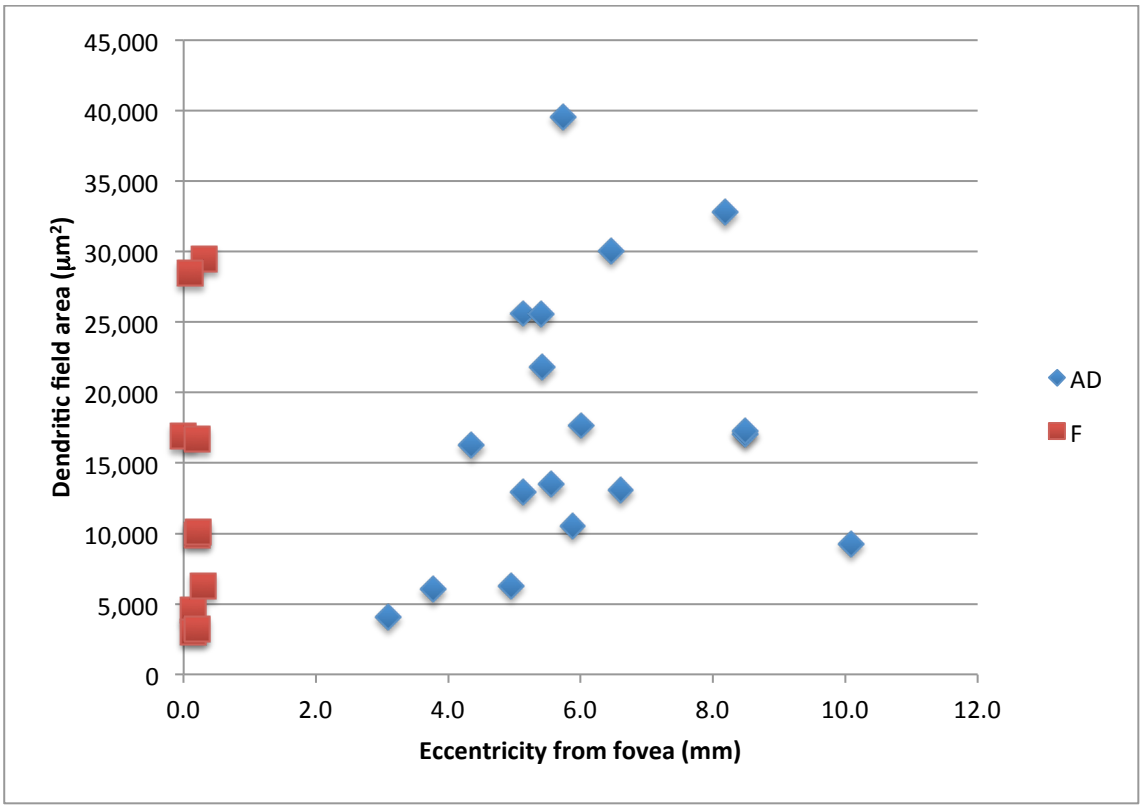

B.

Figure 5.16.

Figure 5.16. The dendritic field areas (μm^2) of bistratified RGCs plotted against eccentricity from the fovea (mm). A. The dendritic field areas of the bistratified RGCs located in the fovea (F) and the yellow field (YF) as the distance (eccentricity) from the fovea changes. B. The dendritic field areas of the bistratified RGCs located in the fovea and the *area dorsalis* (AD).

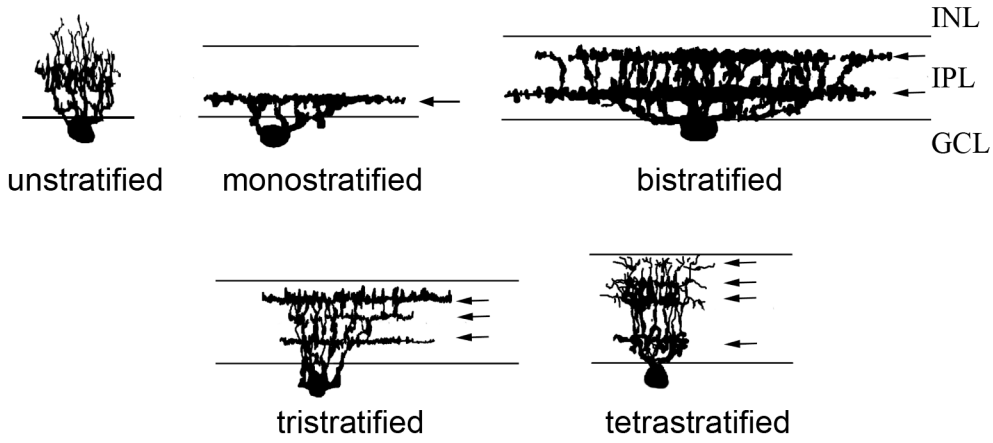

Figure 5.17. Hand-drawn diagrams of the five RGC groups. The arrows point to the horizontally-oriented dendritic arbours.

Table 5.1. Number of RGCs sampled in different retinal regions.

RGC group	**AD**	**F**	**RF**	**YF**	**Total**
Unstratified	187	21	194	87	489
Monostratified	21	12	14	35	82
Bistratified	17	10	27	74	128
Tristratified	14	1	14	20	49
Tetrastratified	4	2	6	5	17
Total	243	46	225	221	765

Chapter 6 - Conclusions

6.1 Conclusions

The studies presented in this thesis have provided further insights into the anatomical organization and potential circuitry in the avian retina, and how it contributes to the processing of various kinds of visual stimuli, especially resolving high spatial detail.

In the three studies, several morphological characteristics were identified in the fovea and the *area dorsalis,* which might contribute to achieving high visual acuity. The first study revealed that the fovea and the *area dorsalis* were both characterised by higher densities of cone photoreceptors and RGCs compared with the periphery (Chapter 3). The second and third studies showed that certain types of bipolar cells and RGCs have proposed candidate midget-like bipolar cells (B7 and B8) and ganglion cells (Chapters 4 and 5). Lastly, estimates of photoreceptor convergence onto RGCs (Chapter 3) indicated that convergence was lower in the two areas associated with high visual acuity. The narrow dendritic field of the midget-like bipolar cell types agrees well with the finding of low photoreceptor convergence onto these cell types. All of these may be important anatomical requirements that enable these neuronal types in the fovea and *area dorsalis* to mediate acute spatial vision.

Another important finding was the difference in the distribution of the neuronal types sampled in the fovea, *area dorsalis*, red field, and yellow field, which suggests that the circuitries in these areas are different. One difference between the fovea and the *area dorsalis* was that the fovea lacked rod photoreceptors, but the *area dorsalis* did not (Chapter 3). The presence of rod photoreceptors in the *area dorsalis* and the pure cone population of the fovea suggest that the circuitries in these two areas are different in which the *area dorsalis* would contain a rod circuitry. Therefore, the differences in the distribution of certain neuronal types suggest that the retinal circuitry, the

interconnections and the pathways for transmission of information between neurons would also be different from the peripheral retina, particularly in the fovea and *area dorsalis*.

There are two possible candidates for the midget-like bipolar cell types, B7 and B8. These cells have morphological dendritic characteristics that might allow input from only one photoreceptor. At the level of the RGC, the circuitry differs from that of the primate midget circuitry. This is because the larger dendritic field size and the thick stratification of the midget-like unstratified RGC suggest that it receives from several bipolar cells and in turn from several photoreceptors. Further experiments are required to characterise the physiology and circuitry that subserves high visual acuity in the pigeon.

The identification of the various bipolar cell and RGC types in the pigeon retina raises many questions concerning their physiology, synaptic connections with each other and other retinal neurons, their role in processing visual stimuli, and whether these properties (yet to be characterised) change in relation to eccentricity from the fovea and *area dorsalis*. The types of bipolar cells and ganglion cells classified by my studies are not an exhaustive catalogue of all the entire population and there are probably other yet to be identified types present in the pigeon retina. The detailed morphological description of each bipolar cell type and ganglion cell group is useful for future investigation as more information is uncovered about their properties. It would be interesting to know if a correlation exists between the dendritic/axonal morphologies of the different cell types and their physiology.

My studies suggest that the two high cell density areas may differ in the circuitry based on the differences in the neuronal types' morphological characteristics. Therefore future studies that investigate other neuronal types need to determine whether all types

are present across the retina, at what proportion, the degree of coverage and which types are connected and their physiological roles, in order to further understand how the pigeon processes visual information in the retina.

REFERENCES

Akagawa K, Barnstable C. 1986. Identification and characterization of cell types in monolayer cultures of rat retina using monoclonal antibodies. Brain Research 383(1-2):110-120.

Ammermüller J, Kolb H. 1995. The organization of the turtle inner retina. I. ON- and OFF-center pathways. The Journal of Comparative Neurology 358(1):1-34.

Amthor FR, Oyster CW, Takahashi ES. 1983. Quantitative Morphology of Rabbit Retinal Ganglion Cells. Proceedings of the Royal Society of London Series B Biological Sciences 217(1208):341-355.

Amthor FR, Oyster CW, Takahashi ES. 1984a. Morphology of on-off direction-selective ganglion cells in the rabbit retina. Brain Research 298(1):187-190.

Amthor FR, Oyster CW, Takahashi ES. 1984b. Morphology of ON-OFF direction-selective ganglion cells in the rabbit retina. Brain Research 298:187-190.

Amthor FR, Takahashi ES, Oyster CW. 1989a. Morphologies of rabbit retinal ganglion cells with complex receptive fields. J Comp Neurol 280(1):97-121.

Amthor FR, Takahashi ES, Oyster CW. 1989b. Morphologies of rabbit retinal ganglion cells with concentric receptive fields. J Comp Neurol 280(1):72-96.

Anderson DH, Fisher SK, Steinberg RH. 1978. Mammalian cones: disc shedding, phagocytosis, and renewal. IOVS 17(2):117-133.

Awatramani GB, Slaughter MM. 2001. Intensity-Dependent, Rapid Activation of Presynaptic Metabotropic Glutamate Receptors at a Central Synapse. The Journal of Neuroscience 21(2):741-749.

Badea TC, Nathans J. 2004. Quantitative analysis of neuronal morphologies in the mouse retina visualized by using a genetically directed reporter. The Journal of Comparative Neurology 480(4):331-351.

Badea TC, Wang Y, Nathans J. 2003. A Noninvasive Genetic/Pharmacologic Strategy for Visualizing Cell Morphology and Clonal Relationships in the Mouse. The Journal of Neuroscience 23(6):2314-2322.

Barlow HB, Levick WR. 1965. The mechanism of directionally selective units in rabbit's retina. J Physiol 178(3):477-504.

Barnstable CJ. 1980. Monoclonal antibodies which recognize different cell types in the rat retina. Nature 286 (5770):231-235.

Berson DM, Isayama T, Pu M. 1999. The eta ganglion cell type of cat retina. J Comp Neurol 408(2):204-219.

Berson DM, Pu M, Famiglietti EV. 1998. The zeta cell: A new ganglion cell type in cat retina. J Comp Neurol 399(2):269-288.

Binggeli RL, Paule WJ. 1969. The pigeon retina: quantitative aspects of the optic nerve and ganglion cell layer. J Comp Neurol 137(1):1-18.

Bloch S, Martinoya C. 1982. Comparing Frontal and Lateral Viewing in the Pigeon. I. Tachistoscopic Visual Acuity as a Function of Distance Behav Brain Res 5:231-244.

Bloomfield S, Miller R. 1986. A functional organization of ON and OFF pathways in the rabbit retina. The Journal of Neuroscience 6(1):1-13.

Blough P. 1971. The visual acuity of the pigeon for distant targets. J Exp Anal Behav 15:57-67.

Blough PM. 1973. Visual acuity in the pigeon. II. Effects of target distance and retinal lesions. J Exp Anal Behav 20(3):333-343.
Boire D, Dufour J, Theoret H, Pitto M. 2001a. Quantitative analysis of the retinal ganglion cell layer in the ostrich, Struthio camelus. Brain Behav Evol 58(6):343-355.
Boire D, Dufour J, Theoret H, Ptito M. 2001b. Quantitative analysis of the retinal ganglion cell layer in the ostrich, Struthio camelus. Brain Behav Evol 58(6):343-355.
Bons N. 1976. Retinohypothalamic pathway in the duck (Anas platyrhynchos). Cell Tissue Res 168(3):343-360.
Bowmaker JK. 1977. The visual pigments, oil droplets and spectral sensitivity of the pigeon. Vision Res 17(10):1129-1138.
Bowmaker JK, Heath LA, Wilkie SE, Hunt DM. 1997. Visual pigments and oil droplets from six classes of photoreceptor in the retinas of birds. Vision Res 37(16):2183-2194.
Bowmaker JK, Hunt DM. 1999. Molecular biology of photoreceptor spectral sensitivity. In: Archer SN, Djamgoz MBA, Loew ER, Partridge JC, Vallerga S, editors. Adaptive mechanisms in the ecology of vision. Dordrecht: Kluwer Academic Publishers. p 439-462.
Bowmaker JK, Martin GR. 1985. Visual pigments and oil droplets in the penguin, *Spheniscus humboldti*. Journal of Comparative Physiology A: Neuroethology, Sensory, Neural, and Behavioral Physiology 156(1):71-77.
Boycott BB, Dowling JE. 1969. Organization of the primate retina: light microscopy. Philos Trans R Soc London (Biol) 225:109-184.
Boycott BB, Hopkins JM. 1991. Cone bipolar cells and cone synapses in the primate retina. Visual Neuroscience 7(1-2):49-60.
Boycott BB, Hopkins JM. 1993. Cone synapses of a flat diffuse cone bipolar cell in the primate retina. J Neurocytol 22(9):765-778.
Boycott BB, Wässle H. 1974. The morphological types of ganglion cells of the domestic cat's retina. J Physiol 240(2):397-419.
Boycott BB, Wässle H. 1991. Morphological Classification of Bipolar Cells of the Primate Retina. Eur J Neurosci 3(11):1069-1088.
Boycott BB, Wässle H. 1999. Parallel processing in the mammalian retina: the Proctor Lecture. Investigative Ophthalmology & Visual Science 40(7):1313-1327.
Braekevelt CR, Richardson KC. 1996. Retinal photoreceptor fine structure in the Australian Galah (*Eolophus roseicapillus*) (Aves). Histol Histopathol 11:555-564.
Bravo H, Pettigrew JD. 1981. The distribution of neurons projecting from the retina and visual cortex to the thalamus and tectum opticum of the barn owl, <I>Tyto alba</I>, and the burrowing owl, <I>Speotyto cunicularia</I>. The Journal of Comparative Neurology 199(3):419-441.
Brecha N, Karten HJ. 1979. Accessory optic projections upon oculomotor nuclei and vestibulocerebellum. Science 203(4383):913-916.
Brecha N, Karten HJ, Hunt SP. 1980. Projections of the nucleus of the basal optic root in the pigeon: An autoradiographic and horseradish peroxidase study. J Comp Neurol 189(4):615-670.
Brown SP, Masland RH. 1999. Costratification of a population of bipolar cells with the direction-selective circuitry of the rabbit retina. The Journal of Comparative Neurology 408(1):97-106.

Budnik V, Mpodozis J, Varela FJ, Maturana HR. 1984. Regional specialization of the quail retina: Ganglion cell density and oil droplet distribution. Neuroscience Letters 51(1):145-150.
Cajal RSY. 1889. Sur la morphologie et les connexions des elements de la retine des oiseaux. Anat Anz 4:111-121.
Cajal RSY. 1972. The Structure of the Retina. Thorpe SA, Glickstein M, translator. Springfield: Charles C Thomas.
Calkins DJ, Schein SJ, Tsukamoto Y, Sterling P. 1994. M and L cones in macaque fovea connect to midget ganglion cells by different numbers of excitatory synapses. Nature 371(6492):70-72.
Calkins DJ, Tsukamoto Y, Sterling P. 1996. Foveal Cones form Basal as well as Invaginating Junctions with Diffuse ON Bipolar Cells. Vision Res 36(21):3373-3381.
Caminos E, Velasco A, Jarrín M, Aijón J, Lara JM. 1999. Protein kinase C-like immunoreactive cells in embryo and adult chicken retinas. Developmental Brain Research 118(1-2):227-230.
Caminos E, Velasco A, Jarrin M, Lillo C. 2000. A comparative study of protein kinase C-like immunoreactive cells in the retina. Brain, Behavior and Evolution 56(6):330-339.
Campbell FW, Green DG. 1965. Optical and retinal factors affecting visual resolution. J Physiol 181(3):576-593.
Campbell FW, Gubisch RW. 1966. Optical quality of the human eye. J Physiol 186:558-578.
Chan TL, Martin PR, Clunas N, Grünert U. 2001a. Bipolar cell diversity in the primate retina: Morphologic and immunocytochemical analysis of a new world monkey, the marmoset Callithrix jacchus. The Journal of Comparative Neurology 437(2):219-239.
Chan TL, Martin PR, Grünert U. 2001b. Immunocytochemical identification and analysis of the diffuse bipolar cell type DB6 in macaque monkey retina. Eur J Neurosci 13(4):829-832.
Chen Y, Naito J. 1999. Morphological classification of ganglion cells in the central retina of chicks. J Vet Med Sci 61(5):537-542.
Chen Y, Naito J. 2009. Morphological properties of chick retinal ganglion cells in relation to their central projections. J Comp Neurol 514(1):117-130.
Cohen E, Sterling P. 1990. Demonstration of Cell Types among Cone Bipolar Neurons of Cat Retina. Philosophical Transactions of the Royal Society of London Series B: Biological Sciences 330(1258):305-321.
Collin SP, Collin HB. 1999. The foveal photoreceptor mosaic in the pipefish, Corythoichthyes paxtoni (Syngnathidae, Teleostei). Histol Histopathol 14:369-382.
Collin SP, Lloyd DJ, Wagner HJ. 2000. Foveate vision in deep-sea teleosts: a comparison of primary visual and olfactory inputs. Philos Trans R Soc Lond B Biol Sci 355(1401):1315-1320.
Connaughton VP, Nelson R. 2000. Axonal stratification patterns and glutamate-gated conductance mechanisms in zebrafish retinal bipolar cells. J Physiol 524(1):135-146.
Coombs J, van der List D, Wang GY, Chalupa LM. 2006. Morphological properties of mouse retinal ganglion cells. Neuroscience 140(1):123-136.
Crawford MLJ. 1977. Central vision of man and macaque: cone and rod sensitivity. Brain Research 119(2):345-356.

Cuenca N, Fern√°ndez E, Kolb H. 1990. Distribution of immunoreactivity to protein kinase C in the turtle retina. Brain Research 532(1,Äì2):278-287.
Curcio CA, Allen KA. 1990. Topography of ganglion cells in human retina. J Comp Neurol 300(1):5-25.
Curcio CA, Packer O, Kalina RE. 1987. A whole mount method for sequential analysis of photoreceptor and ganglion cell topography in a single retina. Vision Res 27(1):9-15.
Curcio CA, Sloan KR, Kalina RE, Hendrickson AE. 1990. Human photoreceptor topography. J Comp Neurol 292(4):497-523.
Dacey D, Petersen M. 1992. Dendritic field size and morphology of midget and parasol ganglion cells of the human retina. Proc Natl Acad Sci 89(20):9666-9670.
Dacey DM. 1989. Monoamine-accumulating ganglion cell type of the cat's retina. J Comp Neurol 288(1):59-80.
Dacey DM. 1993a. Morphology of a small-field bistratified ganglion cell type in the macaque and human retina. Visual Neuroscience 10(06):1081-1098.
Dacey DM. 1993b. The mosaic of midget ganglion cells in the human retina. J Neurosci 13(12):5334-5355.
Dacey DM, Lee BB. 1994. The 'blue-on' opponent pathway in primate retina originates from a distinct bistratified ganglion cell type. Nature 367(6465):731-735.
Dacheux R, Raviola E. 1986. The rod pathway in the rabbit retina: a depolarizing bipolar and amacrine cell. The Journal of Neuroscience 6(2):331-345.
De Robertis E. 1956. Electron microscope observations on the submicroscopic organization of the retinal rods. J Biophys Biochem Cytol 2:319-338.
De Robertis E, Lasansky A. 1958. Submicroscopic Organization of Retinal Cones of the Rabbit. J Biophys Biochem Cytol 4:743-746.
DeVries SH. 2000. Bipolar Cells Use Kainate and AMPA Receptors to Filter Visual Information into Separate Channels. Neuron 28(3):847-856.
DeVries SH, Schwartz EA. 1999. Kainate receptors mediate synaptic transmission between cones and `Off' bipolar cells in a mammalian retina. Nature 397:157-160.
Doi M, Uji Y. 1995. Morphological classification of retinal ganglion cells in mice. J Comp Neurol 356(3):368-386.
Dowling JE. 1979. A new retinal neurone -- the interplexiform cell. Trends in Neurosciences 2:189-191.
Dowling JE, Ehinger B. 1978. The Interplexiform Cell System. I. Synapses of the Dopaminergic Neurons of the Goldfish Retina. Proceedings of the Royal Society of London Series B, Biological Sciences 201(1142):7-26.
Dubin MW. 1970. The inner plexiform layer of the vertebrate retina: a quantitative and comparative electron microscopic analysis. J Comp Neurol 140:479-505.
Euler T, Schneider H, Wässle H. 1996. Glutamate Responses of Bipolar Cells in a Slice Preparation of the Rat Retina. The Journal of Neuroscience 16(9):2934-2944.
Euler T, Wässle H. 1995. Immunocytochemical identification of cone bipolar cells in the rat retina. The Journal of Comparative Neurology 361(3):461-478.
Famiglietti EVJ. 1981. Functional architecture of cone bipolar cells in the mammalian retina. Vision Res 21:1559-1563.
Famiglietti EVJ. 1992a. Dendritic co-stratification of ON and ON-OFF directionally selective ganglion cells with starburst amacrine cells in rabbit retina. J Comp Neurol 324:322-335.

Famiglietti EVJ. 1992b. New metrics for analysis of dendritic branching patterns demonstrating similarities and differences in ON and ON-OFF directionally selective retinal ganglion cells. J Comp Neurol 324:295-321.
Feil R, Brocard J, Mascrez B, LeMeur M, Metzger D, Chambon P. 1996. Ligand-activated site-specific recombination in mice. Proceedings of the National Academy of Sciences 93(20):10887-10890.
Fekete DM, Barnstable CJ. 1983. The subcellular localization of rat photoreceptor-specific antigens. J Neurocytol 12(5):785-803.
Fischer AJ, Stanke JJ, Aloisio G, Hoy H, Stell WK. 2007. Heterogeneity of horizontal cells in the chicken retina. J Comp Neurol 500(6):1154-1171.
Fite KV. 1973. Anatomical and behavioral correlates of visual acuity in the great horned owl. Vision Res 13(2):219-222.
Fite KV, Brecha N, Karten HJ, Hunt SP. 1981. Displaced ganglion cells and the accessory optic system of pigeon. J Comp Neurol 195(2):279-288.
Fite KV, Lister BC. 1981. Bifoveal vision in anolis lizards. Brain Behav Evol 19:144-154.
Fite KV, Rosenfield-Wessels S. 1975. A comparative study of deep avian foveas. Brain Behav Evol 12(1-2):97-115.
Fitzgerald M, Tolley E, Frase S, Zagvazdin Y, Miller R, Hodos W, Reiner A. 2001. Functional and morphological assessment of age-related changes in the choroid and outer retina in pigeons. Visual Neuroscience 18(2):299-317.
Fox R, Lehmkuhle S, Westendorf D. 1976. Falcon visual acuity. Science 192(4236):263-265.
Freed M, Smith R, Sterling P. 1987a. Rod bipolar array in the cat retina: pattern of input from rods and GABA-accumulating amacrine cells. The Journal of Comparative Neurology 266(3):445-455.
Freed MA, Smith RG, Sterling P. 1987b. Rod bipolar array in the cat retina: pattern of input from rods and GABA-accumulating amacrine cells. The Journal of comparative neurology 266(3):445-455.
Friedrich G, Soriano P. 1991. Promoter traps in embryonic stem cells: a genetic screen to identify and mutate developmental genes in mice. Genes & Development 5(9):1513-1523.
Fyk-Kolodziej B, Cai W, Pourcho RG. 2002. Distribution of protein kinase C isoforms in the cat retina. Visual Neuroscience 19(05):549-562.
Galifret Y. 1968. Les diverses aires fonctionnelles de la retine du pigeon. Z Zellforsch Mikrosk Anat 86:535-545.
Gallego A, Baron M, Gayoso M. 1975. Horizontal cells of the avian retina. Vision Research 15(8-9):1029-1030, IN1028.
Gan W-B, Grutzendler J, Wong WT, Wong ROL, Lichtman JW. 2000. Multicolor "DiOlistic" Labeling of the Nervous System Using Lipophilic Dye Combinations. Neuron 27(2):219-225.
Garciá M, Ruiz-Ederra J, Hernández-Barbáchano H, Vecino E. 2005. Topography of pig retinal ganglion cells. J Comp Neurol 486(4):361-372.
Ghosh KK, Bujan S, Haverkamp S, Feigenspan A, Wässle H. 2004. Types of bipolar cells in the mouse retina. The Journal of Comparative Neurology 469(1):70-82.
Grant G, Dowling J. 1995. A glutamate-activated chloride current in cone-driven ON bipolar cells of the white perch retina. The Journal of Neuroscience 15(5):3852-3862.
Grant GB, Dowling JE. 1996. On bipolar cell responses in the teleost retina are generated by two distinct mechanisms. J Neurophysiol 76(6):3842-3849.

Greferath U, Grünert U, Wässle H. 1990. Rod bipolar cells in the mammalian retina show protein kinase C-like immunoreactivity. The Journal of Comparative Neurology 301(3):433-442.
Grünert U, Martin P. 1991. Rod bipolar cells in the macaque monkey retina: immunoreactivity and connectivity. The Journal of Neuroscience 11(9):2742-2758.
Grünert U, Martin PR, Wässle H. 1994. Immunocytochemical analysis of bipolar cells in the macaque monkey retina. The Journal of Comparative Neurology 348(4):607-627.
Grutzendler J, Tsai J, Gan W-B. 2003. Rapid labeling of neuronal populations by ballistic delivery of fluorescent dyes. Methods 30:79-85.
Güntürkün O, Hahmann U. 1999. Functional subdivisions of the ascending visual pathways in the pigeon. Behav Brain Res 98:193–201.
Güntürkün O, Miceli D, Watanabe M. 1993. Anatomy of the avian thalamofugal pathway. In: Zeigler HP, Bischof H, editors. Vision, brain, and behavior in birds. Cambridge: Massachusetts Institute of Technology. p 115-135.
Hahmann U, Güntürkün O. 1993. The Visual Acuity for the Lateral Visual Field of the Pigeon (Columba livia). Vision Res 33:1659-1664.
Hargrave P, Adamus G, Arendt A, McDowell J, Wang J, Szaby A, Curtis D, Jackson R. 1986. Rhodopsin's amino terminus is a principal antigenic site. Experimental Eye Research 42(4):363-373.
Harmening WM, Nikolay P, Orlowski J, Wagner H. 2009. Spatial contrast sensitivity and grating acuity of barn owls. Journal of Vision 9(7).
Harmening WM, Vobig MA, Walter P, Wagner H. 2007. Ocular aberrations in barn owl eyes. Vision Research 47(23):2934-2942.
Hart NS, Hunt DM. 2007. Avian Visual Pigments: Characteristics, Spectral Tuning, and Evolution. The American Naturalist 169(1):S7-S26.
Hayes BP. 1982. The structural organization of the pigeon retina. Progress in Retinal and Eye Research 1:197-226.
Hayes BP. 1984. Cell populations of the ganglion cell layer: displaced amacrine and matching amacrine cells in the pigeon retina. Exp Brain Res 56(3):565-573.
Hayes BP, Holden AL. 1980. Size classes of ganglion cells in the central yellow field of the pigeon retina. Exp Brain Res 39(3):269-275.
Hayes BP, Holden AL. 1983. The distribution of displaced ganglion cells in the retina of the pigeon. Exp Brain Res 49(2):181-188.
Hicks D, Barnstable C. 1986. Lectin and antibody labelling of developing rat photoreceptor cells: an electron microscope immunocytochemical study. J Neurocytol 15(2):219-230.
Hicks D, Barnstable CJ. 1987. Different rhodopsin monoclonal antibodies reveal different binding patterns on developing and adult rat retina. J Histochem Cytochem 35(11):1317-1328.
Hodos W, Bessette BB, Macko KA, Weiss SRB. 1985. Normative data for pigeon vision. Vision Res 25(10):1525-1527.
Hodos W, Erichsen JT. 1990. Lower-field myopia in birds: An adaptation that keeps the ground in focus. Vision Res 30(5):653-657.
Hodos W, Miller RF, Fite KV. 1991. Age-dependent changes in visual acuity and retinal morphology in pigeons. Vision Res 31(4):669-677.
Hoshi H, Liu W-L, Massey SC, Mills SL. 2009. ON Inputs to the OFF Layer: Bipolar Cells That Break the Stratification Rules of the Retina. The Journal of Neuroscience 29(28):8875-8883.

Hubel DH, Wiesel TN. 1960. Receptive fields of optic nerve fibres in the spider monkey. J Physiol 154(3):572-580.
Hughes A. 1977. The topography of vision in mammals of contrasting life style. In: F C, editor. Handbook of Sensory Physiology: The Visual System of Vertebrates. Berlin: Springer Verlag. p 697-756.
Ikushima M, Watanabe M, Ito H. 1986. Distribution and morphology of retinal ganglion cells in the Japanese quail. Brain Research 376(2):320-334.
Inzunna O, Bravo H. 1993. Foveal topography in the optic nerve and primary visual centers in Falconiforms. Anat Rec 235(4):622-631.
Isayama T, Berson DM, Pu M. 2000. Theta ganglion cell type of cat retina. J Comp Neurol 417(1):32-48.
Isayama T, O'Brien BJ, Ugalde I, Muller JF, Frenz A, Aurora V, Tsiaras W, Berson DM. 2009. Morphology of retinal ganglion cells in the ferret (*Mustela putorius furo*). The Journal of Comparative Neurology 517(4):459-480.
Ishikawa T, Yamada E. 1970. The Degradation of the Photoreceptor Outer Segment within the Pigment Epithelial Cell of Rat Retina. Journal of Electron Microscopy 19(1):85-99.
Jane SD, Bowmaker JK. 1988. Tetrachromatic colour vision in the duck (*Anas platyrhynchos*): microspectrophotometry of visual pigments and oil droplets. Journal of Comparative Physiology A: Neuroethology, Sensory, Neural, and Behavioral Physiology 162(2):225-235.
Jasiński A. 1973. Fine structure of capillaries in the pecten oculi of the sparrow, *Passer domesticus*. Cell Tissue Res 146(2):281-292.
Jassik-Gerschenfeld D, Guichard J. 1972. Visual receptive fields of single cells in the pigeon's optic tectum. Brain Research 40(2):303-317.
Jassik-Gerschenfeld D, Teulon J, Ropert N. 1976. Visual receptive field types in the nucleus dorsalateralis anterior of the pigeon's thalamus. Brain Research 108(2):295-306.
Jeon C-J, Masland RH. 1995. A population of wide-field bipolar cells in the rabbit's retina. J Comp Neurol 360(3):403-412.
Job C, Lagnado L. 1998. Calcium and Protein Kinase C Regulate the Actin Cytoskeleton in the Synaptic Terminal of Retinal Bipolar Cells. The Journal of Cell Biology 143(6):1661-1672.
Kaneko A. 1970. Physiological and morphological identification of horizontal, bipolar and amacrine cells in goldfish retina. J Physiol 207(3):623-633.
Karten HJ, Revzin AM. 1966. The afferent connections of the nucleus rotundus in the pigeon. Brain Research 2(4):368-377.
Karten JH, Fite KV, Brecha N. 1977. Specific projection of displaced retinal ganglion cells upon the accessory optic system in the pigeon (Columbia livia). Proc Natl Acad Sci U S A 74(4):1753-1756.
Kato S, Ishita S, Mawatari K, Matsukawa T, Negishi K. 1990. Dopamine Release via Protein Kinase C Activation in the Fish Retina. Journal of Neurochemistry 54(6):2082-2090.
Klug K, Herr S, Ngo IT, Sterling P, Schein S. 2003. Macaque Retina Contains an S-Cone OFF Midget Pathway. J Neurosci 23(30):9881-9887.
Koistinaho J, Sagar SM. 1994. Localization of protein kinase C subspecies in the rabbit retina. Neuroscience Letters 177(1,Äì2):15-18.
Kolb H. 1970. Organization of the Outer Plexiform Layer of the Primate Retina: Electron Microscopy of Golgi-Impregnated Cells. Philos Transac R Soc Lond B Biol Sci 258(823):261-283.

Kolb H. 1979. The inner plexiform layer in the retina of the cat: electron microscopic observations. J Neurocytol 8(3):295-329.
Kolb H, Dekorver L. 1991. Midget ganglion cells of the parafovea of the human retina: A Study by electron microscopy and serial section reconstructions. J Comp Neurol 303(4):617-636.
Kolb H, Linberg KA, Fisher SK. 1992. Neurons of the human retina: A Golgi study. The Journal of Comparative Neurology 318(2):147-187.
Kolb H, Marshak D. 2003. The midget pathways of the primate retina. Doc Ophthalmol 106(1):67-81.
Kolb H, Nelson R, Mariani A. 1981. Amacrine cells, bipolar cells and ganglion cells of the cat retina: A Golgi study. Vision Research 21(7):1081-1114.
Kolb H, Zhang L, Dekorver L. 1993. Differential staining of neurons in the human retina with antibodies to protein kinase C isozymes. Visual Neuroscience 10(02):341-351.
Kong JH, Fish DR, Rockhill RL, Masland RH. 2005. Diversity of ganglion cells in the mouse retina: Unsupervised morphological classification and its limits. J Comp Neurol 489(3):293-310.
Kuffler SW. 1953. DISCHARGE PATTERNS AND FUNCTIONAL ORGANIZATION OF MAMMALIAN RETINA. J Neurophysiol 16(1):37-68.
Leeper HF. 1978. Horizontal cells of the turtle retina. I. Light microscopy of golgi preparations. The Journal of Comparative Neurology 182(5):777-793.
Leventhal AG, Rodieck RW, Dreher B. 1981. Retinal ganglion cell classes in the Old World monkey: morphology and central projections. Science 213(4512):1139-1142.
Li YN, Matsui JI, Dowling JE. 2009. Specificity of the horizontal cell-photoreceptor connections in the zebrafish (Danio rerio) retina. The Journal of Comparative Neurology 516(5):442-453.
Li YN, Tsujimura T, Kawamura S, Dowling JE. 2012. Bipolar cell–photoreceptor connectivity in the zebrafish (Danio rerio) retina. The Journal of Comparative Neurology 520(16):3786-3802.
Lobe CG, Koop KE, Kreppner W, Lomeli H, Gertsenstein M, Nagy A. 1999. Z/AP, a Double Reporter for Cre-Mediated Recombination. Dev Biol 208(2):281-292.
Lockhart M. 1979. Quantitative Morphological Investigations of Retinal Cells in the Pigeon: A Golgi, Light Microscopic Study. In: Granda AM, Maxwell JH, editors. Neural Mechanisms of Behavior in the Pigeon. New York: Plenum Press. p 371-394.
MacNeil MA, Heussy JK, Dacheux RF, Raviola E, Masland RH. 2004. The population of bipolar cells in the rabbit retina. J Comp Neurol 472(1):73-86.
MacNeil MA, Masland RH. 1998. Extreme Diversity among Amacrine Cells: Implications for Function. Neuron 20(5):971-982.
Maier EJ, Bowmaker JK. 1993. Colour vision in the passeriform bird, Leiothrix lutea: correlation of visual pigment absorbance and oil droplet transmission with spectral sensitivity. J Comp Physiol A 172(3):295-301.
Mangrum WI, Dowling JE, Cohen ED. 2002. A morphological classification of ganglion cells in the zebrafish retina. Visual Neuroscience 19(06):767-779.
Mann I. 1924. The function of the pecten. Br J Ophthalmol 8(5):209-226.
Maranto A. 1982. Neuronal mapping: a photooxidation reaction makes Lucifer yellow useful for electron microscopy. Science 217(4563):953-955.
Mariani A. 1984. Bipolar cells in monkey retina selective for the cones likely to be blue-sensitive. Nature 308:184-186.

Mariani AP. 1981. A diffuse, invaginating cone bipolar cell in primate retina. J Comp Neurol 197(4):661-671.
Mariani AP. 1982. Association amacrine cells could mediate directional selectivity in pigeon retina. Nature 298:654-655.
Mariani AP. 1983a. Giant bistratified bipolar cells in monkey retina. Anat Rec 206(2):215-220.
Mariani AP. 1983b. A morphological basis for verticality detectors in the pigeon retina: Asymmetric amacrine cells. Naturwissenschaften 70(7):368-369.
Mariani AP. 1987. Neuronal and synaptic organization of the outer plexiform layer of the pigeon retina. Am J Anat 179:25-39.
Mariani AP, Leure-DuPree AE. 1977. Horizontal cells of the pigeon retina. The Journal of Comparative Neurology 175(1):13-26.
Mariani AP, Leure-Dupree AE. 1978. Photoreceptors and oil droplet colors in the red area of the pigeon retina. J Comp Neurol 182(5):821-837.
Martin PR, Grünert U. 1992. Spatial density and immunoreactivity of bipolar cells in the macaque monkey retina. The Journal of Comparative Neurology 323(2):269-287.
Martinoya C, Rivaud S, Bloch S. 1983. Comparing Frontal and Lateral Viewing in the Pigeon. II. Velocity Thresholds for Movement Discrimination. Behav Brain Res 8:375-385.
Masland RH. 2001. Neuronal diversity in the retina. Current Opinion in Neurobiology 11(4):431-436.
Massey SC, Mills SL. 1996. A calbindin-immunoreactive cone bipolar cell type in the rabbit retina. The Journal of Comparative Neurology 366(1):15-33.
Masu M, Iwakabe H, Tagawa Y, Miyoshi T, Yamashita M, Fukuda Y, Sasaki H, Hiroi K, Nakamura Y, Shigemoto R, Takada M, Nakamura K, Nakao K, Katsuki M, Nakanishi S. 1995. Specific deficit of the ON response in visual transmission by targeted disruption of the mGIuR6 gene. Cell 80(5):757-765.
Matsuura R, Sawada Y, Ishibashi Y. 2010. Development of visual cells in the Pacific bluefin tuna Thunnus orientalis. Fish Physiology and Biochemistry 36(3):391-402.
Maturana HR, Frenk S. 1963. Directional Movement and Horizontal Edge Detectors in the Pigeon Retina. Science 142(3594):977-979.
McCord R, Klein A, Osborne NN. 1996. The occurrence of protein kinase C phi and lambda isoforms in retina of different species. Neurochem Res 21(2):259-266.
McGuire B, Stevens J, Sterling P. 1984. Microcircuitry of bipolar cells in cat retina. The Journal of Neuroscience 4(12):2920-2938.
Meier R, Mihailovic J, Cuénod M. 1974. Thalamic organization of the retmo-thalamo-hyperstriatal pathway in the pigeon (Columba Livia). Experimental Brain Research 19(4):351-364.
Meyer DB. 1977. The avian eye and its adaptations. In: Crescitelli F, editor. The visual system in vertebrates. Berlin: Springer-Verlag. p 549-611.
Meyer DB, May HC. 1973. The topographical distribution of rods and cones in the adult chicken retina. Experimental Eye Research 17(4):347-355.
Miceli D, Reperant J, Medina M, Volle M, Rio J-P. 2006. Distribution of ganglion cells in the pigeon retina labeled via retrograde transneuronal transport of the fluorescent dye rhodamine [beta]-isothiocyanate from the telencephalic visual Wulst. Brain Res 1098(1):94-105.
Mihalkovics. 1873. Untersuchungen uber den Kamm des Vogelauges. Arch f mikros, Anat 9.

Miller WH. 1979. Ocular Optical Filtering. In: Autrum H, editor. Handbook of Sensory Physiology: Comparative physiology and evolution of vision in invertebrates. Berlin: Springer-Verlag. p 69-143.
Mills SL, Massey SC. 1992. Morphology of bipolar cells labeled by DAPI in the rabbit retina. J Comp Neurol 321(1):133-149.
Minami N, Berglund K, Sakaba T, Kohmoto H, Tachibana M. 1998. Potentiation of transmitter release by protein kinase C in goldfish retinal bipolar cells. J Physiol 512(1):219-225.
Morris VB. 1970. Symmetry in a receptor mosaic demonstrated in the chick from the frequencies, spacing and arrangement of the types of retinal receptor. The Journal of Comparative Neurology 140(3):359-397.
Morris VB. 1982. An afoveate area centralis in the chick retina. J Comp Neurol 210(2):198-203.
Morris VB, Shorey CD. 1967. An electron microscope study of types of receptor in the chick retina. The Journal of Comparative Neurology 129(4):313-339.
Müller B, Peichl L. 1991. Rod bipolar cells in the cone-dominated retina of the tree shrew Tupaia belangeri. Visual Neuroscience 6(06):629-639.
Naito J, Chen Y. 2004a. Morphologic analysis and classification of ganglion cells of the chick retina by intracellular injection of lucifer yellow and retrograde labeling with DiI. JComp Neurol 469(3):360-376.
Naito J, Chen Y. 2004b. Morphological features of chick retinal ganglion cells. Anat Sci Int 79(4):213-225.
Nakajima Y, Iwakabe H, Akazawa C, Nawa H, Shigemoto R, Mizuno N, Nakanishi S. 1993. Molecular characterization of a novel retinal metabotropic glutamate receptor mGluR6 with a high agonist selectivity for L-2-amino-4-phosphonobutyrate. Journal of Biological Chemistry 268(16):11868-11873.
Nalbach H-O, Wolf-Oberhollenzer F, Kirschfeld K. 1990. The pigeon's eye viewed through an ophthalmoscopic microscope: Orientation of retinal landmarks and significance of eye movements. Vision Res 30(4):529-540.
Negishi K, Kato S, Teranishi T. 1988. Dopamine cells and rod bipolar cells contain protein kinase C-like immunoreactivity in some vertebrate retinas. Neuroscience Letters 94(3):247-252.
Nelson R, Famiglietti EV, Jr., Kolb H. 1978. Intracellular staining reveals different levels of stratification for on- and off-center ganglion cells in cat retina. J Neurophysiol 41(2):472-483.
Nelson R, Kolb H. 1983. Synaptic patterns and response properties of bipolar and ganglion cells in the cat retina. Vision Research 23(10):1183-1195.
Nomura A, Shigemoto R, Nakamura Y, Okamoto N, Mizuno N, Nakanishi S. 1994. Developmentally regulated postsynaptic localization of a metabotropic glutamate receptor in rat rod bipolar cells. Cell 77(3):361-369.
Oishi T, Kawata A, Hayashi T, Fukada Y, Shichida Y, Yoshizawa T. 1990. Immunohistochemical localization of iodopsin in the retina of the chicken and Japanese quail. Cell Tiss Res 261(3):397-401.
Osborne NN, Wood J, Groome N. 1994. The occurrence of three calcium-independent protein kinase C subspecies (δ, ε and ζ) in retina of different species. Brain Research 637(1,Äì2):156-162.
Packer O, Hendrickson AE, Curcio CA. 1989. Photoreceptor topography of the retina in the adult pigtail macaque (*Macaca nemestrina)*. J Comp Neurol 288(1):165-183.

Pasteels B, Parmentier M, Lawson EM, Verstappen A, Pochet R. 1987. Calcium binding protein immunoreactivity in pigeon retina. Invest Ophthalmol Vis Sci 28(4):658-664.
Pearlman AL, Hughes CP. 1976. Functional role of efferents to the avian retina. I. Analysis of retinal ganglion cell receptive fields. J Comp Neurol 166(1):111-122.
Percival KA, Jusuf PR, Martin PR, Grünert U. 2009. Synaptic inputs onto small bistratified (blue-ON/yellow-OFF) ganglion cells in marmoset retina. The Journal of Comparative Neurology 517(5):655-669.
Percival KA, Martin PR, Grünert U. 2011. Synaptic inputs to two types of koniocellular pathway ganglion cells in marmoset retina. The Journal of Comparative Neurology 519(11):2135-2153.
Perlman I, Kolb H, Nelson R. 2007. S-potentials and horizontal cells. In: Kolb H, Fernandez E, Nelson R, editors. Webvision: The organization of the retina and visual system. Salt Lake City: University of Utah Health Sciences Center.
Perry VH, Oehler R, Cowey A. 1984. Retinal ganglion cells that project to the dorsal lateral geniculate nucleus in the macaque monkey. Neuroscience 12:1101-1123.
Peterson B, Dacey DM. 2000. Morphology of wide-field bistratified and diffuse human retinal ganglion cells. Vis Neurosci 17(4):567-578.
Peterson BB, Dacey DM. 1999. Morphology of wide-field, monostratified ganglion cells of the human retina. Vis Neurosci 16(1):107-120.
Pettigrew JD. 1979. Binocular Visual Processing in the Owl's Telencephalon. Proceedings of the Royal Society of London Series B, Biological Sciences 204(1157):435-454.
Pettigrew JD, Collin SP, Ott M. 1999. Convergence of specialised behaviour, eye movements and visual optics in the sandlance (Teleostei) and the chameleon (Reptilia). Curr Biol 9(8):421-424.
Pettigrew JD, Konishi M. 1976. Effect of monocular deprivation on binocular neurones in the owl's visual Wulst. Nature 264:753-754.
Pignatelli V, Strettoi E. 2004. Bipolar cells of the mouse retina: a gene gun, morphological study. J Comp Neurol 476(3):254-266.
Pochet R, Pasteels B, Seto-ohshima A, Bastianelli E, Kitajima S, Van Eldik LJ. 1991. Calmodulin and calbindin localization in retina from six vertebrate species. J Comp Neurol 314(4):750-762.
Polyak SL. 1941. The Retina. Chicago: University of Chicago Press.
Provis JM. 1979. The distribution and size of ganglion cells in the retina of the pigmented rabbit: A quantitative analysis. J Comp Neurol 185(1):121-137.
Puller C, Ondreka K, Haverkamp S. 2011. Bipolar cells of the ground squirrel retina. The Journal of Comparative Neurology 519(4):759-774.
Qin P, Pourcho RG. 1999. Localization of AMPA-selective glutamate receptor subunits in the cat retina: A light- and electron-microscopic study. Visual Neuroscience 16(01):169-177.
Querubin A, Lee HR, Provis JM, Bumsted O'Brien KM. 2009. Photoreceptor and ganglion cell topographies correlate with information convergence and high acuity regions in the adult pigeon (*Columba livia*) retina. J Comp Neurol 517(5):711-722.
Quesada A, Garcia-Lomas V, Genis-Galvez JM. 1986. The midget bipolar cells in the chick retina. Curr Eye Res 5:85-92.
Quesada A, Prada A, Genis-Galvez JM. 1988. Bipolar cells in the chicken retina. J Morphol 197(3):337-351.

Rahman M, Sugita S, Aoyama M, Sugita S. 2006. Number, distribution and size of retinal ganglion cells in the jungle crow (*Corvus macrorhynchos*). Anatomical Science International 81(4):253-259.
Reiner A, Perkel DJ, Bruce LL, Butler AB, Csillag A, Kuenzel W, Medina L, Paxinos G, Shimizu T, Striedter G, Wild M, Ball GF, Durand S, Gütürkün O, Lee DW, Mello CV, Powers A, White SA, Hough G, Kubikova L, Smulders TV, Wada K, Dugas-Ford J, Husband S, Yamamoto K, Yu J, Siang C, Jarvis ED. 2004. Revised nomenclature for avian telencephalon and some related brainstem nuclei. J Comp Neurol 473(3):377-414.
Remy M, Emmerton J. 1989. Behavioral spectral sensitivities of different retinal areas in pigeons. Behav Neurosci 103:170-177.
Remy M, Güntürkün O. 1991. Retinal afferents to the tectum opticum and the nucleus opticus principalis thalami in the pigeon. The Journal of Comparative Neurology 305(1):57-70.
Revzin AM. 1969. A specific visual projection area in the hyperstriatum of the pigeon (Columba livia). Brain Research 15(1):246-249.
Revzin AM, Karten H. 1967. Rostral projections of the optic tectum and the nucleus rotundus in the pigeon. Brain Research 3(3):264-276.
Reymond L. 1985. Spatial visual acuity of the eagle *Aquila audax*: a behavioural, optical and anatomical investigation. Vision Res 25(10):1477-1491.
Rodieck RW, Binmoeller KF, Dineen J. 1985. Parasol and midget ganglion cells of the human retina. J Comp Neurol 233(1):115-132.
Rodieck RW, Stone J. 1965a. ANALYSIS OF RECEPTIVE FIELDS OF CAT RETINAL GANGLION CELLS. J Neurophysiol 28(5):833-849.
Rodieck RW, Stone J. 1965b. RESPONSE OF CAT RETINAL GANGLION CELLS TO MOVING VISUAL PATTERNS. J Neurophysiol 28(5):819-832.
Romeskie M, Yager D. 1976. Psychophysical studies of pigeon color vision--I. Photopic spectral sensitivity. Vision Res 16(5):501-505.
Rounsley KJ, McFadden SA. 2005. Limits of visual acuity in the frontal field of the rock pigeon (Columba livia). Perception 34(8):983-993.
Saito HA. 1983. Morphology of physiologically identified X-, Y-, and W-type retinal ganglion cells of the cat. J Comp Neurol 221(3):279-288.
Salinas-Navarro M, Mayor-Torroglosa S, Jiménez-López M, Avilés-Trigueros M, Holmes T, Lund R, Villegas-Pérez M, Vidal-Sanz M. 2009. A computerized analysis of the entire retinal ganglion cell population and its spatial distribution in adult rats. Vision Research 49(1):115-126.
Schaeffel F, Wagner H. 1996. Emmetropization and optical development of the eye of the barn owl (*Tyto alba*). Journal of Comparative Physiology A: Neuroethology, Sensory, Neural, and Behavioral Physiology 178(4):491-498.
Sheedlo H, Li L, Barnstable C, Turner J. 1993. Synaptic and photoreceptor components in retinal pigment epithelial cell transplanted retinas of Royal College of Surgeons dystrophic rats. Journal of Neuroscience Research 36(4):423-431.
Shimizu T, Karten HJ. 1993. The avian visual system and the evolution of the neocortex. In: Zeigler HP, Bischof H, editors. Vision, brain, and behavior in birds. Cambridge: Massachusetts Institute of Technology. p 103-114.
Silver R, Witkovsky P, Horvath P, Alones V, Barnstable C, Lehman M. 1988. Coexpression of opsin- and VIP-like-immunoreactivity in CSF-contacting neurons of the avian brain. Cell and Tissue Research 253(1):189-198.

Sjöstrand FS. 1953a. The ultrastructure of the inner segments of the retinal rods of the guinea pig eye as revealed by electron microscopy. Journal of Cellular and Comparative Physiology 42(1):45-70.
Sjöstrand FS. 1953b. The ultrastructure of the outer segments of rods and cones of the eye as revealed by the electron microscope. Journal of Cellular and Comparative Physiology 42(1):15-44.
Slaughter M, Miller R. 1981. 2-amino-4-phosphonobutyric acid: a new pharmacological tool for retina research. Science 211(4478):182-185.
Slonaker J. 1897. A Comparative Study of the Area of Acute Vision in Vertebrates. Journal of Morphology 13:445-494.
Smirnakis SM, Berry MJ, Warland DK, Bialek W, Meister M. 1997. Adaptation of retinal processing to image contrast and spatial scale. Nature 386:69-73.
Snyder AW, Miller WH. 1978. Telephoto lens system of falconiform eyes. Nature 275:127-129.
Song PI, Matsui JI, Dowling JE. 2008. Morphological types and connectivity of horizontal cells found in the adult zebrafish (Danio rerio) retina. The Journal of Comparative Neurology 506(2):328-338.
Stanford LR. 1987. X-cells in the cat retina: relationships between the morphology and physiology of a class of cat retinal ganglion cells. J Neurophysiol 58(5):940-964.
Stein JJ, Berson DM. 1995. On the distribution of gamma cells in the cat retina. Vis Neurosci 12:687-700.
Stein JJ, Johnson SA, Berson DM. 1996. Distribution and coverage of beta cells in the cat retina. J Comp Neurol 372:597-617.
Sterling P, Freed M, Smith R. 1988a. Architecture of rod and cone circuits to the on-beta ganglion cell. Journal of Neuroscience 8(2):623-642.
Sterling P, Freed MA, Smith RG. 1988b. Architecture of rod and cone circuits to the on-beta ganglion cell. J Neurosci 8(2):623-642.
Stone J. 1965. A quantitative analysis of the distribution of ganglion cells in the cat's retina. J Comp Neurol 124(3):337-352.
Stone J. 1983. Parallel processing in the visual system: The classification of retinal ganglion cells and its impact on the neurobiology of vision. Blakemore C, editor. New York: Plenum Press.
Strettoi E, Dacheux RF, Raviola E. 1990. Synaptic connections of rod bipolar cells in the inner plexiform layer of the rabbit retina. The Journal of Comparative Neurology 295(3):449-466.
Strettoi E, Masland R. 1995. The organization of the inner nuclear layer of the rabbit retina. The Journal of Neuroscience 15(1):875-888.
Strettoi E, Novelli E, Mazzoni F, Barone I, Damiani D. 2010. Complexity of retinal cone bipolar cells. Progress in Retinal and Eye Research 29(4):272-283.
Sun W, He S. 2002. Large scale morphological survey of mouse retinal ganglion cells. J Comp Neurol 451:115-126.
Sun W, Li N, He S. 2002. Large-scale morophological survey of rat retinal ganglion cells. Vis Neurosci 19(4):483-493.
Suzuki S, Kaneko A. 1990. Identification of bipolar cell subtypes by protein kinase C-like immunoreactivity in the goldfish retina. Visual Neuroscience 5(03):223-230.
Szmajda BA, Grünert U, Martin PR. 2008. Retinal ganglion cell inputs to the koniocellular pathway. The Journal of Comparative Neurology 510(3):251-268.
Thanos S, Vanselow J, Mey J. 1992. Ganglion cells in the juvenile chick retina and their ability to regenerate axons in vitro. Exp Eye Res 54:377-391.

Uga S, Smelser GK. 1973. Comparative Study of the Fine Structure of Retinal MÜller Cells in Various Vertebrates. Investigative Ophthalmology & Visual Science 12(6):434-448.
Vaquero CF, Velasco A, de la Villa P. 1997. Quantitative measurement of protein kinase C immunoreactivity in rod bipolar cells of the goldfish retina. Brain Research 773(1,Äì2):208-212.
Vardi N. 1998. Alpha subunit of Go localizes in the dendritic tips of ON bipolar cells. The Journal of Comparative Neurology 395(1):43-52.
Vardi N, Matesic DF, Manning DR, Liebman PA, Sterling P. 1993. Identification of a G-protein in depolarizing rod bipolar cells. Visual Neuroscience 10(03):473-478.
Walls GL. 1942. The vertebrate eye and its adaptive radiation. New York: Hafner Publishing Company.
Wässle H, Boycott BB. 1991. Functional architecture of the mammalian retina. Physiol Rev 71(2):447-480.
Wässle H, Grünert U, Martin PR, Boycotts BB. 1994. Immunocytochemical characterization and spatial distribution of midget bipolar cells in the macaque monkey retina. Vision Research 34(5):561-579.
Wassle H, Peichl L, Boycott BB. 1981. Dendritic territories of cat retinal ganglion cells. Nature 292(5821):344-345.
Wässle H, Puller C, Müller F, Haverkamp S. 2009. Cone Contacts, Mosaics, and Territories of Bipolar Cells in the Mouse Retina. The Journal of Neuroscience 29(1):106-117.
Wässle H, Yamashita M, Greferath U, Grünert U, Müler F. 1991. The rod bipolar cell of the mammalian retina. Visual Neuroscience 7(1-2):99-112.
Watanabe M, Rodieck RW. 1989. Parasol and midget ganglion cells of the primate retina. J Comp Neurol 289(3):434-454.
Werblin FS, Dowling JE. 1969. Organization of the retina of the mudpuppy, Necturus maculosus. II. Intracellular recording. J Neurophysiol 32(3):339-355.
Westheimer G. 1960. Modulation thresholds for sinusoidal light distributions on the retina. J Physiol 152(1):67-74.
Wiesel TN. 1960. Receptive fields of ganglion cells in the cat's retina. J Physiol 153(3):583-594.
Wilder HD, Grunert U, Lee BB, Martin PR. 1996. Topography of ganglion cells and photoreceptors in the retina of a New World monkey: the marmoset Callithrix jacchus. Vis Neurosci 13(2):335-352.
Wingstrand KG, Munk O. 1965. The pecten oculi of the pigeon with particular regard to its function. Biol Skr Dan Vid Selsk 14:1-64.
Wortel JF, Wubbels RJ, Nuboer JFW. 1984. Photopic spectral sensitivities of the red and the yellow field of the pigeon retina. Vision Res 24(9):1107-1113.
Yang G, Masland RH. 1992. Direct visualization of the dendritic and receptive fields of directionally selective retinal ganglion cells. Science 258:1949-1952.
Yarczower M, Wolbarsht ML, Galloway WD, Fligsten KE, Malcolm R. 1966. Visual acuity in a stumptail macaque. Science 152:1392-1393.
Yazulla S. 1974. Intraretinal differentiation in the synaptic organization of the inner plexiform layer of the pigeon retina. J Comp Neurol 153(3):309-323.
Yokoyama S. 1997. Molecular Genetic Basis of Adaptive Selection:Examples From Color Vision in Vertebrates. Annu Rev Genet 31(1):315-336.

Young HM, Vaney DI. 1990. The retinae of Prototherian mammals possess neuronal types that are characteristic of non-mammalian retinae. Visual Neuroscience 5(01):61-66.
Young RW. 1967. The renewal of photoreceptor cell outer segments. J Cell Biol 33(1):61-72.
Young RW, Bok D. 1969. Participation of the retinal pigment epithelium in the rod outer segment renewal process. J Cell Biol 42(2):392-403.
Zhang D, Yeh HH. 1991. Protein Kinase C-like immunoreactivity in rod bipolar cells of the rat retina: A developmental study. Visual Neuroscience 6(05):429-437.